Title: MOS4-Associated Complex subunits 3A and 3B modulate *FLM* splicing to repress photoperiod-dependent floral transition

Short title: MAC3A/B regulate FLM AS to repress flowering in SD

Yu-Wen Huang[1,*†], Chih-Yen Tseng[1, 2†], Yi-Tsung Tu[1], Hsin-Yu Hsieh[3],Yu-Sen Wang[1], Yu-Zhen Chen[1], Yun-Tung Ly[4], Shih-Long Tu[3], Chin-Mei Lee[1, 2, 5, 6 *]

[1] Institute of Plant Biology, National Taiwan University, Taipei, 106319, Taiwan
[2] Department of Life Science, National Taiwan University, Taipei, 106319, Taiwan
[3] Institute of Plant and Microbial Biology, Academia Sinica, Taipei, 115201, Taiwan
[4] Department of Agricultural Chemistry, National Taiwan University, Taipei, 106319, Taiwan
[5] The Master Program in Global Agriculture Technology and Genomic Science, National Taiwan University, Taipei, 106319, Taiwan
[6] International Joint Degree Master's Program in Agro-biomedicine in Food and Health, National Taiwan University, Taipei, 100233, Taiwan

[†] These authors contributed equally to the article
[*] Corresponding author: Chin-Mei Lee (Email: chinmeilee@ntu.edu.tw)

The author responsible for the distribution of materials integral to the findings presented in this article in accordance with the policy described in the Instructions for Authors (https://academic.oup.com/plcell/pages/General-Instructions) is: Chin-Mei Lee (chinmeilee@ntu.edu.tw).

Abstract

Plants adjust their flowering time by integrating environmental cues through complex regulatory networks. RNA splicing plays a crucial role in modulating gene expression in response to flowering signals. The MOS4-associated complex (MAC), consisting of the evolutionarily conserved E3 ubiquitin ligases MAC3A and MAC3B, is pivotal in splicing regulation. However, their involvement in floral transition remained unclear. This study observed that *mac3a/mac3b* mutants flowered significantly earlier under short-day (SD) conditions, a phenotype absent under long-day (LD) conditions. This early flowering correlated with upregulation of *FLOWERING LOCUS T* (*FT*) and *SUPPRESSOR OF OVEREXPRESSION OF CO 1* (*SOC1*) compared to wild-type plants. Transcriptomic analysis revealed alterations in transcript levels and splicing profiles of key floral regulators across different flowering pathways. Further exploration identified the thermosensory flowering regulator *FLOWERING LOCUS M* (*FLM*) as being influenced by *MAC3A* and *MAC3B*. Our findings showed that SPL9 bound to *MAC3A* and *MAC3B* promoters to induce their expression under a short photoperiod. Subsequently, MAC3A and MAC3B associated with *FLM* transcripts to modulate their splicing in SD. This study elucidates how the MAC complex, through RNA splicing regulation, integrates environmental signals to modulate flowering, unveiling a new layer of complexity in flowering pathway crosstalk under non-inductive photoperiods.

Introduction

The floral transition from vegetative to reproductive stages represents a captivating and distinctive developmental process in angiosperms. In order to ensure successful reproduction, plants have evolved a sophisticated network that integrates various environmental signals, managing the plants' developmental and metabolic status to control floral transition through multifaceted mechanisms precisely (Takagi et al., 2023; Song et al., 2015; Park et al., 2019; Cho et al., 2017; Teotia et al., 2015; Gendron et al., 2021). This intricate regulatory network is categorized into major pathways, including photoperiod, age, vernalization, autonomous, thermosensory, and gibberellin (GA) pathways, with extensive crosstalk among them that warrants further exploration.

In the photoperiod pathway, the circadian clock integrates signals from the length of the day to regulate the well-known GIGANTEA (GI)-CONSTANS (CO)-FLOWERING LOCUS T

61 (FT) module (Imaizumi et al., 2005; Sawa et al., 2007). The circadian clock orchestrates the
62 rhythmic expression of *GIGANTEA* (*GI*), peaking before dusk (Fowler et al., 1999). During long
63 days (LD), light induces GI to form a complex with FLAVIN-BINDING, KELCH REPEAT, F
64 BOX 1 (FKF1) E3 ubiquitin ligase before dusk, leading to the degradation of CYCLING DOF
65 FACTOR1 and its homologs (CDFs), which otherwise repress *CO* transcription (Sawa et al., 2007;
66 Fornara et al., 2009). In LD conditions, CO protein accumulates and interacts with various
67 transcription factors (TFs), including some B and C subunits of Nuclear Factor Y, namely NF-
68 YB2, NF-YB3, NF-YC3, NF-YC4, and NF-YC9, to activate *FT* expression in leaves (Kumimoto
69 et al., 2008; 2010; Cao et al., 2014). FT, functioning as a mobile florigen, moves to the shoot apical
70 meristem (SAM), where it interacts with FLOWERING LOCUS D (FD), initiating floral transition
71 by promoting the expression of the SAM-expressed floral integrator *SUPPRESSOR OF*
72 *OVEREXPRESSION OF CO 1* (*SOC1*) and activating *LEAFY* (*LFY*) and *APETALA1* (*AP1*)
73 (Corbesier et al., 2007; Jaeger and Wigge, 2007; Li et al., 2011; Lee and Lee, 2010). Conversely,
74 under short days (SD), the formation of the GI-FKF1 complex is reduced due to the
75 unsynchronized accumulation of GI and FKF1 proteins, and *CO* repression by CDFs delays
76 flowering (Sawa et al., 2007). Apart from transcriptional regulation, photoperiod also influences
77 CO protein levels post-translationally (reviewed by Takagi et al., 2023). The activation of *FT* by
78 CO can be counteracted by TEMPRANILLO1 and 2 (TEM1 and TEM2), which directly inhibit
79 *FT* expression (Castillejo and Pelaz, 2008).

80 While extensive research has been conducted on regulating flowering time under inductive
81 photoperiods, the mechanisms governing the repression of floral initiation in non-inductive day
82 lengths remain largely unexplored. The GA pathway plays a significant role in suppressing the
83 expression of *FT* and *SOC1* under SD (Bao et al., 2019). TEM1 and TEM2 downregulate GA
84 biosynthesis genes, such as *GA3OX1* and *GA3OX2*, reducing the levels of bioactive GA, which in
85 turn tightly regulates *SOC1* and *LFY* expression in the shoot apical meristem (SAM) (Osnato et
86 al., 2012; Moon et al., 2005; Eriksson et al., 2006). Additionally, GA repressor DELLA proteins
87 interact with various floral regulators across different pathways. DELLA interacts with and
88 stabilizes the MYC3 transcription factor, which directly represses *FT* or indirectly inhibits the
89 association of the CO/NF-YB activator with the *FT* promoter (Cao et al., 2014; Bao et al., 2019).
90 Furthermore, GA regulates the miR156-SQUAMOSA PROMOTER BINDING PROTEIN-LIKE
91 (SPL) module in the age flowering pathway (Huijser et al., 2011; Park et al., 2017). In juvenile

92 plants, high levels of *miR156* repress *SPL9*, *SPL10*, and *SPL15*, while decreasing *miR156* levels
93 during maturation enhances the expression of *SPL9* and its paralogs (Wang et al., 2009). SPL9
94 promotes the transcription of *pri-miRNA172*, which represses AP2-like TFs, including
95 *SCHLAFMUTZE* (*SMZ*) and *EAT1 TARGETs* (*TOEs*), direct or indirect repressors of *FT* or *SOC1*
96 (Wang and Wang, 2015; Chen, 2004; Mathieu et al., 2009). Under SD, DELLA can interact with
97 SPL9 to inhibit its activity, leading to delayed flowering (Yu et al., 2012). Moreover, DELLA
98 interacts with and stabilizes FLOWERING LOCUS C (FLC), the primary floral repressor in the
99 vernalization and autonomous pathways. FLC, along with other MADS TFs like SHORT
100 VEGETATIVE PHASE (SVP), FLOWERING LOCUS M (FLM), and its homologs, MADS
101 AFFECTING FLOWERINGs (MAFs), recruit histone modifiers to establish repressive epigenetic
102 marks on the *FT* and *SOC1* loci (Li et al., 2008; Li et al., 2016; Gu et al., 2013), thereby facilitating
103 the repression of *FT* and *SOC1* by FLC. Additionally, other floral pathways interact with the
104 photoperiod pathway in a GA-independent manner. Histone Deacetylase 9 (HDA9) represses
105 *AGAMOUS-LIKE 19* (*AGL19*), an *FT* activator, to prevent premature flowering under SD
106 conditions (Kang et al., 2015).
107 Warm temperatures can alleviate the repression of flowering under SD through crosstalk
108 among flowering pathways (Fernández et al., 2016; Jin and Ahn, 2021). The bHLH transcription
109 factors PHYTOCHROME INTERACTING FACTOR 4 and 5 (PIF4 and PIF5) interact with CO
110 to promote *FT* expression at high ambient temperatures under SD (Fernández et al., 2016; Kumar
111 et al., 2012). The expression and activity of PIF4 can be enhanced by the clock/photoperiod
112 regulators EVENING COMPLEX (EC), composed of EARLY FLOWERING 3 (ELF3), ELF4,
113 and LUX ARRHYTHMO (LUX) transcription factors under high temperature conditions (Ezer et
114 al., 2017; Silva et al., 2020; Nieto et al., 2015). The accessibility of PIF4 to the *FT* promoter can
115 be regulated by the RGA DELLA protein, which interacts with the DNA-binding domain of PIF4;
116 however, the flowering regulation by GA appears to be partially independent of PIF4 (de Lucas et
117 al., 2008; Galvão et al., 2015). Furthermore, SVP and FLM more profoundly repress *FT* and *SOC1*
118 expression under SD (Scortecci et al., 2001; Lee et al., 2013; Posé et al., 2013). High temperatures
119 decrease the stability of the SVP protein, thereby reducing its repressive effects on flowering (Lee
120 et al., 2013).
121 RNA splicing emerges as a significant contributor to the modulation of florigen and
122 upstream regulators in response to environmental fluctuations (Posé et al., 2013; Park et al., 2019;

123 Shang et al., 2017; Qi et al., 2019). It generates protein isoforms from spliced RNA variants; some
124 play antagonistic roles in floral pathways, while others modulate RNA stabilities. In the
125 thermosensory flowering pathway, low and high temperatures modulate the alternative splicing of
126 *FLM* (Posé et al., 2013). The major FLM isoform, FLMβ, interacts with SVP to repress *FT* and
127 *SOC1*. Under high ambient temperatures, an increase in *FLMδ*, which encodes a protein that
128 counteracts the function of FLMβ by competing with it for binding to SVP, leads to the
129 derepression of *FT* and *SOC1*. Similar scenario with the photoperiod pathway, *CO* produces two
130 isoforms in a ratio determined by the photoperiods (Gil et al., 2017). COα promotes the expression
131 of *FT*, whereas COβ, encoding a truncated CO protein, interacts and negatively regulates COα by
132 enhancing its degradation by COP1. The ratios of COβ to Coα are higher in SD compared to LD.
133 Furthermore, *PIF4*, another ambient-temperature-sensing flowering regulator, transcribes
134 alternative isoforms (Huang et al., 2022). PIF4-I4R (with 4th intron retained), identified as a
135 translatable splicing isoform, produces a protein that can interact with full-length PIF4, though its
136 specific function remains unknown. The significance of RNA alternative splicing in floral
137 regulation is underscored by observations that mutations in RNA splicing machinery components
138 often lead to altered flowering phenotypes (Park et al., 2019; Shang et al., 2017).
139 The RNA splicing is processed by spliceosomes, and their activities are dynamically
140 regulated by splicing factors associated with them. One such factor is the MOS4-ASSOCIATED
141 COMPLEX (MAC complex), an evolutionarily conserved splicing factor that is crucial for plant
142 RNA splicing (Monaghan et al., 2009; Jia et al., 2017; Li et al., 2019). In Arabidopsis, the MAC
143 complex consists of MAC3A and MAC3B, a pair of U-box type E3 ubiquitin ligase homologs,
144 whose C-terminal WD40 domains predicted to interact with MOS4, AtCDC5, and PRL1 as MAC
145 core proteins. The E3 ubiquitin ligase functions lie in the N-terminal U-box domains of MAC3A
146 and MAC3B to interact with E2 ubiquitin-conjugation enzyme (E2) and facilitate ubiquitin transfer
147 to their substrates. In human cells, the homolog of MAC3A and MAC3B, PRP19, not only
148 transfers ubiquitin to itself for auto-inhibition, it can ubiquitinate the K63 of PRP3, a specific
149 subunit of U4 snRNP, to enhance the association of the U4/U6/U5 snRNP within the spliceosome
150 (de Moura et al., 2018; Song et al., 2010). While the E3 ubiquitin ligase functions of MAC3A and
151 MAC3B in plants remain to be fully explored, their regulatory roles in plant RNA splicing have
152 been evidenced by transcriptome analysis, which revealed misregulation of approximately 11,000
153 genes in 9-day-old *mac3a/mac3b* double mutant seedlings (Li et al., 2019). These splicing defects

may explain a wide range of phenotypes, including circadian rhythm lengthening, growth abnormalities, altered responses to abiotic stress, changes in defense mechanisms, and defects in miRNA biogenesis (Jiang et al., 2023; Tu and Chen, 2022; Monaghan et al., 2009; Jia et al., 2017). Previous reports on the flowering phenotypes under LD conditions have shown that *mac3a* and *mac3b* single knockout mutants, or the *mac3a/mac3b* double knockdown mutant (with the double null mutant being embryonic lethal), exhibit either no differences or moderate delays in flowering (Feke et al., 2020; Li et al., 2019).

Given the pivotal role of alternative splicing in regulating floral transitions and the significant alterations of splicing events observed in the *mac3a/mac3b* seedlings, the previously reported phenotypes under long-day (LD) conditions cannot fully account for this discrepancy (Jia et al., 2017; Li et al., 2019; Feke et al., 2020). Here, we present evidence demonstrating that the Arabidopsis *mac3a/mac3b* double mutant exhibits significantly early flowering under SD while displaying a phenotype similar to the wild type under LD conditions. RNA-sequencing analyses of SD-grown *mac3a/mac3b* mature plants revealed expression and splicing profiles of floral regulators in multiple flowering pathways that were markedly altered. One potential cause for the early flowering phenotype is the involvement of *FLM*, a floral regulator in the ambient temperature flowering pathway. MAC3A/MAC3B can associate with *FLM* RNA to regulate the ratios of *FLMβ* and *FLMδ*, thereby influencing flowering repression. The daylength-specific transcription of *MAC3A* and *MAC3B* may explain their regulatory role only under SD, which is itself regulated by *SPL9*. These findings suggest that the MAC complex might be a central hub coordinating crosstalk among the flowering pathways by regulating RNA splicing under short-day conditions.

Results

MAC3A and *MAC3B* repress flowering in short-day

To comprehensively investigate the roles of *MAC3A* and *MAC3B* in flowering regulation, we measured the flowering times under both long-day (LD, 16 hours of light/8 hours of dark) and short-day (SD, 8 hours of light/16 hours of dark) conditions (Fig.1A and 1B). Aligning with earlier findings, the single mutants of *mac3a* and *mac3b*, as well as the *mac3a/mac3b* double mutant, displayed flowering times similar to the wild type (Col-0) under LD conditions, as determined by the number of rosette leaves at bolting (Figure 1A, left panel) (Li et al., 2019). When the flowering time was assessed by the day of bolting, the *mac3a/mac3b* double mutant manifested a minor delay,

echoing the observations of Feke et al. (2020) (Figure 1A, right panel). Notably, under SD conditions, the *mac3a/mac3b* double mutant exhibited significantly earlier flowering based on both flowering measurement indices, opposite to phenotype in LD (Figure 1B). Further analyses of the floral integrator transcripts, *FT* and *SOC1*, showed elevated peak expressions in the *mac3a/mac3b* double mutant compared to Col-0 under SD. This finding supports early flowering phenotypes in the *mac3a/mac3b* mutant under SD (Figure 1C).

The flowering phenotype of *mac3a/mac3b* mutant does not correlate with *CONSTANS* levels.

To ascertain if *CO* mediated the upregulation of *FT* and *SOC1* in the *mac3a/mac3b* mutant, we analyzed the expression patterns of *CO*. Remarkably, the expression profiles of *CO* in the *mac3a/mac3b* double mutant were not significantly different compared to wildtype under SD conditions (Figure 2A and 2B). Further examination of *CO* expression in the *mac3a* and *mac3b* single mutants or *mac3a/mac3b* double mutants in SD or LD conditions did not correlate to the observed flowering phenotypes nor the expression of *FT* (Figure 2A, Figure 1B-1C). Given the roles of MAC3A and MAC3B in RNA splicing, we next investigated whether these factors might influence the balance between two splice variants of CO, namely COα and COβ, which in turn could modulate *FT* expression (Figure 2C-2E). Consistent with prior findings, *COα* levels surpassed those of *COβ* towards the end of the day, resulting in a higher *COα* to *COβ* ratio in the wild type under SD (Figure 2D) (Gil et al., 2017). However, the *mac3a/mac3b* mutant presented a reduced *COα* to *COβ* ratio due to increased *COβ* expression. This pattern does not account for the elevated *FT* expression nor the early flowering observed in the *mac3a/mac3b* mutant (Figure 2C and 2D, Figure 1B and 1C).

Transcriptome analyses of *mac3a/mac3b* mutant indicate alterations in various flowering pathways

Recognizing that MAC3A and MAC3B can impact transcriptome by supporting proper RNA splicing, we posited that their regulatory function in splicing might underlie the accelerated flowering observed in *mac3a/mac3b* mutants under SD conditions. To test this hypothesis, we performed RNA sequencing on 40-day-old SD-grown *mac3a/mac3b* mutants and wild-type (Col-0) plants, which were still in their vegetative growth phase. The analysis revealed 605 differentially expressed genes (DEGs) between the *mac3a/mac3b* mutants and Col-0 ($|\log2(\text{fold change})| \geq 1.5$

216 and FDR≤ 10%) (Figure 3A). Of these, 371 genes were upregulated, while 234 were
217 downregulated. Gene Ontology (GO) enrichment analysis of the DEGs highlighted significant
218 associations with biological processes such as circadian rhythm, response to stimulus, and post-
219 embryonic development (Figure 3B).

220 To explore the affected flowering pathways in the *mac3a/mac3b*, we compared the DEG
221 list with genes involving flowering initiation classified by Bouché et al. (2016). It revealed
222 differential gene expression across multiple flowering pathways, including circadian
223 clock/photoperiod, vernalization, age, and GA pathways in the *mac3a/mac3b* mutants (Figure 3C).
224 Notably, morning-phased central clock regulators, like *CCA1*, *LHY*, and *PRR9,* were upregulated,
225 whereas evening-phased regulators, such as *ELF4, LUX, TOC1*, and *PRR3,* exhibited reduced
226 expression. This shift suggests a circadian clock phase delay, aligning with previous findings (Feke
227 et al., 2019). Despite these changes, the observed decrease in *CO* expression with log2(fold change)
228 = -2.899 identified through RNA sequencing, potentially due to phase delays, does not fully
229 account for the *mac3a/mac3b* mutant's early flowering phenotype (Figure 1B).

230 Investigating beyond photoperiodic influences, we found that the age and vernalization
231 pathways also experienced significant alterations (Figure 3C). In the age pathway, *miRNA156*-
232 targeted *SPL5* was downregulated, whereas *SPL15* was upregulated. On the other hand, *pri-*
233 *miRNA172*, which is downstream of *SPL15*, showed decreased transcript levels. These changes
234 suggest that the age pathway might not primarily drive the early flowering observed in the
235 *mac3a/mac3b* mutants. Conversely, in the vernalization pathway, the floral repressor *FLC* was
236 downregulated, and the floral activator *AGL19* was upregulated. We further confirmed their
237 expression by RT-qPCR. The *mac3a/mac3b* mutants exhibited overall lower *FLC* expression
238 compared to the wildtype under SD, and the other two MADS TFs, FLM, and SVP, which complex
239 with FLC to repress *FT*, were not significantly changed (Supplemental Figure S1A-S1C). However,
240 the expression of *AGL19* was not higher in the *mac3a/mac3b* mutants (Supplemental Figure S1D).
241 These data imply that *MAC3A/MAC3B* partially modulates the flowering time under SD conditions
242 through *FLC* in the vernalization/autonomous pathway (Figure 3B and Supplemental Figure S1).
243

244 **Mutations in *MAC3A* and *MAC3B* lead to severe RNA splicing defects**

245 Given the established involvement of *MAC3A/MAC3B* in RNA splicing, prior research has
246 highlighted a marked increase in abnormal alternative splicing events, predominantly intron

247 retention, in *mac3a/mac3b* mutants (Li et al., 2019). This alteration in RNA splicing presents a
248 plausible avenue to elucidate the genetic contributors to the early flowering observed in
249 *mac3a/mac3b* mutants under SD conditions. Consequently, we identified differentially
250 alternatively spliced transcripts in our RNA-sequencing dataset with 12,031 events encoded by
251 6,836 genes differential alternative splicing events (DASs) in the *mac3a/mac3b* mutants (Table 1).
252 Consistent with earlier findings, the analysis revealed that over 98% of DASs or 11,876 events
253 within 6,778 genes in the *mac3a/mac3b* mutants were characterized by increased intron retention
254 (IR) (Table 1 and Figure 4A). The remaining DASs were exon skipping (ES) and alterations in
255 donor/acceptor splice sites (AltDA) involving transcription from 150 genes (Table 1 and Figure
256 4B).

257 Gene ontology (GO) analysis of the DASs showed significant enrichment of terms associated
258 with developmental processes and the RNA splicing machinery (Figure 4C). Additionally, the
259 altered RNA splicing in *mac3a/mac3b* mutants affected genes integral to primary metabolic
260 pathways, RNA processing, and responses to environmental stimuli, potentially leading to the
261 observed pleiotropic effects on flowering initiation and growth attenuation (Figure 1B; Li et al.,
262 2018; Li et al., 2019; Feke et al., 2020; Guo et al., 2024).

263 A subsequent comparison of genes within the DAS list with established regulators of
264 flowering initiation (Bouché et al., 2016) revealed a significant overlap: 136 genes from the DAS
265 list were among the 306 known to regulate flowering (Figure 5A). As noted, 135 of these genes
266 exhibited upregulated retained introns in the *mac3a/mac3b* mutant. These results underscore the
267 critical role of *MAC3A/MAC3B* in safeguarding splicing fidelity under SD conditions.

268

269 **Changes in the ratios of *FLOWERING LOCUS M* isoforms in the *mac3a/mac3b* mutant**

270 To elucidate the specific regulators whose DAS defects contribute to the upregulation of *FT*
271 and *SOC1*, and consequently the early flowering phenotype in *mac3a/mac3b* mutants, we focused
272 on identifying overlaps among the DAS gene list, known flowering regulators, and potential
273 transcription factors (TFs) upstream of the DEGs (Figure 5A). By analyzing the promoter regions
274 of each DEG for potential upstream regulators, we identified enriched TFs based on the frequency
275 of downstream genes present in the DEG list. Among these TFs, 38 exhibited DAS, with three
276 playing roles in flowering initiation: *LHY*, *PIF4*, and *FLM* (Figure 5A-5B).

277 *LHY*, a circadian clock gene acting upstream of *CO* in the photoperiod pathway, showed
278 reduced inclusion of the 4th exon (Figure 5C). However, our earlier findings have excluded *CO*'s
279 alterations as a primary factor for the early flowering observed in *mac3a/mac3b* mutants (Figure
280 2). In the *mac3a/mac3b* mutants, significant retention of the 1st and 4th introns of *PIF4* was
281 observed (Figure 5C and Supplemental Figure S2A), potentially leading to truncated protein
282 isoforms with missing or incomplete bHLH DNA binding domain (Supplemental Figure S2A-
283 S2B). Other PIF alternative transcripts may go through nonsense-mediated decay. Overall, it can
284 lead to less functional PIF4 proteins. Given PIF4's role as a positive regulator of *FT* as Kumar et
285 al. (2012) reported, these splicing defects could be expected to decrease *FT* expression,
286 contradicting our observations (Figure 1C).
287 Furthermore, *FLM*, a repressor in the thermosensory flowering pathway, exhibited increased
288 inclusion of the 3rd exon and reduced inclusion of the 2nd exon in *mac3a/mac3b* mutants (Figure
289 5C and 6A). The alternatively splicing patterns of *FLM* lead to two isoforms, *FLMβ* and *FLMδ*,
290 with opposing roles in regulating flowering thermosensitivity (Posé et al., 2013). *FLMδ*,
291 characterized by the retention of the 3rd exon and exclusion of the 2nd, mitigates *FLMβ*'s
292 repression of *FT*. The prevalence of *FLMδ* over *FLMβ* in *mac3a/mac3b* mutants under SD
293 conditions could explain the upregulation of *FT* and the consequent early flowering (Figure 6A-
294 6B). However, this alteration was not observed under LD conditions (Figure 6C), indicating that
295 *MAC3A/MAC3B*'s regulation of *FLM* splicing is SD-specific. To ascertain if *MAC3A/MAC3B*
296 directly influence *FLM* splicing, RNA-immunoprecipitation (RIP) was performed using
297 Arabidopsis expressing FLAG-tagged *MAC3A*, revealing enrichment of *FLM* transcripts with
298 qPCR (Figure 6D and Supplemental Figure S4). These findings suggest that MAC3A/MAC3B
299 directly modulate the splicing of *FLM*, adjusting the ratio of *FLMβ* to *FLMδ* to regulate flowering
300 time under SD conditions.
301
302 **Photoperiod regulates the transcript levels of *MAC3A* and *MAC3B***
303 To elucidate the specific regulatory mechanisms of *MAC3A* and *MAC3B* on flowering under
304 SD conditions, we analyzed their transcript levels under both SD and LD conditions (Figure 7A-
305 7B). Notably, under SD conditions, both *MAC3A* and *MAC3B* transcripts exhibited peak
306 expression levels between 12 to 16 hours after dawn, a pattern not observed under LD conditions.
307 This distinct expression profile prompted further investigation into whether post-translational

308 mechanisms also contribute to regulating *MAC3A* and *MAC3B*, specifically their protein
309 abundance in Arabidopsis. To this end, we analyzed protein levels in transgenic Arabidopsis lines
310 overexpressing FLAG-tagged *MAC3A* across both photoperiods (Supplemental Figure S3). In the
311 *MAC3A* overexpressing lines, the protein abundance of *MAC3A* transgene remained consistently
312 similar in SD and LD conditions. These findings indicate that the regulation of *MAC3A* and
313 *MAC3B* in response to photoperiod changes is primarily transcriptional, with their peak transcript
314 levels under SD potentially playing a pivotal role in modulating flowering time.
315
316 **SPL9 binds to the *MAC3A* and *MAC3B* promoters to regulate their photoperiodic expression**
317 To elucidate the mechanism driving increased *MAC3A* and *MAC3B* expression under SD
318 conditions, we aimed to identify transcription factors interacting with both *MAC3A* and *MAC3B*
319 promoters. We utilized PlantPAN 4.0 (http://plantpan.itps.ncku.edu.tw/plantpan4, Chow et al.,
320 2019) for promoter analysis and identified 649 known TF binding motifs within the 1.5 kb
321 promoter regions of *MAC3A* and *MAC3B* (Figure 7C). A total of 243 common motifs were found
322 in both promoters, implicating 364 TFs as potential upstream regulators. Among them, 38 TFs
323 associated with flowering initiation. To further identify the potential regulators, we performed
324 correlation analysis between the expression profiles of these TFs (sourced from the Photo-Graph
325 database https://gendron-lab.shinyapps.io/PhotoGraph/; Leung et al., 2023) and *MAC3A/MAC3B*
326 expression under LD and SD (Figure 7A-7B). Finally, we identified four TFs, SPL9, TEM1, CDF1,
327 and NF-YB3 whose mRNA patterns showed significant correlations with *MAC3A* and *MAC3B*
328 expressions (Figure 7C-7D and Supplemental Figure S5).
329 Among these candidates, we chose SPL9, an activator that promotes the age-dependent
330 flowering initiation pathway (Schwarz et al., 2008), for further investigation due to the following
331 reasons. Firstly, previous genome-wide DNA Affinity Purification Sequencing (or DAP-Seq)
332 analyses showed that SPL9 interacted with the *MAC3B* promoter (ReMap2022 database,
333 https://remap2022.univ-amu.fr/; Chèneby et al., 2020). Additionally, both CDF1 and NF-YB3
334 regulate flowering through *CO* predominantly under LD conditions (Imaizumi et al., 2005;
335 Kumimoto et al., 2008), which may not be the CO-independent pathways that *MAC3A* and *MAC3B*
336 involved in. Finally, TEM1 functions as a repressor of *FT* (Castillejo and Pelaz, 2008). However,
337 the expression of *TEM1* was positively correlated with *MAC3A* and *MAC3B*, which is supposed to
338 be an activator of *MAC3A* and *MAC3B*. (Supplemental Figure S5).

339 We performed yeast one-hybrid assays to confirm that SPL9 binds to *MAC3A* and *MAC3B*
340 promoters, shown by increased β-galactosidase activity compared to controls (Figure 8A). This
341 interaction was further validated in Arabidopsis through Chromatin-immunoprecipitation (ChIP)
342 assays with miRNA156-resistant SPL9-GFP (rSPL9-GFP) transiently expressed in the Col-0,
343 revealing strong enrichment of rSPL9-GFP on some SPL9 binding sites (SPB-box, GTAC) of
344 *MAC3A* and *MAC3B* promoters (Figure 8B). To assess the activity of SPL9 on *MAC3A* and
345 *MAC3B* expression under photoperiodic changes, we examined *MAC3A* and *MAC3B* expressions
346 in the Col-0, *spl9*, and *mac3a/mac3b* mutants under both SD and LD (Figure 9A-9B). The SPL9
347 has higher expression in SD and peaks at ZT8 (Figure 7D), corresponding to higher expression of
348 the *MAC3A and MAC3B* with peaks at ZT12 or ZT16 (Figure 7A-7B). In the *spl9* mutant, the
349 higher expression of *MAC3A* and *MAC3B* in Col-0 during the evening (ZT12 to ZT20) in SD was
350 decreased (Figure 9A). Meanwhile, the *MAC3A* and *MAC3B* expression was not affected much by
351 the *SPL9* mutation in LD (Figure 9B). However, the mutation of *SPL9* did not entirely reduce
352 *MAC3A* and *MAC3B* expression levels to that in the *mac3a/mac3b* double mutant, suggesting other
353 regulators exist (Figure 9A-9B). We further employed transient overexpression of *rSPL9-GFP* in
354 seedlings to confirm SPL9's regulatory role under SD, and it induced *MAC3A* and *MAC3B*
355 expressions (Figure 9C-9D). Overall, our findings highlight *SPL9* as a regulator of *MAC3A* and
356 MAC3B, partially accounting for promoting their expression under SD conditions for flowering
357 time controls.
358
359 **Discussion**
360 Alternative splicing critically regulates floral transition in response to environmental cues,
361 yet the underlying regulators and mechanisms remain largely unexplored (Park et al., 2019; Shang
362 et al., 2017; Qi et al., 2019). Disruptions of proteins involved in the RNA splicing process
363 frequently result in flowering time anomalies across both LD and SD conditions. Notably,
364 mutations in U1 snRNP components, such as *RBP45d* and *PRP39a*, or the factors associated with
365 3' splicing site recognition—U2 snRNP auxiliary factors U2AF35a, U2AF35b, and U2AF65a—
366 all lead to delayed flowering in LD and SD (Chang et al., 2022; Wang et al., 2007; Wang and
367 Brendel, 2006; Park et al., 2019). This study unveils the roles of MAC3A and MAC3B, key
368 components of the MOS4-associated complex (MAC) splicing factor, specifically repressing floral
369 transition under SD conditions. We discovered that the photoperiod influences *MAC3A/MAC3B*

370 expression through SPL9 transcription factors, driving higher expression levels in SD. While
371 transcriptome analysis suggests that alterations in transcripts and splicing profiles across various
372 flowering pathways contribute to regulating flowering time, our findings specifically point to
373 MAC3A/MAC3B's direct impact on *FLM* splicing under SD conditions. Additionally, an indirect
374 effect on *FLC* expression emerges as another mechanism by which *MAC3A* and *MAC3B* suppress
375 flowering under SD, highlighting a nuanced role of alternative splicing and photoperiodic
376 regulation in floral transition.
377
378 **MAC3A and MAC3B modulate the ratios of *FLM* isoform to regulate flowering in**
379 **response to photoperiod and temperature signals**
380 Utilizing a combination of differentially expressed and alternatively spliced gene data,
381 along with RIP-qPCR and expression analysis, we have identified *FLM* as a direct splicing target
382 of MAC3A and MAC3B under SD conditions (Figure 5 and 6). *FLM* functions at the crossroads
383 of the thermosensory and autonomous flowering pathways, with its splicing of isoforms modulated
384 by temperature. The alterations of *FLM* splicing also have been found in various splicing regulator
385 mutants under ambient temperature conditions (Jin and Ahn, 2021; Posé et al., 2013). Our results
386 extend this understanding by revealing that *FLM* splicing is also influenced by photoperiod,
387 suggesting a mechanism whereby *FLM* isoform regulation serves as an integration point for
388 photoperiod and temperature cues, facilitating flowering in response to elevated temperatures
389 under SD conditions. This finding offers a molecular basis for previous observations of genetic
390 interactions between *FLM-SVP* and photoperiod flowering pathways (Scortecci et al., 2003). The
391 potential for *MAC3A* and *MAC3B* to also respond to ambient temperatures to further integrate
392 photoperiod and temperature signals through *FLM* splicing warrants additional study.
393 Beyond *MAC3A* and *MAC3B*, the *GLYCINE-RICH RNA-BINDING PROTEINs*, *GRP7* and
394 *GRP8*, have been shown to regulate *FLM* isoform splicing (Steffen et al., 2019). GRP7
395 preferentially binds to *FLMβ* over *FLMδ* at lower temperatures under SD. The *grp7/grp8* mutants
396 exhibit reduced *FLMβ* levels, a pattern mirrored in *mac3a/mac3b* mutants alongside decreased
397 *GRP7* expression, suggesting a collaborative role in modulating *FLMβ* (Figure 6). Additionally,
398 our findings highlight intron retention in *PIF4* transcripts within *mac3a/mac3b* mutants (Figure 5
399 and Supplemental Figure S2), potentially impacting *FT* expression and, by extension, flowering,
400 suggesting a broader role for *MAC3A* and *MAC3B* in mediating temperature-responsive flowering

401 pathways under SD. Future research is poised to unravel the intricate molecular and genetic
402 interactions between *MAC3A*, *MAC3B*, and other splicing factors in adjusting *FLM* isoform ratios
403 and orchestrating seasonal flowering responses.
404
405 **The *FLC* expression may be indirectly regulated by MAC3A and MAC3B**
406 In SD conditions, the *mac3a/mac3b* mutants exhibit significantly earlier flowering, a
407 phenomenon attributed, in part, to the decreased expression of the floral repressor *FLOWERING*
408 *LOCUS C* (*FLC*) within the vernalization and autonomous pathways. This reduction in *FLC*
409 expression alleviates repression on key flowering promoters *FT* and *SOC1*, facilitating early
410 flowering (Supplemental Figure S1A and Figure 1C). While the direct influence of MAC3A and
411 MAC3B on *FLC* expression appears to be limited, their role in modulating *FLC* through indirect
412 pathways is evident, particularly in the context of epigenetic regulation and post-transcriptional
413 RNA processing (Qi et al., 2019; Herr et al., 2006; Whittaker and Dean, 2017). *COOLAIR*, a long
414 non-coding antisense RNA, initially represses *FLC* during vernalization by altering the chromatin's
415 H3K36me3 and H3K27me3 modifications (Qi et al., 2019). In the autonomous pathway, RNA
416 processing factors further regulate the *FLC* expression by the 3'-end processing of its antisense
417 *COOLAIR* transcripts (Qi et al., 2019; Whittaker and Dean, 2017). Given that *MAC3A* and *MAC3B*
418 have been established to impact mRNA biosynthesis (Li et al., 2018), their potential effect on
419 *COOLAIR* processing and, consequently, on *FLC* expression in *mac3a/mac3b* mutants warrants
420 further investigation.
421 Additionally, transcriptome analysis revealed changes in *GRP7* expression, a known
422 interactor with *COOLAIR*, suggesting a possible regulatory link between *MAC3A*, *MAC3B*, *GRP7*,
423 and *FLC* expression (Figure 3C) (Xiao et al., 2015). Interestingly, the regulatory dynamics of
424 *MAC3A/MAC3B* and *GRP7* diverge; *MAC3A/MAC3B* seem to specifically influence *FLC*
425 expression under SD, contrasting with *GRP7*'s broader regulatory scope across photoperiods (Xiao
426 et al., 2015; Steffen et al., 2019). Despite *GRP7* being downregulated in *mac3a/mac3b* mutants,
427 this does not mask the *mac3a/mac3b* early flowering phenotype (Figure 1A and 3C). This suggests
428 that under SD, MAC3A and MAC3B are crucial for maintaining *FLC* expression, potentially
429 gating the autonomous flowering pathway and highlighting a nuanced role in flowering regulation.
430
431 **SPL9 may integrate multiple signals to regulate *MAC3A* and *MAC3B***

432 In this study, we identified SPL9 binding to the promoters of *MAC3A* and *MAC3B in vivo*,
433 activating their expressions specifically during the SD evening. Furthermore, overexpression of
434 miRNA156-resistant *rSPL9* resulted in increased levels of *MAC3A* and *MAC3B* expressions, while
435 mutation of *SPL9* led to a diminished peak of *MAC3B* and *MAC3B* expression at ZT12 under SD
436 conditions (Figure 9A). These findings provide partial insights into the photoperiodic-specific
437 regulation of *FLM* splicing and flowering by *MAC3A* and *MAC3B*.
438 How does SPL9 perceive photoperiodic signals? Our observations suggest that *SPL9*
439 expression is regulated by photoperiods, with higher expression levels observed during the daytime
440 under both LD and SD conditions (Figure 7D). As a pivotal component of the age-dependent
441 flowering pathway, SPL9 is known to be post-transcriptionally suppressed by *miRNA156*
442 (Schwarz et al., 2008; Wang et al., 2009). The phytochrome-PIF light-sensing module suppresses
443 *miRNA156* expression in response to shading environments, thereby mediating shade-avoidance
444 responses (Xie et al., 2017). Hence, it is plausible that PIFs are implicated in the photoperiod-
445 dependent regulation of *SPL9* expression. Furthermore, the observed peak of *SPL9* expression
446 before light-off under short days may account for the higher *MAC3A* and *MAC3B* expression levels
447 under these conditions (Figure 7A, 7B, and 7D). Since MAC3A and MAC3B are involved in
448 miRNA biosynthesis, their mutants have reduced levels of mature miRNAs, resulting in the de-
449 repression of miR156-targeted *SPLs* (Li et al., 2018). If SPL9 indeed activates *MAC3A* and
450 *MAC3B*, it suggests the existence of a potential negative feedback loop between *miR156/SPLs* and
451 *MAC3A/MAC3B*, which could explain the redundancy observed between *MAC3A* and *MAC3B*.
452 Additionally, our data suggest that *SPL9, MAC3A,* and *MAC3B* may modulate temperature-
453 responsive flowering initiation as plants age, given that *SPL9* expression gradually accumulates
454 with plant age. Moreover, the differential expression of *miR156*-targeted *SPL5* and *SPL15* in the
455 DEGs of *mac3a/mac3b* (Addo-Quaye et al., 2008) (Figure 3C) further hints at the existence of a
456 complex underlying regulatory network. Specifically, while *SPL5* is down-regulated, *SPL15* is up-
457 regulated, suggesting intricate interactions within this network.
458
459 **Potential versatile molecular functions of MAC3A and MAC3B in regulating flowering**
460 MAC3A and MAC3B are bona fide U-box-containing E3 ubiquitin ligases, supported by
461 evidence demonstrating their ability to auto-ubiquitinate themselves or other substrates (Li et al.,
462 2018; Guo et al., 2024; Yu et al., 2024). The functions of these E3 ubiquitin ligases are crucial for

463 modulating various biological processes, including miRNA biogenesis, lateral root emergence,
464 and organ size control. However, whether the E3 functions are critical for their role in SD-specific
465 flowering time regulation remains to be explored. In human cells, the homologs of MAC3A and
466 MAC3B, PRP19, have been shown to ubiquitinate spliceosome subunits, affecting their assembly
467 and activities (de Moura et al., 2018; Song et al., 2010). This suggests that the E3 ubiquitin ligase
468 functions of MAC3A and MAC3B might be vital for regulating splicing in the flowering pathways.
469 Furthermore, in addition to their role as E3 ubiquitin ligases, MAC3A and MAC3B have been
470 reported to interact with histone modifiers such as HISTONE DEACETYLASE 15 (HDA15) (Tu
471 and Chen et al., 2022). Moreover, recent findings indicate that MAC3A and MAC3B associate
472 with cryptochromes or other proteins to form biomolecular condensates in the nucleus under
473 specific conditions, suggesting a potential role in regulating gene expression through epigenetic or
474 transcriptional mechanisms beyond RNA splicing (Li et al., 2018; Jia et al., 2023).
475
476 **Materials and methods**
477 **Plant Materials and Growth Conditions**
478 All *Arabidopsis thaliana* lines utilized in this study were derived from the Columbia-0 (Col-0)
479 genetic background. The *mac3a* (SALK_089300), *mac3b* (SALK_050811), and the *mac3a/mac3b*
480 double mutants (CS69985) were as characterized by Monaghan et al. (2009). Additionally, the
481 *spl9* mutant (*spl9-4*, SAIL_150_B05) was identified in the work of Xu et al. (2016). All mutant
482 lines were obtained from the Arabidopsis Biological Resource Center (ABRC) and confirmed
483 through genotyping and PCR.
484
485 Seed vernalization was performed by soaking in sterilized water at 4°C for three days in darkness,
486 followed by sowing on the soil. For seedlings grown on plates, seeds underwent sterilization with
487 70% ethanol and 0.1% TRITON® X-100, then were plated on 1/2 strength Murashige and Skoog
488 (MS) medium (Caisson, Cat# MSP02) supplemented with 0.8% agar (Duchefa Biochemie, Cat#
489 P1003). Plates were kept at 4°C in the dark for three days before being moved to growth chambers.
490 Growth conditions for plants, whether in soil or on plates, included long-day (LD) conditions (16
491 hours of light/8 hours of dark) or short-day (SD) conditions (8 hours of light/16 hours of dark),
492 maintained at 22°C with light intensities ranging from 85 to 120 μmol m^{-2} s^{-1}.
493

494 Flowering time was quantitatively assessed using two metrics: the date of flowering, when the
495 inflorescence stem reached a length of 1 cm, and the total leaf count, recorded once the
496 inflorescence stem achieved a length of 7 cm. Each experimental replicate comprised 15-20 plants
497 per genetic line.
498
499 **Reverse Transcription Quantitative PCR (RT-qPCR)**
500 To quantify RNA expression, *Arabidopsis thaliana* seedlings grown for 10 days under LD
501 conditions and 14 days under SD conditions were harvested. The harvested seedlings were flash-
502 frozen in liquid nitrogen and ground into a fine powder using a ball grinder (Retsch, MM400).
503 Total RNA was then extracted from the tissue powder using TRIzol Reagent (Invitrogen, Cat#
504 15596-018) following the manufacturer's instructions. DNase treatment (Promega, Cat# M6101)
505 was applied to the extracted RNA samples to eliminate potential DNA contamination. Finally, the
506 RNA concentrations and 260/280 ratios were measured with NanoDrop One (ThermoFisher)
507 before frozen storage of the RNA samples.
508
509 For reverse transcription, 1000 ng of DNase-treated RNA was used in a 20 µL reaction employing
510 oligo-dT primers and random hexamers according to the protocol provided by Takara (Cat#
511 RR014B). The relative expression levels of the target genes were assessed via qPCR. For this, 4
512 µL of 10-fold diluted cDNA was combined with 5 µL of iQ SYBR Green Supermix (Bio-Rad,
513 Cat# 170-8880) and 0.5 µL of each 10 µM forward and reverse primers, bringing the total reaction
514 volume to 10 µL. These qPCR reactions were conducted using the CFX Connect Real-Time
515 System (Bio-Rad) following a three-step PCR protocol.
516
517 This study incorporated three biological replicates for each qPCR experiment. Expression levels
518 were normalized to the internal control gene *UBQ10* (AT4G05320).
519
520 **RNA-sequencing Analyses of Differentially Expressed Genes (DEG) and Differential**
521 **Alternative Spliced (DAS) Events**
522 Leaves from 40-day-old Arabidopsis thaliana Columbia-0 (Col-0) and *mac3a/mac3b* mutants
523 grown on the soil under short-day conditions were collected at Zeitgeber time 16 (ZT16). Total
524 RNA was extracted using the RNeasy Plant Mini Kit (QIAGEN, Cat# 74904), with subsequent

525 removal of genomic DNA contamination employing the RNase-Free DNase Set (Qiagen, Cat#
526 79254). RNA-sequencing (RNA-seq) libraries for triple replicates of both Col-0 and *mac3a/mac3b*
527 were prepared utilizing the Illumina TruSeq toolkit (Illumina, Cat# FC-122-1001). Paired-end
528 reads were processed with Trimmomatic (Bolger et al., 2014) to excise undesired Illumina adaptor
529 sequences and poly-G repetitions.
530
531 Differential gene expression (DEG) analysis employed the STAR algorithm (Dobin et al., 2013)
532 for alignment to the Arabidopsis TAIR10 genome using Araport11 (201606 released) annotations.
533 Counts of aligned reads were generated with HTSeq (Anders et al., 2013), followed by
534 normalization and comparative analysis with DESeq2 (Love et al., 2014). Statistical significance
535 was assessed by p-values, with a false discovery rate (FDR) threshold set to 10% for identifying
536 DEGs.
537
538 For alternative splicing event detection, reads were aligned to transcript coordinates from
539 Araport11 using Bowtie2 (Langmead and Salzberg, 2012), applying a minimum identity threshold
540 of 0.95. Unmapped reads were further processed with BLAT (Kent, 2002) against the TAIR10
541 genome, requiring an identity threshold of 0.9 and at least 8 base matches on both ends. Previously
542 established "Read Analysis & Comparison Kit in Java" pipeline (RackJ, http://rackj.sourceforge.net)
543 (Chang et al., 2022) then aggregated these mappings to identify sample-sensitive alternative
544 splicing events, including intron retention, exon skipping, and donor-acceptor changes, using Chi-
545 square tests. Events showing significant differences and fold-change among replicates were
546 selected, setting an FDR threshold of 5%.
547
548 The IR events were identified by the Chi-square test of reads with or without IR between Col-0
549 and *mac3a/mac3b* mutants, with fold change criteria of $|Log_2(\text{Fold change})| > 3$. Similarly,
550 Alternative Donor/Acceptor sites (AltDA) events were identified by the Chi-square of the number
551 of reads test with or without event-supportive exons, with fold change criteria of $|Log_2(\text{Fold}$
552 $\text{change})| > 1$. The statistic method used on AltDA events was applied to ES events with fold change
553 criteria of $|Log_2(\text{Fold change})| > 0.585$. For ES events, reads were also normalized by the
554 expression (read depth) of exons nearby as a different comparison strategy, with fold change
555 criteria of $|Log_2(\text{Fold change})| > 0.585$. ES events from both comparison methods were accepted

556 and combined as a category in this table. Out of the identified alternative splicing events, the
557 differentially alternative splicing events were selected by significance and fold-change among
558 replicates. Events showing significant differences and fold-change among replicates were selected,
559 setting an FDR threshold of 5%.
560
561 To identify key transcription factors (TFs) implicated in the *mac3a/mac3b* mutants, DEG lists
562 underwent TF enrichment analysis via FunTFBS (PlantRegMap, http://plantregmap.gao-
563 lab.org/tf_enrichment.php; Tian et al., 2019). Gene Ontology (GO) annotations for DEGs and DAS
564 genes were analyzed using the g:GOst feature on the g:Profiler website
565 (https://biit.cs.ut.ee/gprofiler/gost; Raudvere et al., 2019) for enriched GO terms. This study used
566 the calculation method published by Storey and Tibshirani (2003) to estimate the FDR. Data
567 visualization was accomplished with the ggplot2 package in R (Wickham, 2016).
568
569 **Generation of *FLAG-MAC3A*-overexpressing Transgenic Arabidopsis**
570 To construct *35S::6xHis-3xFLAG-MAC3A* (or called *FLAG-MAC3A*-overexpression lines) in the
571 *mac3a/mac3b* mutant background, the *MAC3A* coding sequence was subcloned into the *pB7-HFN*
572 plant binary vector (Huang et al., 2016). This vector was then transformed into Agrobacterium
573 tumefaciens strain *GV3101*, which was used to introduce the construct into the *mac3a/mac3b*
574 double mutant using the floral dip method (Clough and Bent, 1998). Selection of homozygous T3
575 plants was performed by screening on 1/2 MS medium supplemented with 10 µg/mL glufosinate
576 ammonium (Cyrusbiosciences, Cat# 101-77182-82-2).
577
578 **RNA-Immunoprecipitation Quantitative PCR (RIP-qPCR)**
579 RNA immunoprecipitation (RIP) was conducted on 15-day-old *mac3a/mac3b* and MAC3A-
580 FLAG-overexpression *Arabidopsis* seedlings harvested at ZT12, following a modified protocol
581 from Terzi and Simpson (2009). Seedlings were cross-linked with 1% formaldehyde under vacuum
582 infiltration for 20 minutes, with the reaction quenched using 200 mM glycine for an additional 5
583 minutes under vacuum. After four washes with ddH2O and drying, the samples were frozen in
584 liquid nitrogen and pulverized.
585

586 The pulverized tissue was incubated in 30 mL of buffer 1 (400 mM sucrose, 10 mM Tris-HCl pH
587 8.0, 10 mM $MgCl_2$, 5 mM β-mercaptoethanol, 1 mM PMSF, 1× Roche cOmplete EDTA-free
588 Protease Inhibitor Cocktail, and 50 U/mL Invitrogen™ SUPERase•In™ RNase Inhibitor) on ice
589 for 30 minutes. Following filtration through miracloth and centrifugation at 3000 g for 30 minutes
590 at 4°C, the pellet was resuspended in buffer 2 (250 mM sucrose, 10 mM Tris-HCl pH 8.0, 10 mM
591 $MgCl_2$, 5 mM β-mercaptoethanol, 1 mM PMSF, 1× cOmplete EDTA-free Protease Inhibitor
592 Cocktail, and 50 U/mL SUPERase•In™ RNase Inhibitor), then centrifuged at 12000 g for 10
593 minutes at 4°C. The subsequent pellet was suspended in buffer 3 (1.7 M sucrose, 10 mM Tris-HCl
594 pH 8.0, 2 mM $MgCl_2$, 5 mM β-mercaptoethanol, 1 mM PMSF, 1× cOmplete EDTA-free Protease
595 Inhibitor Cocktail, and 50 U/mL SUPERase•In™ RNase Inhibitor), centrifuged at 16000 g for 20
596 minutes at 4°C, and the resulting nuclei pellets were resuspended in buffer 4 (50 mM Tris-HCl pH
597 8.0, 10 mM EDTA pH8.0, 1% SDS, 1 mM PMSF, 1× cOmplete EDTA-free Protease Inhibitor
598 Cocktail, and 160 U/mL SUPERase•In™ RNase Inhibitor) for 10 minutes on ice. Nucleic acids
599 were fragmented using a Branson Digital Sonifier SFX 250, with a cycle of 15 minutes on and 1
600 minute off, repeated 20 times (totaling 5 minutes), followed by centrifugation at 15000 g for 10
601 minutes at 4°C.
602
603 The nuclear extract was then diluted with RIP dilution buffer (16.7 mM Tris-HCl pH 8.0, 1.2 mM
604 EDTA pH8.0, 167 mM NaCl, 0.5% Triton X-100, 1 mM PMSF, 1× cOmplete EDTA-free Protease
605 Inhibitor Cocktail, and 160 U/mL SUPERase•In™ RNase Inhibitor) and incubated with anti-
606 FLAG® antibody magnetic beads (Merck, Cat# M8823) overnight at 4°C with gentle rotation.
607 Beads were washed four times in RIP wash buffer (50 mM Tris-HCl pH 8.0, 10 mM EDTA pH8.0,
608 300 mM NaCl, 0.5% Triton X-100, 0.1 % SDS, 1 mM PMSF, 1× cOmplete EDTA-free Protease
609 Inhibitor Cocktail, and 40 U/mL SUPERase•In™ RNase Inhibitor) and treated with proteinase K
610 (Sigma, Cat# p2308). RNA was extracted using TRIzol reagent (Invitrogen, Cat# 15596-018), and
611 residual genomic DNA was removed with RQ1 RNase-free DNase (Promega, Cat# M6101).
612
613 **Protein Extraction and Immunoblot**
614 Protein was extracted from *Arabidopsis thaliana* seedlings, previously ground to a powder using
615 a freezer mill (Retsch, MM400) in liquid nitrogen. The extraction buffer contained 4 M Urea, 100
616 mM Tris-HCl (pH 6.8), 5% SDS, 15% Glycerol, supplemented with 0.4% protease inhibitor

617 cocktail (Roche, Cat# 04693132001), 0.5% β-mercaptoethanol (PanReac AppliChem, Cat#
618 A11080100), and 0.2% bromophenol blue dye (Sigma, Cat# 62625289). Samples were
619 subsequently boiled for 5 minutes at 105°C, followed by centrifugation at 13,000 g for 5 minutes
620 to collect the supernatant. The clarified protein extracts were either analyzed immediately or stored
621 at -80°C.
622
623 For immunoblot analysis, around 5 μg of the protein samples were subjected to 10% SDS-PAGE
624 for separation. Proteins were then transferred to PVDF membranes (Millipore, Cat# IPVH00010)
625 at 4°C. The membranes were blocked with 5% non-fat milk in TBST buffer (20 mM Tris-base,
626 150 mM NaCl, 0.1% Tween 20) for 1 hour at room temperature, followed by overnight incubation
627 at 4°C with a 1:5000 dilution of anti-FLAG antibody (Sigma, Cat# F1804) in the blocking solution.
628 After washing thrice with TBST, the membranes were incubated with an HRP-conjugated
629 secondary antibody (Promega, Cat# W4021, 1:10,000 dilution) in blocking solution, washed three
630 times in TBST, and developed using Clarity Western ECL Substrate (Bio-Rad, Cat# 1705061) for
631 imaging on a 5200 Chemiluminescent Imaging System (Tanon). This procedure was
632 independently replicated with three biological samples.
633
634 **Promoter Analysis and Identification of Transcription Factors**
635 Promoter sequences for *MAC3A* (-1487 to +266) and *MAC3B* (-1468 to +224) were retrieved from
636 the TAIR10 genome, with transcription start sites determined according to Araport11 annotations
637 (June 2016 release). These sequences were analyzed using the PlantPAN 4.0 Promoter Analysis
638 tool (http://plantpan.itps.ncku.edu.tw/plantpan4; Chow et al., 2019), opting for a comparison
639 against the PlantPAN 3.0 database. The analysis yielded predicted motifs within the promoter
640 regions and identified associated transcription factors.
641
642 To pinpoint TFs potentially governing the photoperiod-specific expression of *MAC3A* and *MAC3B*,
643 we accessed expression data for candidate TFs under long and short days at various times of the
644 day from the Photo-Graph database (https://gendron-lab.shinyapps.io/PhotoGraph/; Leung et al.,
645 2023). This expression data was juxtaposed against the relative expression patterns of *MAC3A* and
646 *MAC3B* under similar conditions, as quantified by RT-qPCR (Figures 7A and 7B). The correlation
647 between the expressions of the predictive TFs and *MAC3A/MAC3B* was assessed by Pearson's

648 correlation coefficient (r), with a significance threshold set at $p < 0.05$. Furthermore, these
649 candidate TFs were cross-referenced with known flowering-related genes. Candidates fitting all
650 criteria were selected for subsequent validation.
651
652 **Yeast One-Hybrid Assays**
653 The promoter regions of *MAC3A* (-1487 to +266) and *MAC3B* (-1487 to +266) were cloned into
654 *pLacZi-GW* reporter vectors, which incorporate a Gateway cassette between the *SmaI* and *XhoI*
655 sites of the original *pLacZi* vectors (Clontech). Concurrently, the coding sequence of the *SPL9*
656 transcription factor, obtained from the ABRC in the form of *pENTR-D-TOPO-SPL9* (Pruneda-Paz,
657 2014), was recombined into *pGADT7-GW* using the Gateway LR reaction following the protocol
658 provided by Invitrogen (Cat# 11791019).
659
660 Yeast strain *YM4271* was transformed with linearized DNA-bait vectors: *pLacZi*,
661 *pMAC3Apro::LacZi*, or *pMAC3Bpro::LacZi*, each digested with *ApaI*. Simultaneously, the *Y187*
662 yeast strain was transformed with the SPL9 TF-prey vector (*pGADT7-SPL9*) or the negative
663 control (*pGADT7-GW*). Transformants were selected on the uracil-dropout medium for bait strains
664 and leucine-dropout medium for prey strains, respectively. Diploids were generated through yeast
665 mating in the YPDA medium and selected on synthetic dropout (-Met-Leu-Ura) medium.
666
667 Single colonies representing each prey-bait combination were cultivated in a liquid medium.
668 Cultures were normalized to the same cell density (OD600= 0.3), spotted onto agar plates, and
669 allowed to grow. To assay β-galactosidase activity, a sterile filter paper was applied to the colony
670 spots for replicates of colonies. The filter paper was then subjected to three freeze-thaw cycles in
671 liquid nitrogen to lyse the yeast cells. β-Galactosidase activity was detected by immersing the filter
672 paper in X-gal solution (16.6 µl of 20 mg/mL X-gal stock, 6.7µL of β-mercaptoethanol, 1mL of
673 Z-buffer [60 mM Na_2HPO_4, 60 mM NaH_2PO_4, 10 mM KCl, 1 mM $MgSO_4$, pH 7.0]) and
674 incubating at 37°C until blue color development, indicative of TF-prey binding to DNA-baits. This
675 procedure is adapted from Fuxman Bass et al. (2016).
676
677 **Transient Expression of GFP-rSPL9 in Arabidopsis with Agrobacterium-mediated**
678 **enhanced seedling transformation (AGROBEST)**

679 To engineer a miRNA156-resistant version of *SPL9* (*rSPL9*), synonymous substitutions (744-764
680 base in the coding sequence, 5'-CGCCTTAAGCTTGTTAAGC-3') were introduced into *SPL9*'s
681 coding sequence via site-directed mutagenesis using the overlapping-PCR technique (Wang et al.,
682 2008). The modified PCR product, lacking the stop codon, was cloned into the *pENTR-D-TOPO*
683 vector (Invitrogen, Cat# K240020). For plant expression, the *rSPL9* was then transferred into
684 *pEarleyGate103* (Earley et al., 2006), yielding *pEG103-rSPL9* for GFP-tagged *rSPL9* expression.
685
686 For *rSPL9-GFP* overexpression in Arabidopsis, the AGROBEST method (Wu et al., 2014) was
687 employed. Briefly, constructs of *pEG103-rSPL9* (*rSPL9-GFP*) and *pB7-HFN-GFP* (*35S::6xHis-*
688 *3xFLAG-GFP*) were transformed into Agrobacterium strain *C58C1*. Cultures were grown in LB
689 broth with 12.5 μM Rifamycin and 50 μM Kanamycin (for *pEG103-rSPL9*) or 100 μM
690 Spectinomycin (for *pB7-HFN-GFP*) and then induced with 200 μM acetosyringone (Sigma, Cat#
691 D134406) in AB-MES buffer (17.2 mM K_2HPO_4, 8.3 mM NaH_2PO_4, 18.7 mM NH_4Cl, 2 mM KCl,
692 1.25 mM $MgSO_4$, 100 μM $CaCl_2$, 10 μM $FeSO_4$, 50 mM MES, 2% glucose (w/v), pH 5.5) to a
693 final OD600 of 0.6-1.0. Post-induction, Agrobacteria were diluted to OD600= 0.04 in fresh AB-
694 MES buffer with 200 μM acetosyringone for plant infection.
695
696 For Chromatin Immunoprecipitation (ChIP) assays, 4-day-old Arabidopsis seedlings grown under
697 SD conditions were co-cultured with an equal volume of Agrobacterium suspension and 1/2MS
698 medium in the SD white-light growth chamber. After two days, seedlings were rinsed with 1/2MS
699 with 10 μM Timentin (Gold Biotechnology, Cat# T104-2), transferred into a fresh 1/2MS medium,
700 and then left for another day to optimize the expression. Protein expression of rSPL9-GFP was
701 verified by SDS-PAGE and immunoblotting using an anti-GFP antibody (Abcam, Cat# ab290,
702 1:10,000 dilution) and HRP-conjugated secondary antibody (Promega, Cat# W4011, 1:4,000
703 dilution).
704
705 To assess the impact on *MAC3A* and *MAC3B* transcript levels, 11-day-old seedlings underwent a
706 similar process, with an additional step of vacuum infiltration to ensure effective agrobacteria
707 penetration.
708
709 **Chromatin Immunoprecipitation (ChIP)**

710 The ChIP assay was conducted with modifications to the protocol established by Gendrel et al.
711 (2005). Initially, 2 g of Arabidopsis seedlings underwent cross-linking to preserve protein-DNA
712 interactions. To improve nucleus extraction efficiency, samples were incubated on ice for 30
713 minutes in nucleus extraction buffer 1. Following extraction, chromatin was fragmented to an
714 optimal size using a Branson Ultrasonics™ Sonifier™ (SFX250) set at 12% power for 5 minutes.
715 For the immunoprecipitation (IP) step, the anti-GFP antibody (Abcam, Cat# ab290) targeted the
716 rSPL9-GFP fusion protein, and Protein G mag Sepharose (Cytiva, Cat# 28967070) was employed
717 to isolate the immunocomplexes.
718
719 After reverse cross-linking, protease K (Sigma, Cat# P2308) treatment was applied to digest
720 proteins, facilitating the recovery of DNA. DNA extraction was performed using a Phenol-
721 Chloroform-Isoamyl alcohol mixture (Sigma, Cat# 77617), and the DNA was resuspended in 200
722 µL of ddH2O. qPCR analysis was then used to assess the enrichment of the *MAC3A* and *MAC3B*
723 promoters, utilizing specific primers targeting regions with and without predicted SPL9 binding
724 motifs. As a negative control, primers amplifying the *ACTIN2* region were included.
725
726 **Statistical analysis**
727 Statistical analysis for experiments was performed using the software Graphpad Prism 10.
728 Student's t-test, one-way ANOVA (non-parametric Kruskal-Wallis test), or two-way ANOVA
729 were adopted. The P values of post-hoc tests used are individually indicated in the figures. For
730 one-way ANOVA and two-way ANOVA, P values were used to indicate significant differences
731 between multiple groups with Dunn's or Šídák's post-hoc statistical test, respectively (ns, no
732 significant difference; *, $P< 0.05$; **, $P< 0.01$; ***, $P< 0.001$). Each experiment was performed
733 with at least three biological replicates. The results are presented as mean values ± standard error
734 of the mean (SE).
735
736 **Accession numbers**
737 Sequence data from this article can be found in The Arabidopsis Information Resource under the
738 following accession numbers: *MAC3A* (AT1G04510), *MAC3B* (AT2G33340), *CO* (AT5G15840),
739 *FT* (AT1G65480), *SOC1* (AT2G45660), *FLC* (AT5G10140), *SVP* (AT2G22540), *FLM*
740 (AT1G77080), *AGL19* (AT4G22950), *SPL9* (AT2G42200), *ACT2* (AT3G18780), and *UBQ10*

741 (AT4G05320). The sequencing data generated in this study have been deposited into GEO with a
742 code: GSE 261591.
743
744 **Acknowledgments**
745 We thank Dr. Shu-Hsing Wu, Dr. Huang-Lung Tsai, Dr. Ming-Jung Liu, and Dr. Mei-Chun Cheng
746 for valuable discussion. We also thank Shu-Jen Chou in the Genomic Technology Core Laboratory
747 and Wen-Dar Lin at the Bioinformatics Core Laboratory of the Institute of Plant and Microbial
748 Biology, Academia Sinica, for technical assistance.
749
750 **Author Contributions**
751 The study was conceptualized, and the manuscript was written by C.M.L., C.Y.T., and Y.W.H..
752 Y.W.H., C.Y.T., and Y.T.T. designed and executed the experiments. S.L.T., H.Y.H., and C.Y.T.
753 analyzed the RNA-sequencing data. Y.S.W., Y.Z.C., and Y.T.L. prepared the materials and
754 conducted the experiments.
755
756 **Funding**
757 C.M.L.: NSTC-110-2311-B-002-025-, NSTC-111-2311-B-002-025-, NSTC-112-2311-B-002-
758 025-, NTU-CC-110L893604, NTU-CC-111L893004, and NTU-CC-112L891804
759 S.L.T.: NSTC-111-2311-B-001-004-, NSTC-112-2311-B-001-004-
760 C.Y.T.: NSTC-112-2813-C-002-208-B, PhD fellowship from NSTC and NTU
761 Y.T.T.: NTU-CC-111L4000, NTU-CC-112L4000, NTU-CC-113L4000
762 Y.S.W.: MOE Industry-Academia Cooperative PhD fellowship
763
764 **Conflict of Interest**
765 The authors declare that the research was conducted in the absence of any commercial or
766 financial relationships that could be construed as a potential conflict of interest.
767
768 **References**
769 **Addo-Quaye C, Eshoo TW, Bartel DP, Axtell MJ. (2008)** Endogenous siRNA and miRNA
770 targets identified by sequencing of the Arabidopsis degradome. Curr Biol. **18(10):**758-762.

771 **Anders S, Pyl PT, Huber W.** (2015) HTSeq--a Python framework to work with high-throughput
772 sequencing data. Bioinformatics. **31(2):**166-9.
773 **Bao S, Hua C, Huang G, Cheng P, Gong X, Shen L, Yu H.** (2019) Molecular Basis of Natural
774 Variation in Photoperiodic Flowering Responses. Dev. Cell **50(1):**90-101.
775 **Bolger AM, Lohse M, Usadel B.** (2014) Trimmomatic: a flexible trimmer for Illumina sequence
776 data. Bioinformatics. **30(15):**2114-20.
777 **Bouché F, Lobet G, Tocquin P, Périlleux C.** (2016) FLOR-ID: an interactive database of
778 flowering-time gene networks in Arabidopsis thaliana. Nucleic Acids Res. **44(D1):**D1167-
779 71.
780 **Castillejo C, Pelaz S.** (2008) The balance between CONSTANS and TEMPRANILLO activities
781 determines FT expression to trigger flowering. Curr. Biol. **18(17):**1338-43.
782 **Cao S, Kumimoto RW, Gnesutta N, Calogero AM, Mantovani R, Holt BF.** (2014) A distal
783 CCAAT/NUCLEAR FACTOR Y complex promotes chromatin looping at the
784 FLOWERING LOCUS T promoter and regulates the timing of flowering in Arabidopsis.
785 Plant Cell. **26(3):**1009-17.
786 **Chang P, Hsieh HY, Tu SL.** (2002) The U1 snRNP component RBP45d regulates temperature-
787 responsive flowering in Arabidopsis. Plant Cell. **34(2):**834-851.
788 **Chen X.** (2004) A microRNA as a translational repressor of APETALA2 in Arabidopsis flower
789 development. Science. **303(5666):**2022-25.
790 **Chèneby J, Ménétrier Z, Mestdagh M, Rosnet T, Douida A, Rhalloussi W, Bergon A, Lopez**
791 **F, Ballester B.** (2020) ReMap 2020: a database of regulatory regions from an integrative
792 analysis of Human and Arabidopsis DNA-binding sequencing experiments. Nucleic Acids
793 Res. **48(D1):**D180-8.
794 **Cho LH, Yoon J, An G.** (2017) The control of flowering time by environmental factors. Plant J.
795 **90(4):**708-719.
796 **Chow CN, Lee TY, Hung YC, Li GZ, Tseng KC, Liu YH, Kuo PL, Zheng HQ, Chang WC.**
797 (2019) PlantPAN3.0: a new and updated resource for reconstructing transcriptional regulatory
798 networks from ChIP-seq experiments in plants. Nucleic Acids Res. **47(D1):**D1155-63.
799 **Clough SJ, Bent AF.** (1998) Floral dip: a simplified method for Agrobacterium-mediated
800 transformation of Arabidopsis thaliana. Plant J. **16(6):**735-43.

801 **Corbesier L, Vincent C, Jang S, Fornara F, Fan Q, Searle I, Giakountis A, Farrona S, Gissot**
802 **L, Turnbull C, Coupland G.** (2007) FT protein movement contributes to long-distance
803 signaling in floral induction of Arabidopsis. Science. **316(5827):**1030-33.
804 **de Lucas M, Davière JM, Rodríguez-Falcón M, Pontin M, Iglesias-Pedraz JM, Lorrain S,**
805 **Fankhauser C, Blázquez MA, Titarenko E, Prat S.** (2008) A molecular framework for
806 light and gibberellin control of cell elongation. Nature. **451(7177):**480-4.
807 **de Moura TR, Mozaffari-Jovin S, Szabó CZK, Schmitzová J, Dybkov O, Cretu C, Kachala**
808 **M, Svergun D, Urlaub H, Lührmann R, Pena V.** (2018) Prp19/Pso4 Is an Autoinhibited
809 Ubiquitin Ligase Activated by Stepwise Assembly of Three Splicing Factors. Mol Cell.
810 **69(6):**979-92.
811 **Dobin A, Davis CA, Schlesinger F, Drenkow J, Zaleski C, Jha S, Batut P, Chaisson M,**
812 **Gingeras TR.** (2013) STAR: ultrafast universal RNA-seq aligner. Bioinformatics. **29(1):**15-
813 21.
814 **Earley KW, Haag JR, Pontes O, Opper K, Juehne T, Song K, Pikaard CS.** (2006) Gateway-
815 compatible vectors for plant functional genomics and proteomics. Plant J. **45(4):**616-29.
816 **Eriksson S, Böhlenius H, Moritz T, Nilsson O.** (2006) GA4 is the active gibberellin in the
817 regulation of LEAFY transcription and Arabidopsis floral initiation. Plant Cell. **18(9):**2172-
818 2181
819 **Ezer D, Jung JH, Lan H, Biswas S, Gregoire L, Box MS, Charoensawan V, Cortijo S, Lai X,**
820 **Stöckle D, Zubieta C, Jaeger KE, Wigge PA.** (2017) The evening complex coordinates
821 environmental and endogenous signals in Arabidopsis. Nat. Plants. **3:**17087.
822 **Feke A, Liu W, Hong J, Li MW, Lee CM, Zhou EK, Gendron JM.** (2019) Decoys provide a
823 scalable platform for the identification of plant E3 ubiquitin ligases that regulate circadian
824 function. Elife. **8:**e44558.
825 **Feke AM, Hong J, Liu W, Gendron JM.** (2020) A Decoy Library Uncovers U-Box E3 Ubiquitin
826 Ligases That Regulate Flowering Time in Arabidopsis. Genetics. **215(3):**699-712.
827 **Fernández V, Takahashi Y, Le Gourrierec J, Coupland G.** (2016) Photoperiodic and
828 thermosensory pathways interact through CONSTANS to promote flowering at high
829 temperature under short days. Plant J. **86(5):**426-40.

830 **Fornara F, de Montaigu A, Sánchez-Villarreal A, Takahashi Y, Ver Loren van Themaat E,**
831 **Huettel B, Davis SJ, Coupland G.** (2015) The GI-CDF module of Arabidopsis affects
832 freezing tolerance and growth as well as flowering. Plant J. **81(5):**695-706.
833 **Fowler S, Lee K, Onouchi H, Samach A, Richardson K, Morris B, Coupland G, Putterill J.**
834 (1999) GIGANTEA: a circadian clock-controlled gene that regulates photoperiodic flowering
835 in Arabidopsis and encodes a protein with several possible membrane-spanning domains.
836 EMBO J. **18(17):**4679-88.
837 **Fuxman Bass JI, Reece-Hoyes JS, Walhout AJ.** (2016) Colony Lift Colorimetric Assay for β-
838 Galactosidase Activity. Cold Spring Harb Protoc. **2016(12):**pdb.prot088963.
839 **Galvão VC, Collani S, Horrer D, Schmid M.** (2015) Gibberellic acid signaling is required for
840 ambient temperature-mediated induction of flowering in Arabidopsis thaliana. Plant J.
841 **84(5):**949-62.
842 **Gendrel AV, Lippman Z, Martienssen R, Colot V.** (2005) Profiling histone modification
843 patterns in plants using genomic tiling microarrays. Nat Methods. **2(3):**213-8.
844 **Gendron JM, Leung CC, Liu W.** (2021) Energy as a seasonal signal for growth and reproduction.
845 Curr Opin Plant Biol. **63:**102092.
846 **Gil KE, Park MJ, Lee HJ, Park YJ, Han SH, Kwon YJ, Seo PJ, Jung JH, Park CM.** (2017)
847 Alternative splicing provides a proactive mechanism for the diurnal CONSTANS dynamics
848 in Arabidopsis photoperiodic flowering. Plant J. **89:**128-40.
849 **Gu X, Le C, Wang Y, Li Z, Jiang D, Wang Y, He Y.** (2013) Arabidopsis FLC clade members
850 form flowering-repressor complexes coordinating responses to endogenous and
851 environmental cues. Nat Commun. **4:**1947.
852 **Guo X, Zhang X, Jiang S, Qiao X, Meng B, Wang X, Wang Y, Yang K, Zhang Y, Li N, Chen**
853 **T, Kang Y, Yao M, Zhang X, Wang X, Zhang E, Li J, Yan D, Hu Z, Botella JR, Song**
854 **CP, Li Y, Guo S.** (2024) E3 ligases MAC3A and MAC3B ubiquitinate UBIQUITIN-
855 SPECIFIC PROTEASE14 to regulate organ size in Arabidopsis. Plant Physiol. **194(2):**684-
856 97.
857 **Huang CK, Lin WD, Wu SH.** (2022) An improved repertoire of splicing variants and their
858 potential roles in Arabidopsis photomorphogenic development. Genome Biol. **23(1):**50.
859 **Huang H, Alvarez S, Bindbeutel R, Shen Z, Naldrett MJ, Evans BS, Briggs SP, Hicks LM,**
860 **Kay SA, Nusinow DA.** (2016) Identification of Evening Complex Associated Proteins in

861 Arabidopsis by Affinity Purification and Mass Spectrometry. Mol Cell Proteomics.
862 **15(1):**201-17.
863 **Huijser P, Schmid M.** (2011) The control of developmental phase transitions in plants.
864 Development. **138(19):**4117-29.
865 **Imaizumi T, Schultz TF, Harmon FG, Ho LA, Kay SA.** (2005) FKF1 F-box protein mediates
866 cyclic degradation of a repressor of CONSTANS in Arabidopsis. Science. **309(5732):**293-7.
867 **Jin S, Ahn JH.** (2021) Regulation of flowering time by ambient temperature: repressing the
868 repressors and activating the activators. New Phytol. **230(3):**938-42.
869 **Jia M, Chen X, Shi X, Fang Y, Gu Y.** (2023) Nuclear transport receptor KA120 regulates
870 molecular condensation of MAC3 to coordinate plant immune activation. Cell Host Microbe.
871 **31(10):**1685-1699.e7.
872 **Jia T, Zhang B, You C, Zhang Y, Zeng L, Li S, Johnson KCM, Yu B, Li X, Chen X.** (2017)
873 The Arabidopsis MOS4-Associated Complex Promotes MicroRNA Biogenesis and Precursor
874 Messenger RNA Splicing. Plant Cell. **29(10):**2626-43.
875 **Jiang B, Zhong Z, Su J, Zhu T, Yueh T, Bragasin J, Bu V, Zhou C, Lin C, Wang X.** (2023)
876 Co-condensation with photoexcited cryptochromes facilitates MAC3A to positively control
877 hypocotyl growth in Arabidopsis. Sci Adv. **9(32):**eadh4048.
878 **Jaeger KE, Wigge PA.** (2007) FT protein acts as a long-range signal in Arabidopsis. Curr Biol.
879 **17(12):**1050-4.
880 **Kang MJ, Jin HS, Noh YS, Noh B.** (2015) Repression of flowering under a noninductive
881 photoperiod by the HDA9-AGL19-FT module in Arabidopsis. New Phytol. **206(1):**281-94.
882 **Kent WJ.** (2002) BLAT--the BLAST-like alignment tool. Genome Res. **12(4):**656-64.
883 **Kumar SV, Lucyshyn D, Jaeger KE, Alós E, Alvey E, Harberd NP, Wigge PA.** (2012)
884 Transcription factor PIF4 controls the thermosensory activation of flowering. Nature.
885 **484(7393):**242-5.
886 **Kumimoto RW, Adam L, Hymus GJ, Repetti PP, Reuber TL, Marion CM, Hempel FD,**
887 **Ratcliffe OJ.** (2008) The Nuclear Factor Y subunits NF-YB2 and NF-YB3 play additive roles
888 in the promotion of flowering by inductive long-day photoperiods in Arabidopsis. Planta.
889 **228(5):**709-23.

890 **Kumimoto RW, Zhang Y, Siefers N, Holt BF 3rd.** (2010) NF-YC3, NF-YC4 and NF-YC9 are
891 required for CONSTANS-mediated, photoperiod-dependent flowering in Arabidopsis
892 thaliana. Plant J. **63(3):**379-91.
893 **Kyung J, Jeon M, Lee I.** (2022) Recent advances in the chromatin-based mechanism of
894 FLOWERING LOCUS C repression through autonomous pathway genes. Front Plant Sci.
895 **13:**964931.
896 **Langmead B, Salzberg SL.** (2012) Fast gapped-read alignment with Bowtie 2. Nat Methods.
897 **9(4):**357-9.
898 **Lee J, Lee I.** (2010) Regulation and function of SOC1, a flowering pathway integrator. J Exp Bot.
899 **61(9):**2247-54.
900 **Lee JH, Ryu HS, Chung KS, Posé D, Kim S, Schmid M, Ahn JH.** (2013) Regulation of
901 temperature-responsive flowering by MADS-box transcription factor repressors. Science.
902 **342(6158):**628-32.
903 **Leung CC, Tarté DA, Oliver LS, Wang Q, Gendron JM.** (2023) Systematic characterization of
904 photoperiodic gene expression patterns reveals diverse seasonal transcriptional systems in
905 Arabidopsis. PLoS Biol. **21(9):**e3002283.
906 **Li C, Gu M, Shi N, Zhang H, Yang X, Osman T, Liu Y, Wang H, Vatish M, Jackson S, Hong**
907 **Y.** (2011) Mobile FT mRNA contributes to the systemic florigen signalling in floral induction.
908 Sci Rep. **1:**73.
909 **Li D, Liu C, Shen L, Wu Y, Chen H, Robertson M, Helliwell CA, Ito T, Meyerowitz E, Yu**
910 **H.** (2008) A repressor complex governs the integration of flowering signals in Arabidopsis.
911 Dev Cell. **15(1):**110-20.
912 **Li M, An F, Li W, Ma M, Feng Y, Zhang X, Guo H.** (2016) DELLA proteins interact with FLC
913 to repress flowering transition. J Integr Plant Biol. **58(7):**642-55.
914 **Li S, Liu K, Zhou B, Li M, Zhang S, Zeng L, Zhang C, Yu B.** (2018) MAC3A and MAC3B,
915 Two Core Subunits of the MOS4-Associated Complex, Positively Influence miRNA
916 Biogenesis. Plant Cell. **30:**481-94.
917 **Li Y, Yang J, Shang X, Lv W, Xia C, Wang C, Feng J, Cao Y, He H, Li L, Ma L.** (2019) SKIP
918 regulates environmental fitness and floral transition by forming two distinct complexes in
919 Arabidopsis. New Phytol. **224(1):**321-35**.**

920 **Love MI, Huber W, Anders S.** (2014) Moderated estimation of fold change and dispersion for
921 RNA-seq data with DESeq2. Genome Biol. **15(12):**550.
922 **Mathieu J, Yant LJ, Mürdter F, Küttner F, Schmid M.** (2009) Repression of flowering by the
923 miR172 target SMZ. PLoS Biol. **7(7):**e1000148.
924 **Moon J, Lee H, Kim M, Lee I.** (2005) Analysis of flowering pathway integrators in Arabidopsis.
925 Plant Cell Physiol. **46(2):**292-9.
926 **Monaghan J, Xu F, Gao M, Zhao Q, Palma K, Long C, Chen S, Zhang Y, Li X.** (2009) Two
927 Prp19-like U-box proteins in the MOS4-associated complex play redundant roles in plant
928 innate immunity. PLoS Pathog. **5:**e1000526.
929 **Nieto C, López-Salmerón V, Davière, JM, Prat S.** (2015) ELF3-PIF4 interaction regulates plant
930 growth independently of the evening complex. Curr. Biol. **25:**187-93.
931 **Osnato M, Castillejo C, Matías-Hernández L, Pelaz S.** (2012) TEMPRANILLO Genes Link
932 Photoperiod and Gibberellin Pathways to Control Flowering in Arabidopsis. Nat. Commun
933 **3(1):** 808.
934 **Park J, Oh D-H, Dassanayake M, Nguyen KT, Ogas J, Choi G, Sun T-p** (2017) Gibberellin
935 signaling requires chromatin remodeler PICKLE to promote vegetative growth and phase
936 transitions. Plant Physiol **173(2):**1463-74.
937 **Park HY, Lee HT, Lee JH, Kim JK.** (2019) Arabidopsis U2AF65 Regulates Flowering Time
938 and the Growth of Pollen Tubes. Front Plant Sci. **10:**569.
939 **Park YJ, Lee JH, Kim JY, Park CM.** (2019) Alternative RNA Splicing Expands the
940 Developmental Plasticity of Flowering Transition. Front Plant Sci. **10:**606.
941 **Posé D, Verhage L, Ott F, Yant L, Mathieu J, Angenent GC, Immink RG, Schmid M.** (2013)
942 Temperature-dependent regulation of flowering by antagonistic FLM variants. Nature.
943 **503:**414-7.
944 **Pruneda-Paz JL, Breton G, Nagel DH, Kang SE, Bonaldi K, Doherty CJ, Ravelo S, Galli M,**
945 **Ecker JR, Kay SA.** (2014) A genome-scale resource for the functional characterization of
946 Arabidopsis transcription factors. Cell Rep. **8(2):**622-32.
947 **Raudvere U, Kolberg L, Kuzmin I, Arak T, Adler P, Peterson H, Vilo J.** (2019) g:Profiler: a
948 web server for functional enrichment analysis and conversions of gene lists (2019 update).
949 Nucleic Acids Res. **47(W1):**W191-8.

950 **Qi HD, Lin Y, Ren QP, Wang YY, Xiong F, Wang XL.** (2019) RNA Splicing of FLC Modulates
951 the Transition to Flowering. Front Plant Sci. **10:**1625.
952 **Sawa M, Nusinow DA, Kay SA, Imaizumi T.** (2007) FKF1 and GIGANTEA complex formation
953 is required for day-length measurement in Arabidopsis. Science. **318(5848):**261-5.
954 **Schwarz S, Grande AV, Bujdoso N, Saedler H, Huijser P.** (2008) The microRNA regulated
955 SBP-box genes SPL9 and SPL15 control shoot maturation in Arabidopsis. Plant Mol Biol.
956 **67(1-2):**183-95.
957 **Scortecci KC, Michaels SD, Amasino RM.** (2001) Identification of a MADS-box gene,
958 FLOWERING LOCUS M, that represses flowering. Plant J. **26(2):**229-36.
959 **Shang X, Cao Y, Ma L.** (2017) Alternative Splicing in Plant Genes: A Means of Regulating the
960 Environmental Fitness of Plants. Int J Mol Sci. **18(2):**432.
961 **Silva CS, Nayak A, Lai X, Hutin S, Hugouvieux V, Jung JH, López-Vidriero I, Franco-**
962 **Zorrilla JM, Panigrahi KCS, Nanao MH, Wigge PA, Zubieta C.** (2020) Molecular
963 mechanisms of evening complex activity in Arabidopsis. Proc. Natl. Acad. Sci. USA.
964 **117(12):**6901-9.
965 **Song EJ, Werner SL, Neubauer J, Stegmeier F, Aspden J, Rio D, Harper JW, Elledge SJ,**
966 **Kirschner MW, Rape M.** (2010) The Prp19 complex and the Usp4Sart3 deubiquitinating
967 enzyme control reversible ubiquitination at the spliceosome. Genes Dev. **24:**1434-47.
968 **Song YH, Shim JS, Kinmonth-Schultz HA, Imaizumi T.** (2015) Photoperiodic flowering, time
969 measurement mechanisms in leaves. Annu Rev Plant Biol. **66:**441-64.
970 **Steffen A, Elgner M, Staiger D.** (2019) Regulation of Flowering Time by the RNA-Binding
971 Proteins AtGRP7 and AtGRP8. Plant Cell Physiol. **60(9):**2040-2050.
972 **Storey JD, Tibshirani R.** (2003) Statistical significance for genomewide studies. Proc Natl Acad
973 Sci U S A. **100(16):**9440-5.
974 **Takagi H, Hempton AK, Imaizumi T.** (2023) Photoperiodic flowering in Arabidopsis:
975 Multilayered regulatory mechanisms of CONSTANS and the florigen FLOWERING LOCUS
976 T. Plant Commun. **4(3):**100552.
977 **Teotia S, Tang G.** (2015) To bloom or not to bloom: role of microRNAs in plant flowering. Mol
978 Plant. **8**:359-77.
979 **Terzi LC, Simpson GG.** (2009) Arabidopsis RNA immunoprecipitation. Plant J. **59(1):**163-8.

980 **Tian F, Yang DC, Meng YQ, Jin J, Gao G.** (2020) PlantRegMap: charting functional regulatory
981 maps in plants. Nucleic Acids Res. **48(D1):**D1104-13.
982 **Tu YT, Chen CY, Huang YS, Chang CH, Yen MR, Hsieh JA, Chen PY, Wu K.** (2022)
983 HISTONE DEACETYLASE 15 and MOS4-associated complex subunits 3A/3B coregulate
984 intron retention of ABA-responsive genes. Plant Physiol. **190(1):**882-97.
985 **Wang BB, Brendel V.** (2006) Molecular characterization and phylogeny of U2AF35 homologs
986 in plants. Plant Physiol. **140(2):**624-36.
987 **Wang C, Tian Q, Hou Z, Mucha M, Aukerman M, Olsen OA.** (2007) The Arabidopsis thaliana
988 AT PRP39-1 gene, encoding a tetratricopeptide repeat protein with similarity to the yeast pre-
989 mRNA processing protein PRP39, affects flowering time. Plant Cell Rep. **26(8):**1357-66.
990 **Wang H, Wang H.** (2015) The miR156/SPL Module, a Regulatory Hub and Versatile Toolbox,
991 Gears up Crops for Enhanced Agronomic Traits. Mol Plant. **8(5):**677-88.
992 **Wang JW, Czech B, Weigel D.** (2009) miR156-regulated SPL transcription factors define an
993 endogenous flowering pathway in Arabidopsis thaliana. Cell. **138(4):**738-49.
994 **Wang JW, Schwab R, Czech B, Mica E, Weigel D.** (2008) Dual effects of miR156-targeted SPL
995 genes and CYP78A5/KLUH on plastochron length and organ size in Arabidopsis thaliana.
996 Plant Cell. **20(5):**1231-43.
997 **Whittaker C, Dean C.** (2017) The FLC Locus: A Platform for Discoveries in Epigenetics and
998 Adaptation. Annu Rev Cell Dev Biol. **33:**555-575.
999 **Wickham H.** (2016) ggplot2: Elegant Graphics for Data Analysis. Springer-Verlag New York.
1000 ISBN 978-3-319-24277-4.
1001 **Wu HY, Liu KH, Wang YC, Wu JF, Chiu WL, Chen CY, Wu SH, Sheen J, Lai EM.** (2014)
1002 AGROBEST: an efficient Agrobacterium-mediated transient expression method for versatile
1003 gene function analyses in Arabidopsis seedlings. Plant Methods. **10**:19.
1004 **Xiao J, Li C, Xu S, Xing L, Xu Y, Chong K.** (2015) JACALIN-LECTIN LIKE1 Regulates the
1005 Nuclear Accumulation of GLYCINE-RICH RNA-BINDING PROTEIN7, Influencing the
1006 RNA Processing of FLOWERING LOCUS C Antisense Transcripts and Flowering Time in
1007 Arabidopsis. Plant Physiol. **169(3):**2102-17.
1008 **Xie Y, Liu Y, Wang H, Ma X, Wang B, Wu G, Wang H.** (2017) Phytochrome-interacting factors
1009 directly suppress MIR156 expression to enhance shade-avoidance syndrome in Arabidopsis.
1010 Nat Commun. **8(1):**348.

1011 **Xu M, Hu T, Zhao J, Park MY, Earley KW, Wu G, Yang L, Poethig RS.** (2016)
1012 Developmental Functions of miR156-Regulated SQUAMOSA PROMOTER BINDING
1013 PROTEIN-LIKE (SPL) Genes in Arabidopsis thaliana. PLoS Genet. **12(8):**e1006263.
1014 **Yu S, Galvão VC, Zhang YC, Horrer D, Zhang TQ, Hao YH, Feng YQ, Wang S, Schmid M,**
1015 **Wang JW.** (2012) Gibberellin regulates the Arabidopsis floral transition through miR156-
1016 targeted SQUAMOSA promoter binding-like transcription factors. Plant Cell **24:**3320-32.
1017 **Yu Z, Qu X, Lv B, Li X, Sui J, Yu Q, Ding Z.** (2024) MAC3A and MAC3B mediate **degradation**
1018 of the transcription factor ERF13 and thus promote lateral root emergence. Plant Cell.
1019 koae047.

Table1. The differentially alternative spliced (DAS) events in the *mac3a/mac3b* mutant compared to Col-0 under SD

The number of DAS events, including intron retention (IR), exon skipping (ES), alternative donor/acceptor splicing site (AltDA), and their corresponding gene number was listed. The IR, AltDA, or ES events were identified by the Chi-square test of reads with or without IR AltDA or ES in between Col-0 and *mac3a/mac3b* mutants, respectively. Out of the identified alternative splicing events, the differentially alternative splicing events were selected by significance and fold-change among replicates. The false discovery rate (FDR) of accepted p-values is limited to 5%.

	***mac3a/mac3b* v.s. WT**			
	Events	**%**	**Genes**	**%**
total	**12031**	**100.00**	**6836**	**100.00**
IR	**11876**	**98.71**	**6778**	**99.15**
ES	**150**	**1.24**	**146**	**2.14**
AltDA	**5**	**0.04**	**4**	**0.06**

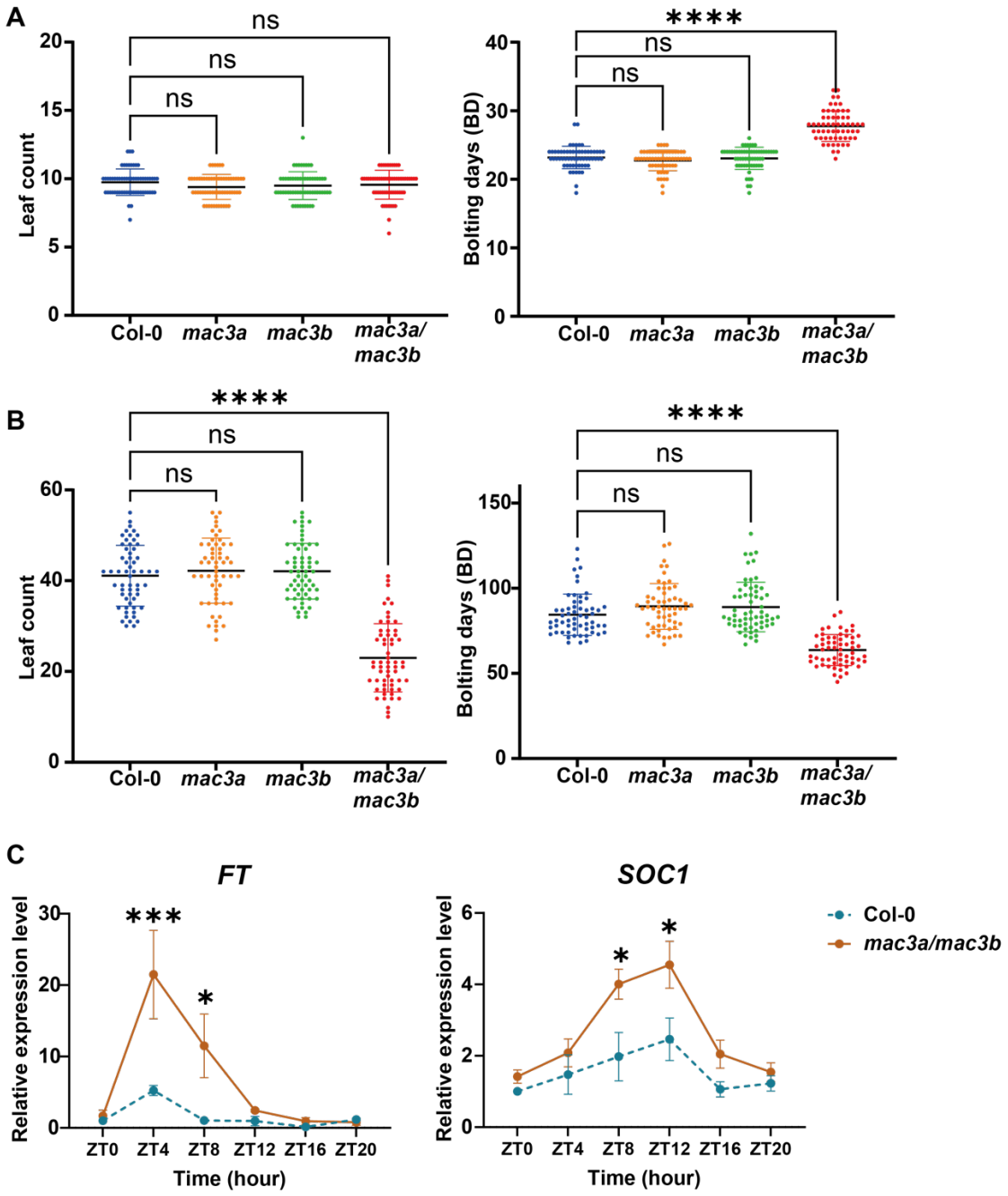

Figure 1. The flowering phenotypes of Col-0, *mac3a*, *mac3b*, and *mac3a/mac3b* mutants in long-day (LD) and short-day (SD)

The flowering time of Col-0, *mac3a*, *mac3b*, and *mac3a/mac3b* mutants grown under **(A)** LD (16h light/8h dark) or **(B)** SD (8h light/16h dark) was measured by rosette leaf number (left panel) when inflorescence reached 7 cm and bolting day (right panel) when inflorescence reached 1 cm. Data were collected from three biological replicates (n≥ 56) and analyzed using ANOVA and Kruskal-Wallis test: ****, p< 0.0001; ns, not significant. **(C)** The transcript levels of *FT* (left panel) and *SOC1* (right panel) of Col-0 and *mac3a/mac3b* seedlings in SD. The samples were harvested every 4 hours after light on (Zeitgeber time 0, ZT0), and the expression levels were measured by RT-qPCR. The relative expression levels were normalized with *UBQ10* and compared to the Col-0 at ZT0. The error bars indicated standard deviations from three biological replicates. Data were analyzed using ANOVA and the Kruskal-Wallis test: ***, p< 0.001; *, p< 0.05.

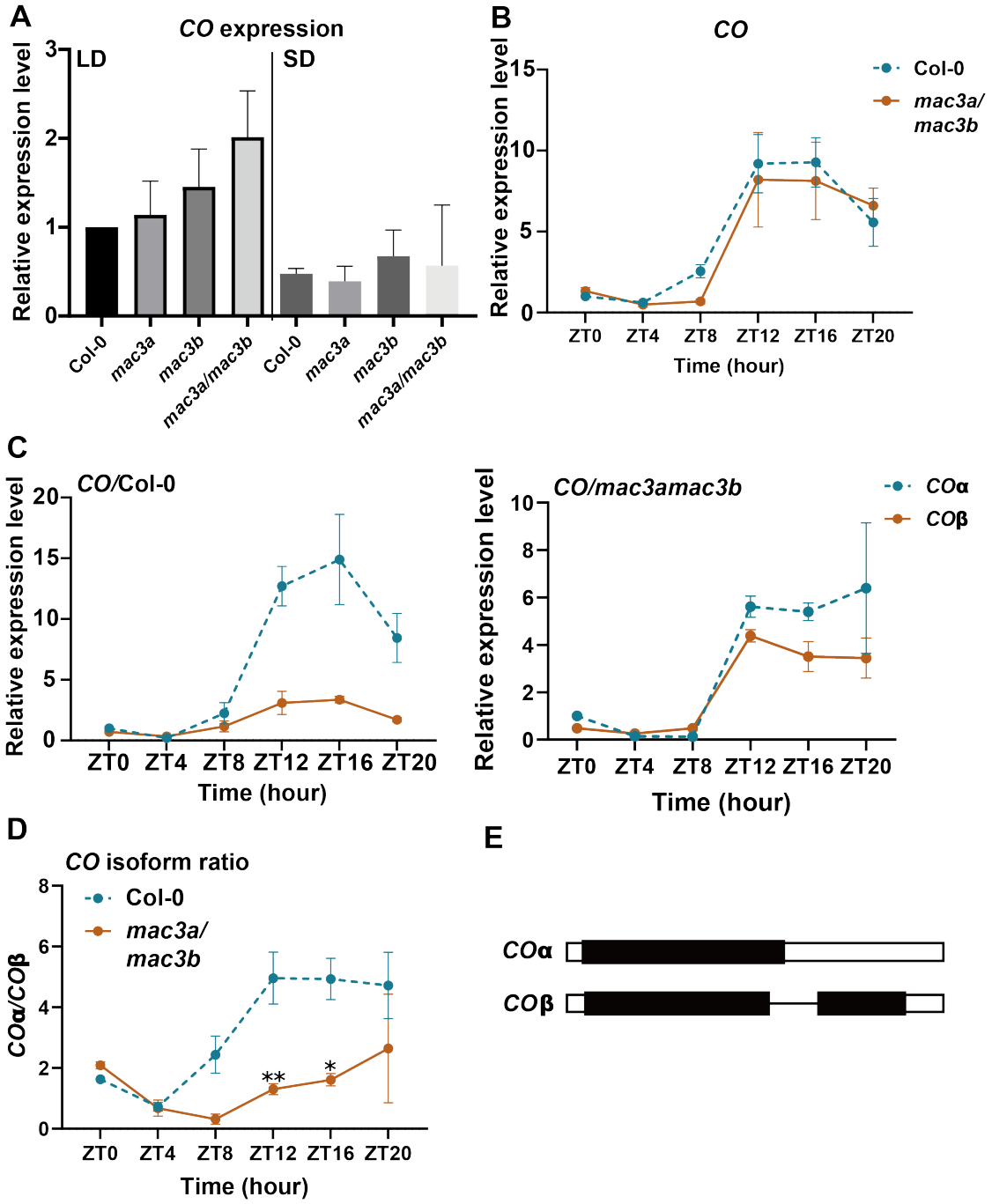

Figure 2. The expression of *CO* and its isoforms measured by RT-qPCR

(A) The relative transcript levels of *CO* in Col-0, *mac3a*, *mac3b*, and *mac3a/mac3b* mutants harvested at ZT16 under LD (16h light/8h dark) and ZT8 under SD (8h light/16h dark). The samples were harvested every 4 hours since dawn (ZT0). All time points were normalized with *UBQ10* expression and compared to the Col-0 sample at ZT0. **(B)** The diurnal expression profile of *CO* in Col-0 and *mac3a/mac3b* mutants under SD. **(C)** The relative expression of *COα* and *COβ* in Col-0 (left panel) and *mac3a/mac3b* (right panel) in SD. **(D)** The ratios of *COα* over *COβ* in Col-0 and *mac3a/mac3b* mutants in SD. **(E)** The diagram of transcript structure and the resulting protein isoforms of *COα* and *COβ*. The black rectangles are exons, and the lines connecting them are introns. The black bars are protein-coding regions. The error bars indicated standard deviations from three biological replicates. Data were analyzed using ANOVA and the Kruskal-Wallis test: **, $p < 0.01$; *, $p < 0.05$.

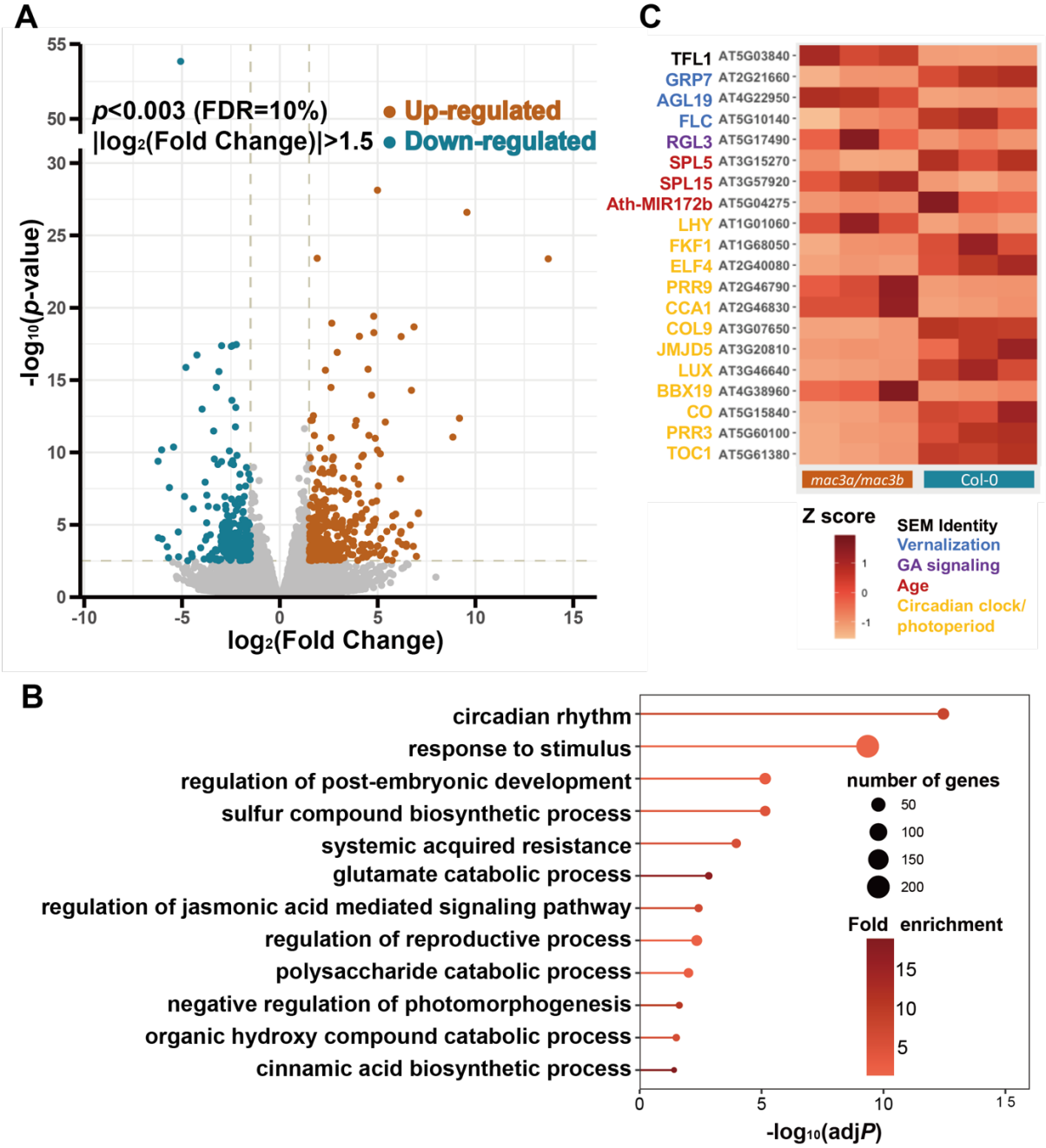

Figure 3. The differentially expressed genes (DEG) of SD-grown *mac3a/mac3b* mutant and their Gene ontology (GO) analysis

(A) The volcano plot of differentially expressed genes (DEG) in *mac3a/mac3b* mutants under SD compared to that in Col-0. The fold changes were calculated by comparing the means of normalized reads in three biological replicates of *mac3a/mac3b* and Col-0, and the p-values were calculated by T-Test of normalized reads. The up-regulated genes were marked in brown-orange, and the down-regulated genes were marked in blue with the criteria of $|\log_2(\text{fold change})| > 1.67$ and 10% FDR of accepted P values. **(B)** The top-ranked gene ontology (GO) of the biological processes category for the DEG. Selected GO terms were plotted on the lollipop plot, with gene numbers for each GO term in the DEG list represented by the dot size, and the darkness of the lollipops indicated the fold enrichment. **(C)** Heat map of DEG genes involved in flowering regulation. The color represents the Z-score, calculated by the normalized gene expression reads between samples. The genes belonging to specific flowering pathways were color-coded. FDR: false discovery rate.

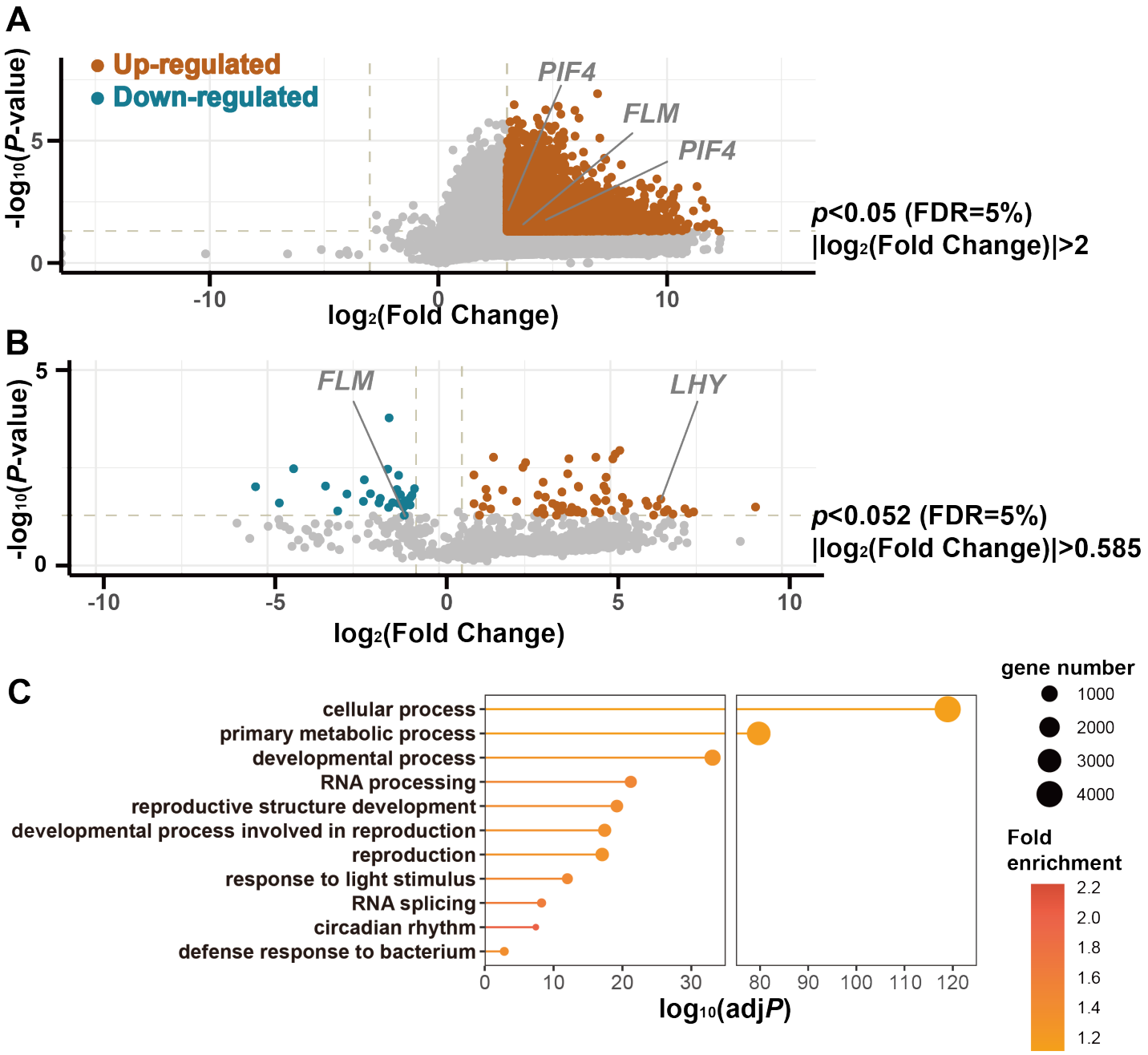

Figure 4. The differentially alternative spliced (DAS) events of SD-grown *mac3a/mac3b* mutant and their Gene ontology (GO) analysis

(A) The volcano plot of differentially intron retention (DIR) events between Col-0 and *mac3a/mac3b* identified by supporting reads ratio (|$\log_2$(fold change)|> 3, FDR< 0.05). **(B)** The volcano plot of differentially exon skipping (DES) events between Col-0 and *mac3a/mac3b* identified by supporting reads ratio (|$\log_2$(fold change)|> 0.585, FDR < 0.05). Genes related to flowering regulation, such as *PIF4*, *FLM*, and *LHY*, were labeled. **(C)** The top-ranked gene ontology (GO) of biological processes for all differential alternative spliced events. Selected GO terms were plotted on the lollipop plot, with gene numbers exhibiting in the dot size and the darkness of the lollipops for the fold enrichment. FDR: false discovery rate.

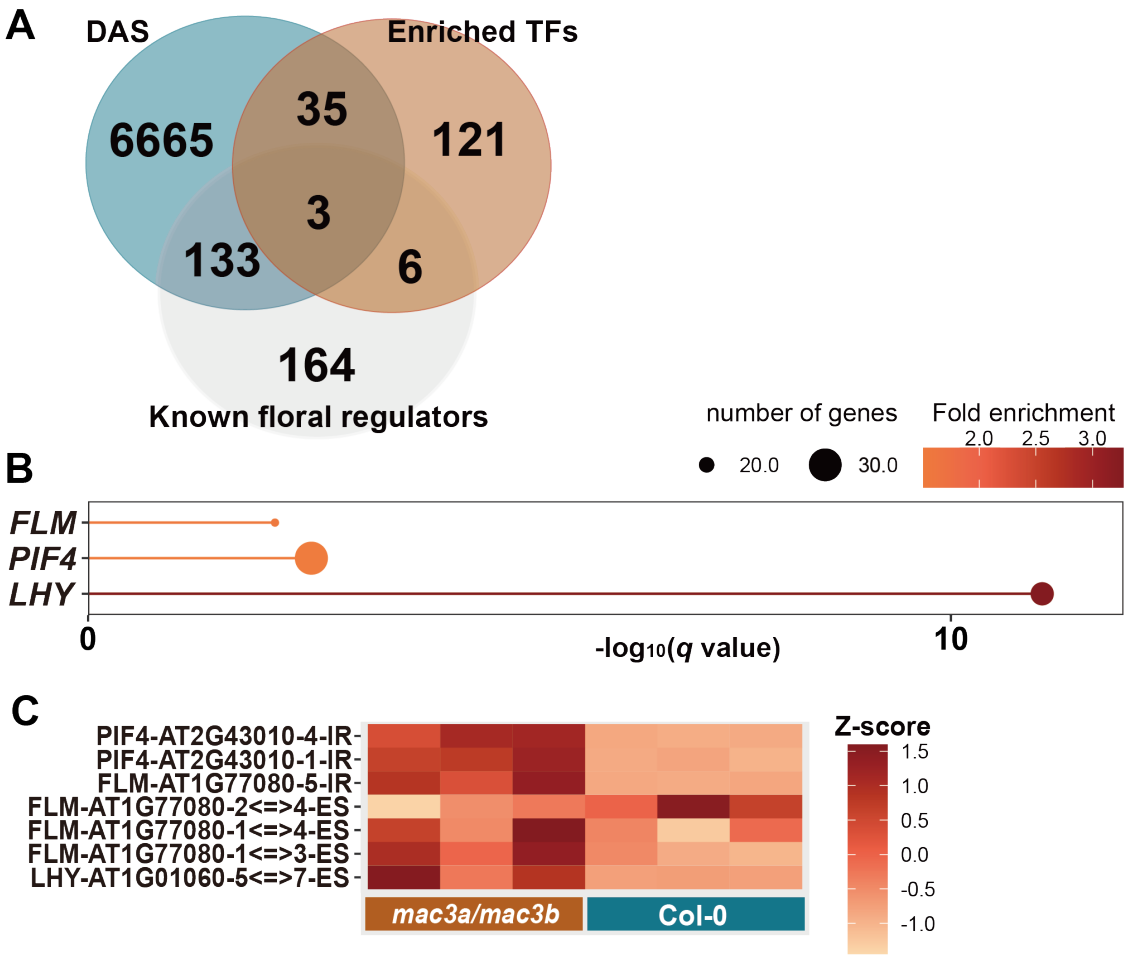

Figure 5. Identification of potential alternatively spliced targets of MAC3A and MAC3B for their flowering time regulation

(A) The Venn diagram represents the intersection of genes with differentially alternative spliced (DAS) events (Blue), the enriched transcription factors (TFs) upstream of the differentially expressed gene (DEG) (Orange), and known floral regulators (Grey). **(B)** *FLM*, *PIF4*, and *LHY* are the genes that overlap among these lists. The lollipop plot represents the numbers of DEG in the *mac3a/mac3b* potentially as downstream targets of FLM, PIF4, or LHY. The gene numbers were exhibited in the size of the dot, and the fold enrichment was shown in the darkness of the lollipops. **(C)** Heatmap of *FLM*, *PIF4*, and *LHY* DAS events found in the *mac3a/mac3b*. The color represented the Z-score among samples from respective normalized values of splicing events. The label of each row refers to the gene name, TAIR ID, and the location of the event.

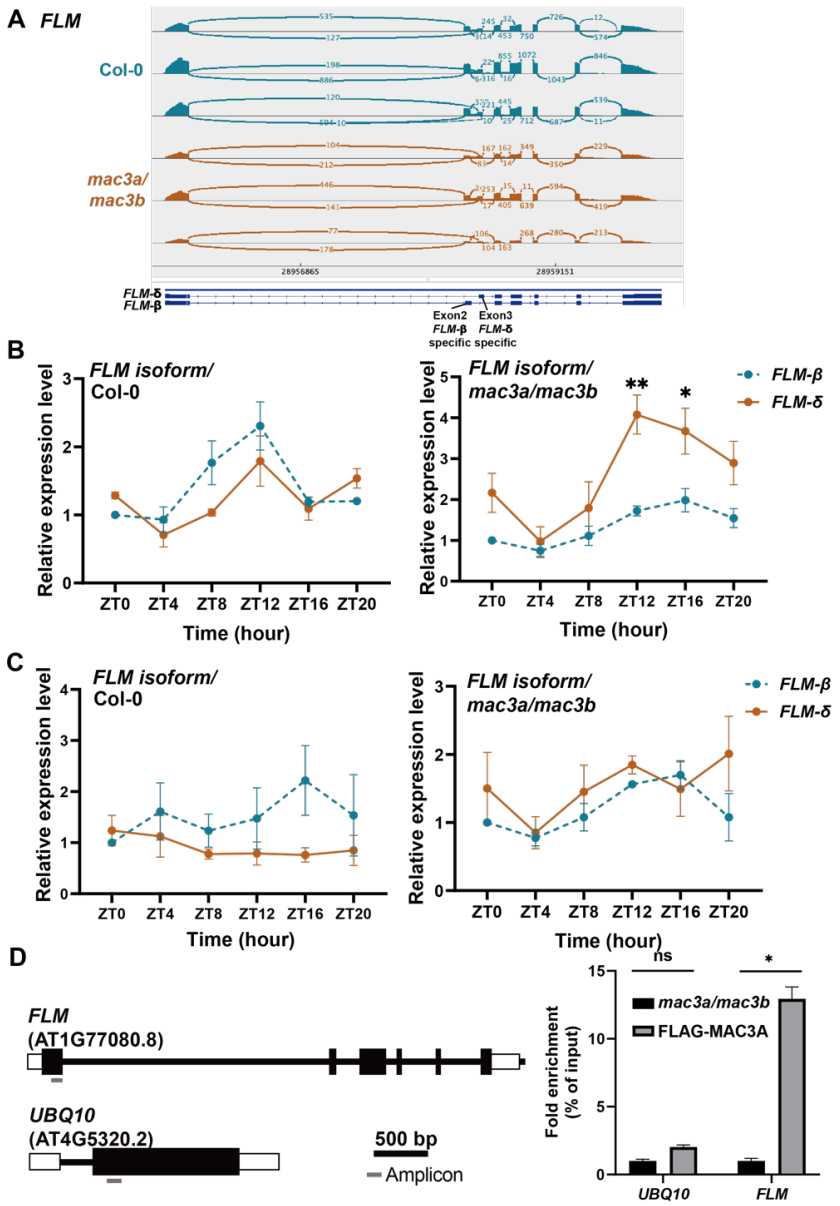

Figure 6. MAC3A and MAC3B regulate *FLM* splicing

(A) The sashimi plots on *FLM* locus in Col-0 (Blue) and *mac3a/mac3b* (Orange). The height of the base represented the relative read depth, and the read number across junctions was shown between specific splicing junctions. The *FLMβ*-specific 2nd exon and *FLMδ*-specific third exon were indicated. **(B and C)** The relative expression levels of *FLMβ* and *FLMδ* were measured with RT-qPCR in Col-0 (left panel) and *mac3a/mac3b* (right panel) seedlings under SD (B) and LD (C). All time points were normalized with *UBQ10* expression and compared to the *FLMβ* expression at ZT0. Error bars represented the standard deviations of three biological replicates. Data were analyzed using ANOVA and the Kruskal-Wallis test: *, $p< 0.05$; **, $p< 0.01$. **(D)** RNA-Immunoprecipitation followed by qPCR (RIP-qPCR) with anti-FLAG antibody in the FLAG-tagged MAC3A/*mac3amac3b* (FLAG-MAC3A) and *mac3amac3b* control. The locations of the amplicons were illustrated in the *FLM* and *UBQ10* gene structure (left panel), and the locations of the amplicons were labeled underneath the gene structure. The enrichment of immunoprecipitated RNA was calculated relative to the input RNA. The *mac3a/mac3b* mutant and the transcript of *UBQ10* were used as control and negative control, respectively. The values shown are means ± SD. Statistical analysis was performed using a two-tailed paired t-test (ns, non-significant, *$P< 0.05$). The other two biological replicates were included in the Supplemental Figure S4.

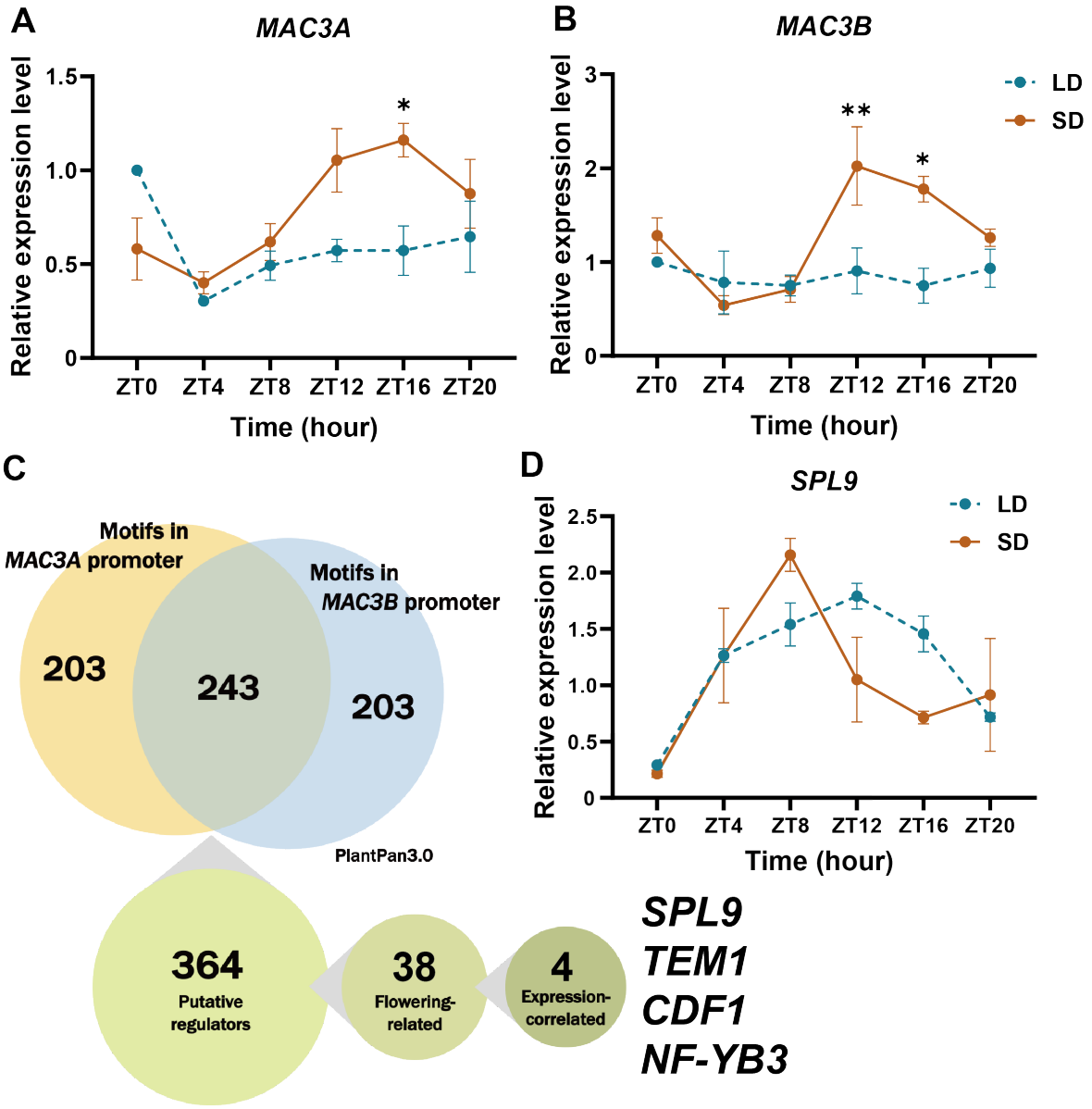

Figure 7. Identification of the upstream regulators mediating the photoperiodic expression of *MAC3A* and *MAC3B*

(A and B) The relative diurnal expression pattern of *MAC3A* (A) and *MAC3B* (B) in LD and SD were measured with RT-qPCR. The expression was normalized with *UBQ10* and compared to the expression at ZT0 in LD. Error bars showed the standard deviations of three biological replicates, and the data were statistically tested using the Kruskal-Wallis test: **, $p < 0.01$; *, $p < 0.05$. **(C)** The pipeline of identifying *MAC3A* and *MAC3B* upstream regulators. The TF binding motifs on the ~1.5 kb of *MAC3A* and *MAC3B* promoters were identified with the PlantPAN4 database (http://plantpan.itps.ncku.edu.tw/plantpan4, Chow et al., 2019), respectively. Then, 364 putative TFs binding to the motifs in both *MAC3A* and *MAC3B* promoters were selected. The TFs belonging to the flowering regulators in the list were further selected through analyses of their diurnal expression correlating with *MAC3A* and *MAC3B* shown in A and B. The diurnal expression data were extracted from the Photo-Graph database (https://gendron-lab.shinyapps.io/PhotoGraph/; Leung et al., 2023). **(D)** RT-qPCR measured the expression of *SPL9* under LD and SD. The expression was normalized with *UBQ10*. The error bars are the standard deviations of the mean from three biological replicates.

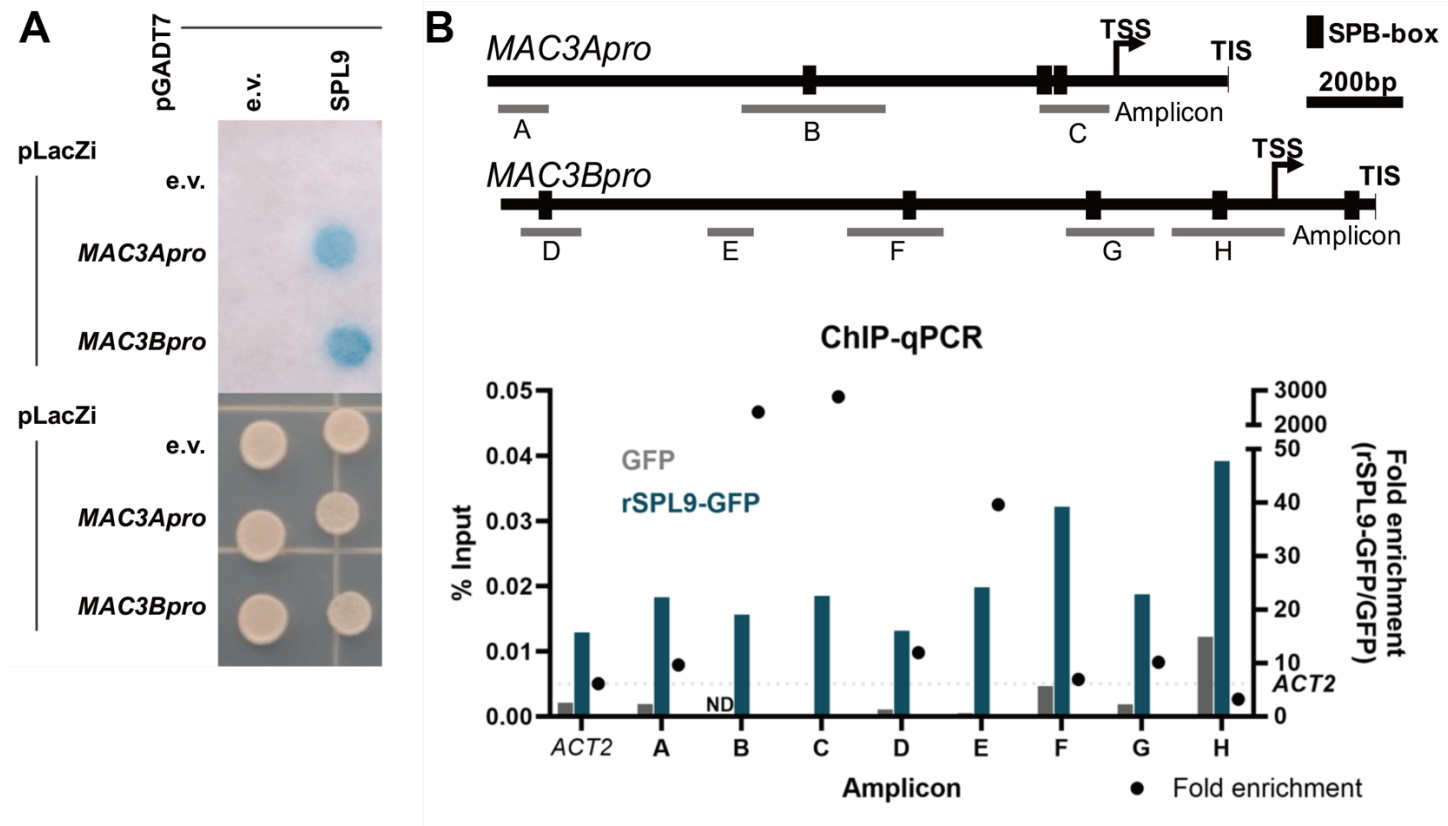

Figure 8. SPL9 interacts with the promoters of *MAC3A* and *MAC3B*

(A) SPL9 interacts with the *MAC3A* and *MAC3B* promoters in the yeast one-hybrid assays. The yeast bearing the *pLacZi* promoter-reporter vectors and *pGADT7* vectors expressing *SPL9* were grown on synthetic dropout medium (SD-Leu-Ura-Met). The colonies were blotted on the filter paper to test the β-Galactosidase (β-Gal) activity. The blue color indicates the interaction between 1.5 kb promoter fragments of *MAC3A* and *MAC3B* in the *pLacZi* vectors and the transcription factors in the *pGADT7* vectors. Empty vectors (e.v.) were used as negative control. **(B)** The chromatin immunoprecipitation (ChIP) assays in the Arabidopsis seeding expressing *rSPL9-GFP* or *GFP* only. The locations of SPL9 predicted binding sites (SPB-box, black boxes) were illustrated in the *MAC3A* and *MAC3B* promoters (upper panel). The amplicons were designed to surround SBP-Box (greys boxes labeled with A to H) or *ACTIN2* (*ACT2*) as controls. The chromatins in the Arabidopsis seedlings expressing *rSPL9-GFP* (dark blue bars) or *GFP* (grey bars) along with Col-0 were immunoprecipitated with anti-GFP antibody, and the relative enrichments of immunoprecipitated DNA relative to input were calculated as "%input." shown as a bar graph. The fold enrichment (black dots) was calculated by dividing "%input" in SPL9-GFP with "%input" in GFP. The grey horizontal dashed line represents the fold enrichment of negative control, *ACT2*. The "ND" stands for not detectable, and the transcription start site (TSS) and the translation initiation site (TIS) were labeled. Only one replicate is presented here.

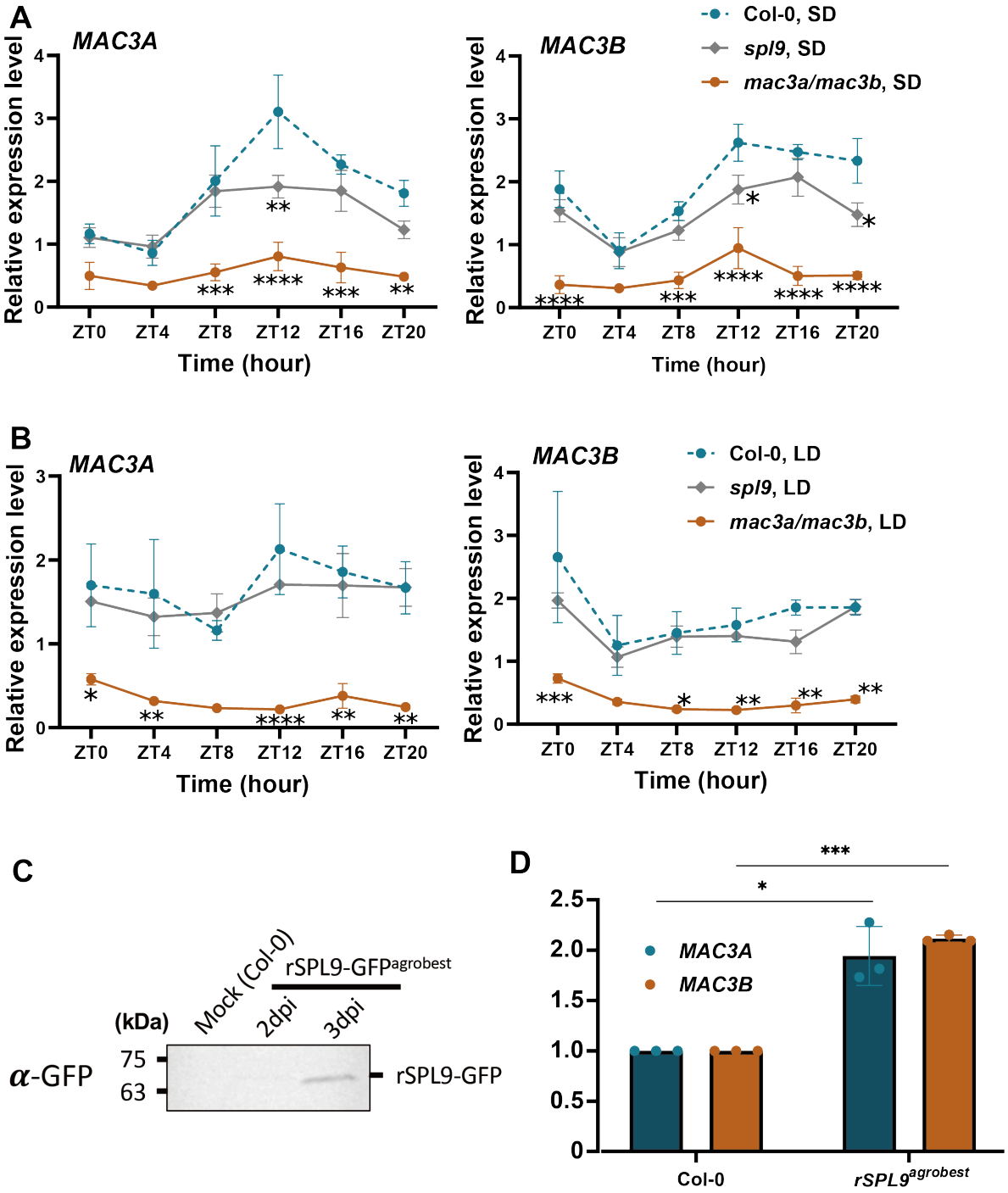

Figure 9. SPL9 activates *MAC3A* and *MAC3B* expression

(A and B) The diurnal expression of *MAC3A* (left panel) and *MAC3B* (right panel) in Col-0, *spl9*, and *mac3a/mac3b* mutant in SD (A) and LD (B) was measured with RT-qPCR. The samples were harvested every 4 hours after light on (ZT0). The significance of the differences between genotypes within time points was calculated from three biological replicates using two-way ANOVA with Dunnett's test. **(C)** Transient expression of *rSPL9-GFP* with the AGROBEST infection strategy. The rSPL9-GFP protein was detected by anti-GFP antibody in Western blotting to confirm their expression. **(D)** The expression of *MAC3A* and *MAC3B* in *rSPL9-GFP* over-expressed or Col-0 seedlings. The significance of the differences between the three biological repeats was tested using a T-Test. Significances were annotated by star marks (*:P< 0.05, **:P< 0.01, ***:P< 0.001, ****:P< 0.0001).

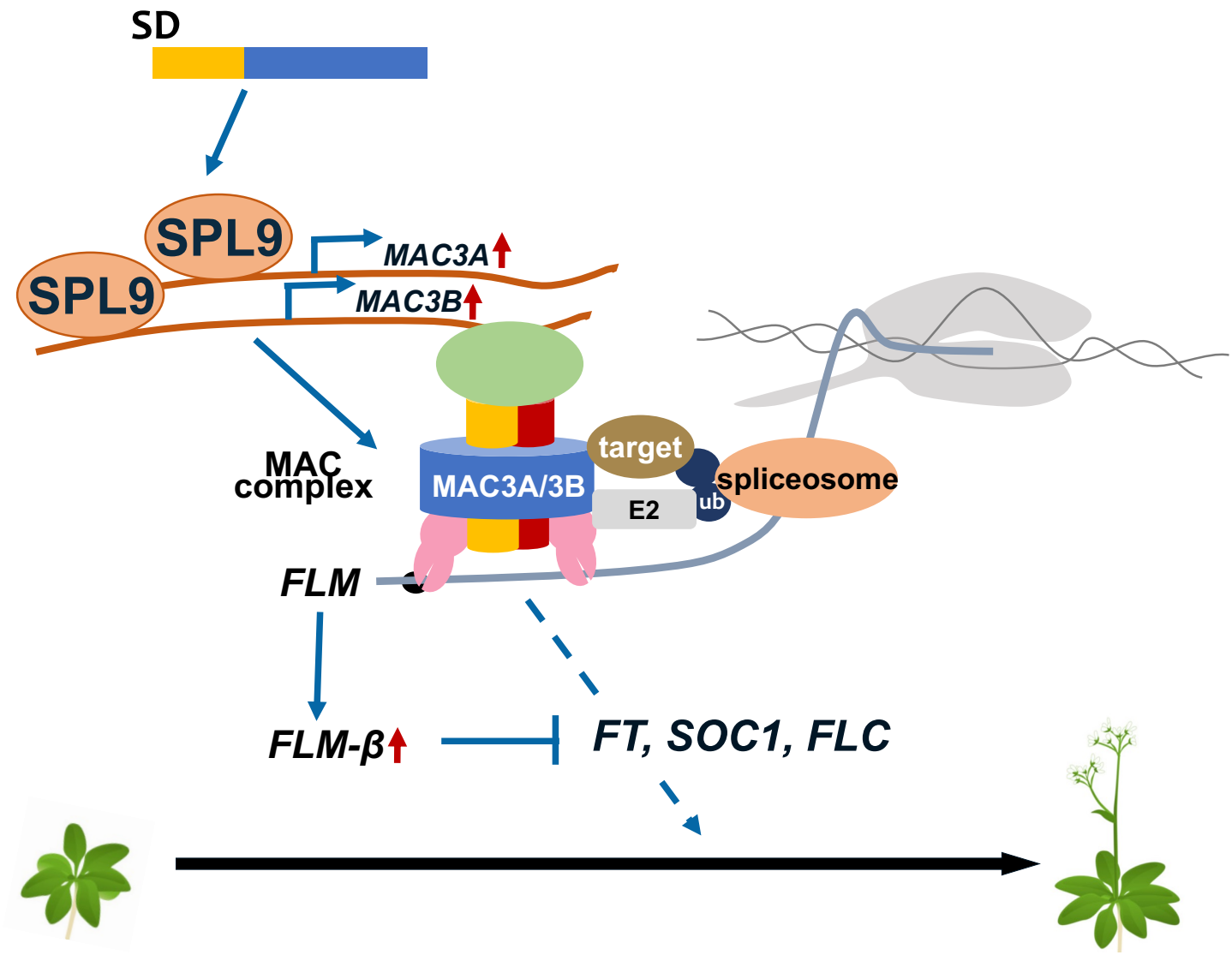

Figure 10. Proposed model of MAC3A and MAC3B mediated photoperiod signal to regulate flowering under SD

The working model of MAC3A and MAC3B repressing floral transition under SD. MAC3A and MAC3B proper the RNA splicing of *FLMβ* under SD, potentially acting with spliceosome, repressing floral transition. Under SD, SPL9 activates *MAC3A* and *MAC3B* transcription, which may enable MAC3A and MAC3B to modulate floral transition.

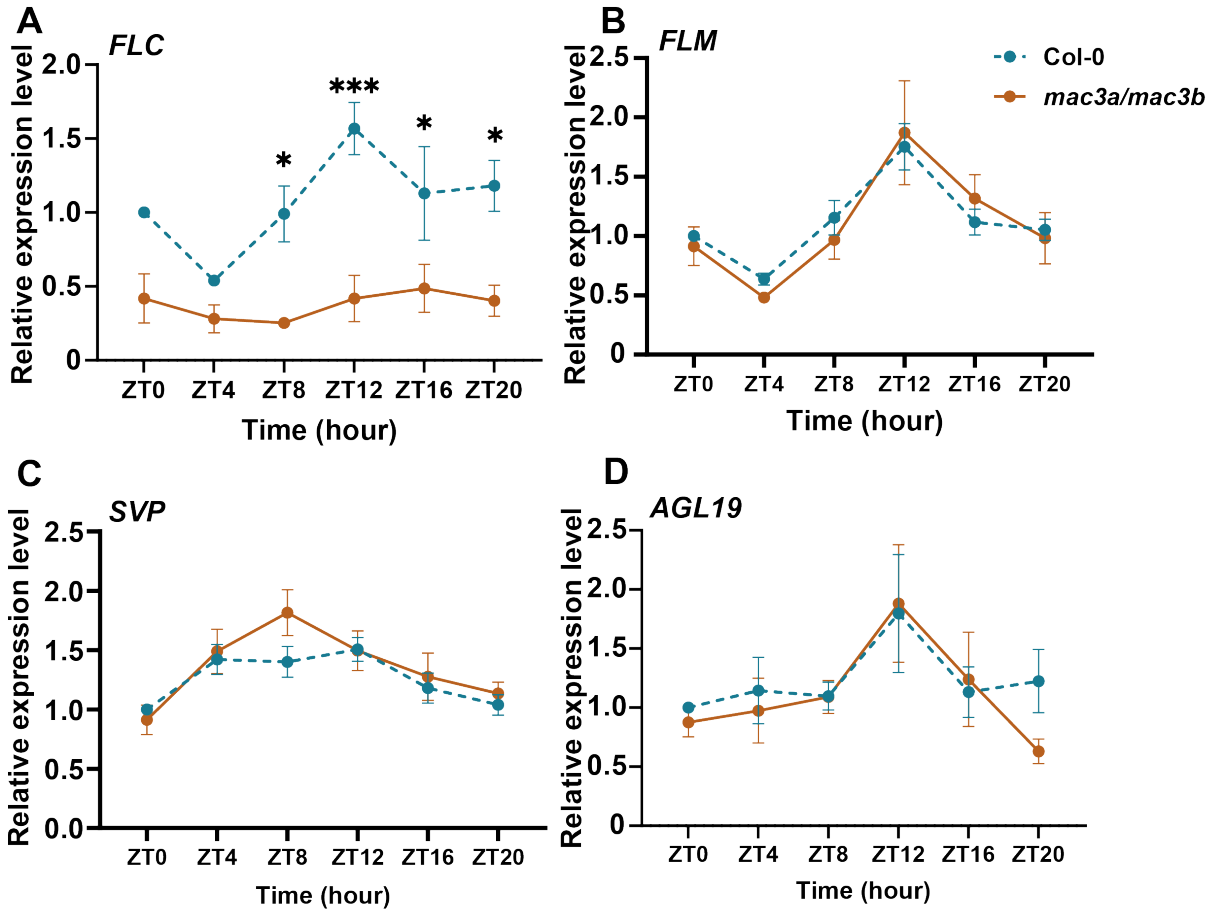

Supplemental Figure S1. The expression of *FLC*, *FLM*, *SVP*, and *AGL19* in SD measured by RT-qPCR

The diurnal expression levels of **(A)** *FLC*, **(B)** *FLM*, **(C)** *SVP*, and **(D)** *AGL19* in the Col-0 and *mac3a/mac3b* mutant seedlings under SD were measured by RT-qPCR. The relative expression levels were normalized with *UBQ10* and compared to Col-0 at ZT0. Error bars indicated standard deviations of three biological replicates. Data were analyzed using ANOVA and the Kruskal-Wallis test: ***, $p < 0.001$; *, $p < 0.05$.

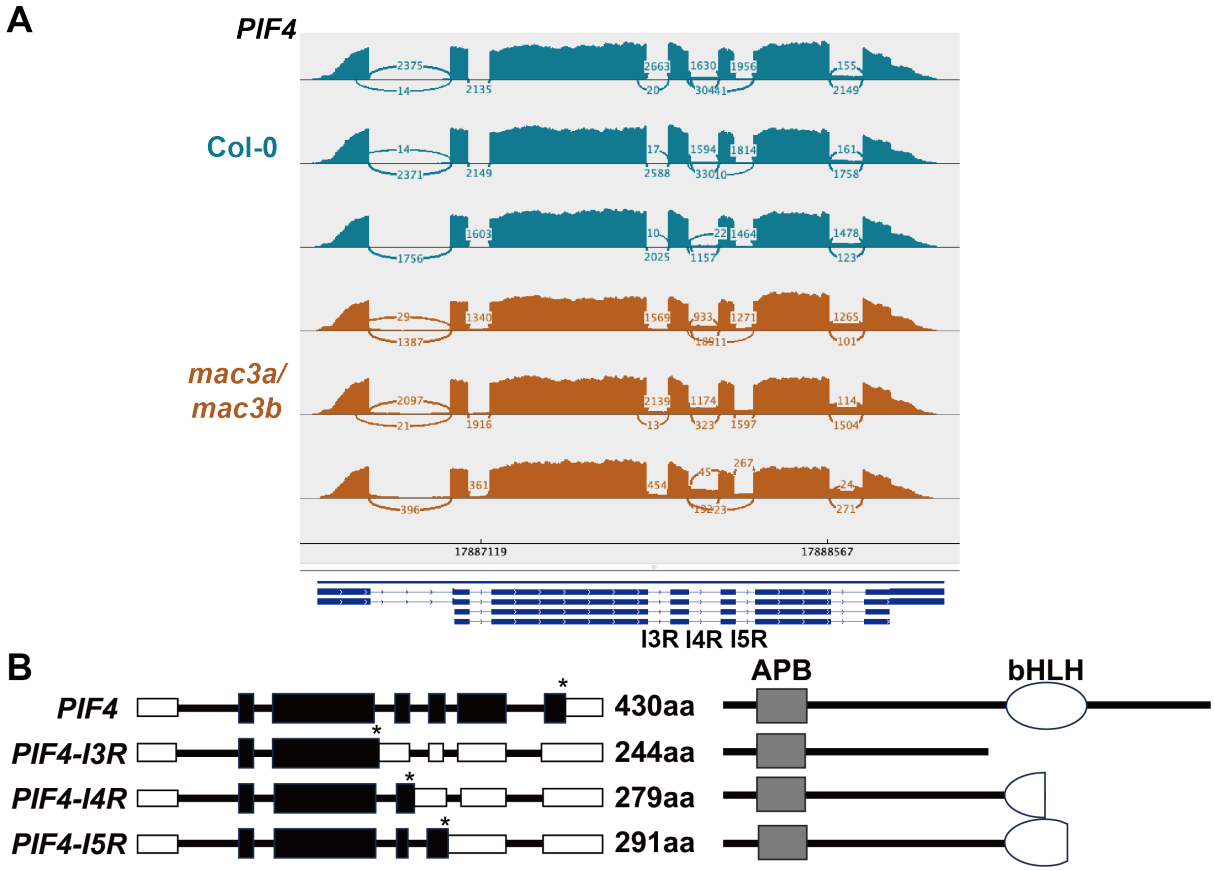

Supplemental Figure S2. Alternatively spliced events of *PIF4* were identified in the *mac3a/mac3b* mutant

(A) The sashimi plots demonstrate the splicing events found in Col-0 (Blue) and *mac3a/mac3b* (Orange) on the *PIF4* locus. The height of the base represents the relative read depth, and the read number across junctions was shown between specific splicing junctions. Intron 3, 4, and 5 (I3R, I4R, and I5R) annotated the IR events that may happen on the *PIF4* locus. In differentially alternative splicing events, only the I3R event out of these three events passes our statistical criteria, while its annotation is "PIF4-AT2G43010-4-IR" in Figure 5. The different annotations of intron numbers were due to the procedures of the RackJ algorithm. **(B)** The predicted *PIF4* isoforms with different retained introns. PIF4 and its intron-retained form of transcripts were drawn with untranslated regions (UTR) in white blocks, coding sequence (CDS) in black blocks, spliced introns in black lines, and translation stop codon in the star above (left). On the right panel, predicted peptides encoded from specific transcripts were annotated with active phyB-binding (APB, grey box) and complete/truncated bHLH (complete/sliced white oval) domains.

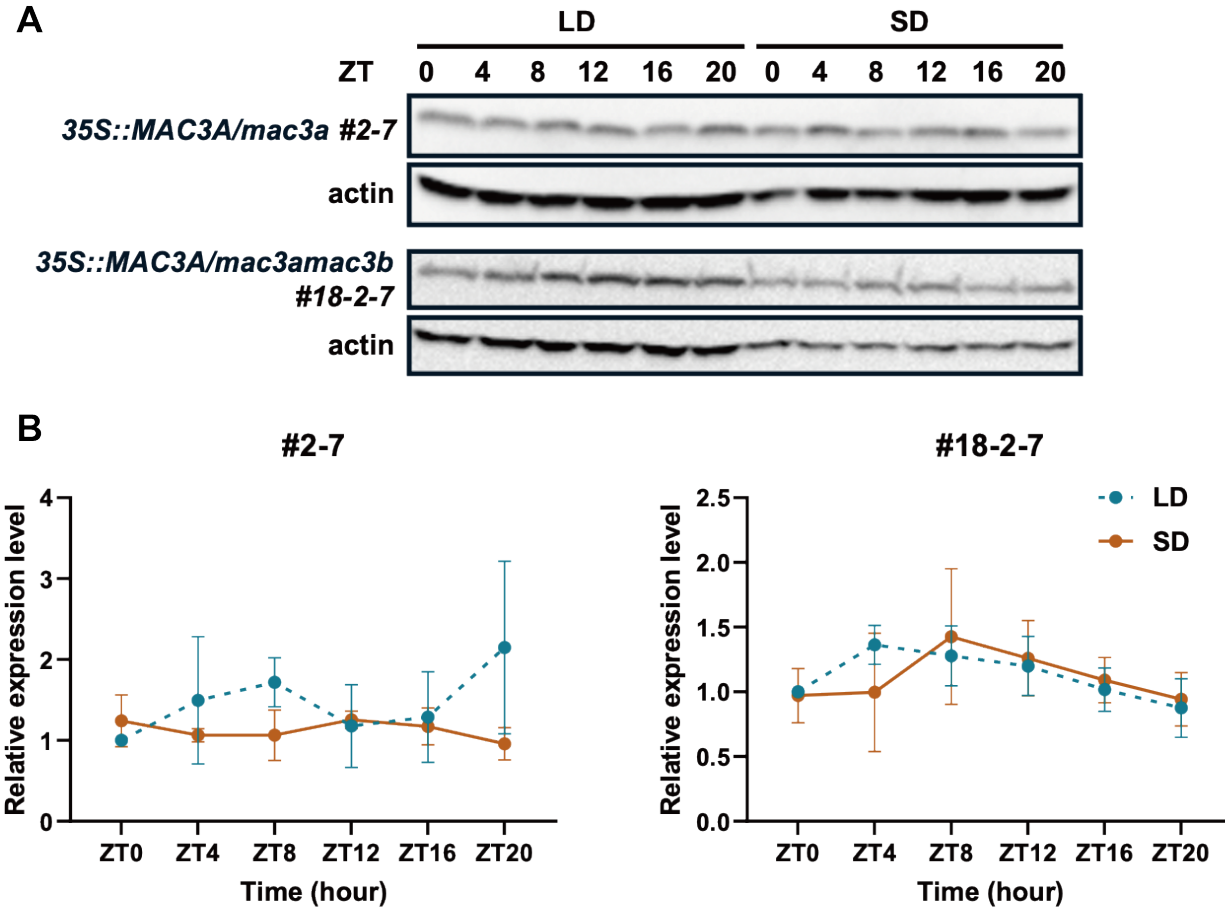

Supplemental Figure S3. Diurnal protein profiles of *35S::FLAG-MAC3A* in LD and SD

(A) The representative diurnal protein levels of *FLAG-MAC3A* fusions driven by the *CaMV 35S* promoter in the *mac3a* (*35S::MAC3A/mac3a*) or *mac3a/mac3b* (*35S::MAC3A/mac3amac3b*) Arabidopsis mutant in LD and SD. The 10-day-old seedlings in LD and 14-day-old seedlings in SD were harvested every 4 hours after light on (ZT0) for 24 hours. MAC3A proteins were immunologically detected using an anti-FLAG antibody, and actin levels were used as an internal control. **(B)** The quantification analysis of *35S::MAC3A* protein expression levels was plotted. Data were collected from three biological replicates and statistically analyzed using the Kruskal-Wallis test with no significant differences.

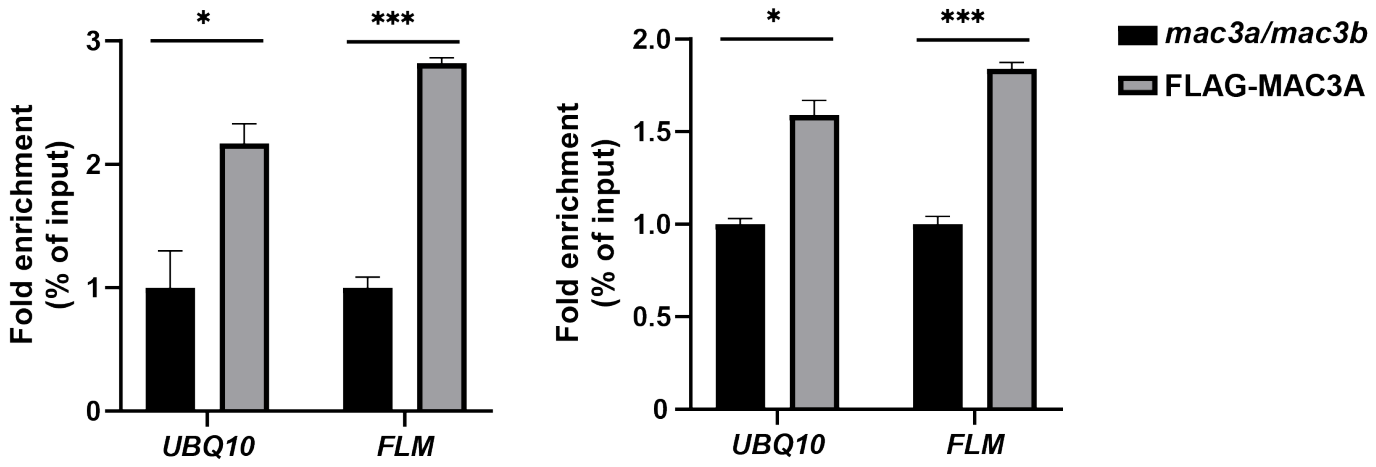

Supplemental Figure S4. The biological repeats of FLAG-MAC3A RIP-qPCR

RNA-Immunoprecipitation followed by qPCR (RIP-qPCR) with anti-FLAG antibody in the FLAG-tagged *MAC3A*/*mac3amac3b* (FLAG-MAC3A) and *mac3amac3b* control. The enrichment of immunoprecipitated RNA was calculated relative to the input RNA. The *mac3amac3b* mutant and the transcript of *UBQ10* were used as negative controls, respectively. The values shown are means ± SD. Statistical analysis was performed using a two-tailed paired t-test (ns, non-significant, *P< 0.05; ***P< 0.001). The representative replicates are shown in Figure 6D.

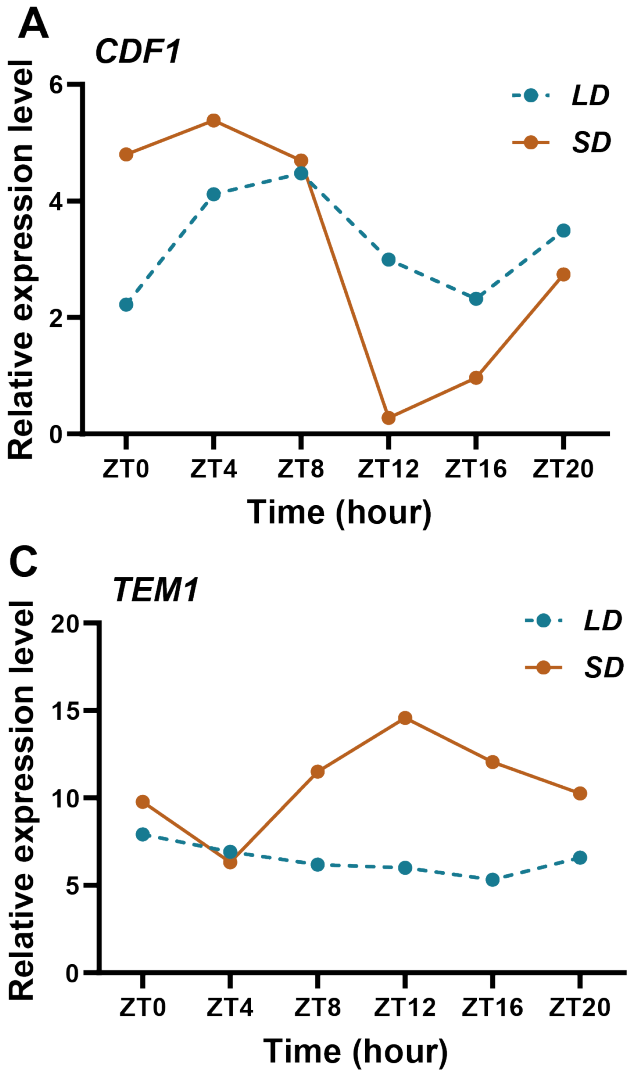

D

Correlation pair		Pearson's *r*	*P* value
SPL9	*MAC3A*	-0.593	0.0421
	MAC3B	-0.731	0.0069
CDF1	*MAC3A*	-0.830	0.0008
	MAC3B	-0.693	0.0125
TEM1	*MAC3A*	0.697	0.0118
	MAC3B	0.725	0.0076
NF-YB3	*MAC3A*	0.762	0.0040
	MAC3B	0.718	0.0086

Supplemental Figure S5. The expression profiles of *CDF1*, *NF-YB3*, and *TEM1* under LD and SD on the Photo-Graph database and their correlation to *MAC3A* and *MAC3B*

(A-C) The diurnal expression of (A) *CDF1*, (B) *NF-YB3*, and (C) *TEM1* under LD and SD were retrieved from the RPKM of RNA-seq data on the Photo-graph database (https://gendron-lab.shinyapps.io/PhotoGraph/; Leung et al., 2023). The dot noted the mean of normalized reads. The expression values under LD were represented by blue dots with lines and SD by orange dots with lines. The relative expression levels **(D)** The correlation between the expression pattern of *MAC3A* and *MAC3B* (Figure 7A and 7B) with *SPL9*, *CDF1*, *NF-YB3*, and *TEM1* across a day under LD and SD. The correlation was calculated in Pearson's r, by gene expression of correlation pair genes under LD and SD, and the significances of Pearson's r were shown on its right side.

Table1. The differentially alternative spliced (DAS) events in the *mac3a/mac3b* mutant compared to Col-0 under SD

The number of DAS events, including intron retention (IR), exon skipping (ES), alternative donor/acceptor splicing site (AltDA), and their corresponding gene number was listed. The IR, AltDA, or ES events were identified by the Chi-square test of reads with or without IR AltDA or ES in between Col-0 and *mac3a/mac3b* mutants, respectively. Out of the identified alternative splicing events, the differentially alternative splicing events were selected by significance and fold-change among replicates. The false discovery rate (FDR) of accepted p-values is limited to 5%.

	***mac3a/mac3b* v.s. WT**			
	Events	**%**	**Genes**	**%**
total	**12031**	**100.00**	**6836**	**100.00**
IR	**11876**	**98.71**	**6778**	**99.15**
ES	**150**	**1.24**	**146**	**2.14**
AltDA	**5**	**0.04**	**4**	**0.06**

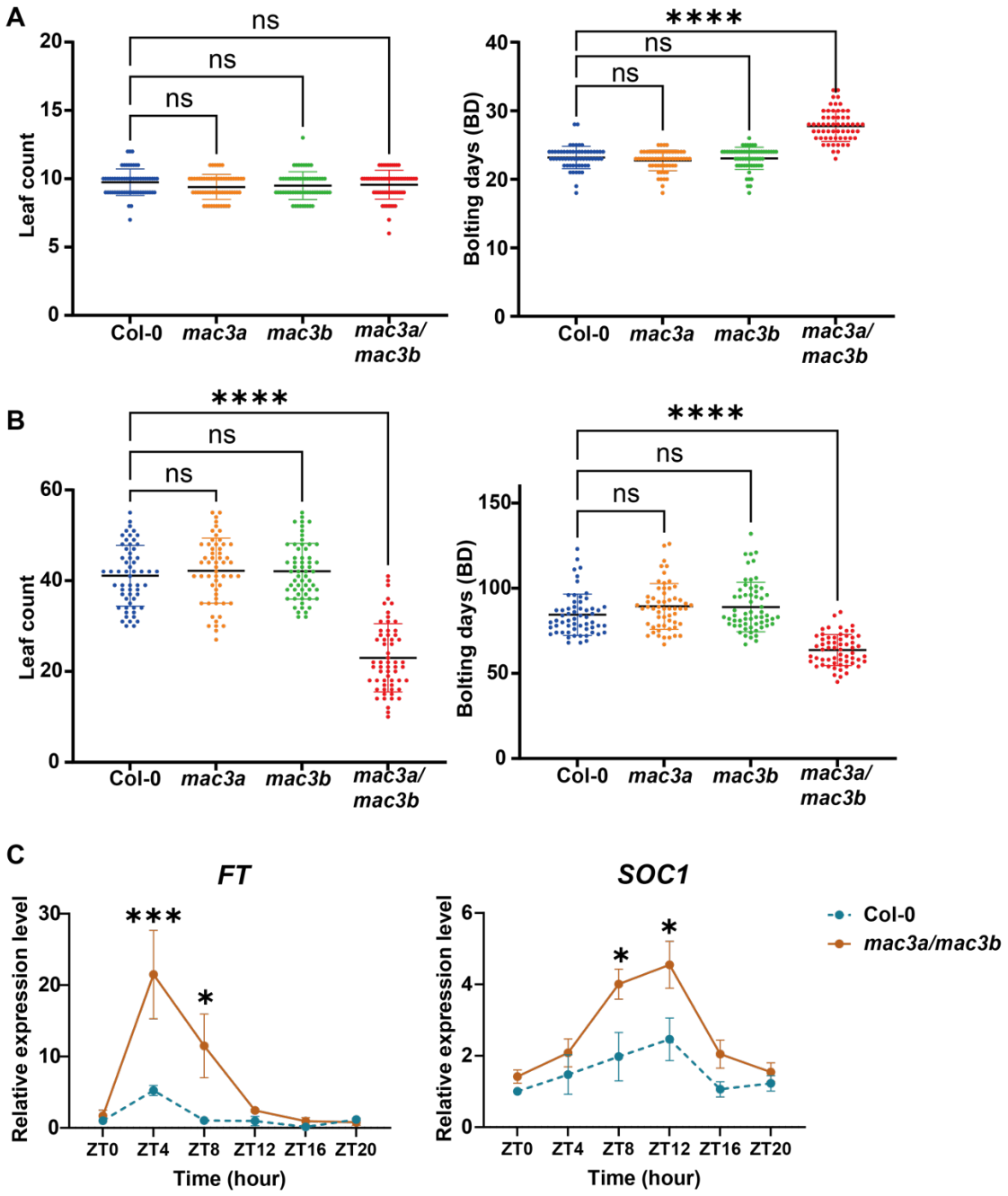

Figure 1. The flowering phenotypes of Col-0, *mac3a*, *mac3b*, and *mac3a/mac3b* mutants in long-day (LD) and short-day (SD)

The flowering time of Col-0, *mac3a*, *mac3b*, and *mac3a/mac3b* mutants grown under **(A)** LD (16h light/8h dark) or **(B)** SD (8h light/16h dark) was measured by rosette leaf number (left panel) when inflorescence reached 7 cm and bolting day (right panel) when inflorescence reached 1 cm. Data were collected from three biological replicates (n≥ 56) and analyzed using ANOVA and Kruskal-Wallis test: ****, p< 0.0001; ns, not significant. **(C)** The transcript levels of *FT* (left panel) and *SOC1* (right panel) of Col-0 and *mac3a/mac3b* seedlings in SD. The samples were harvested every 4 hours after light on (Zeitgeber time 0, ZT0), and the expression levels were measured by RT-qPCR. The relative expression levels were normalized with *UBQ10* and compared to the Col-0 at ZT0. The error bars indicated standard deviations from three biological replicates. Data were analyzed using ANOVA and the Kruskal-Wallis test: ***, p< 0.001; *, p< 0.05.

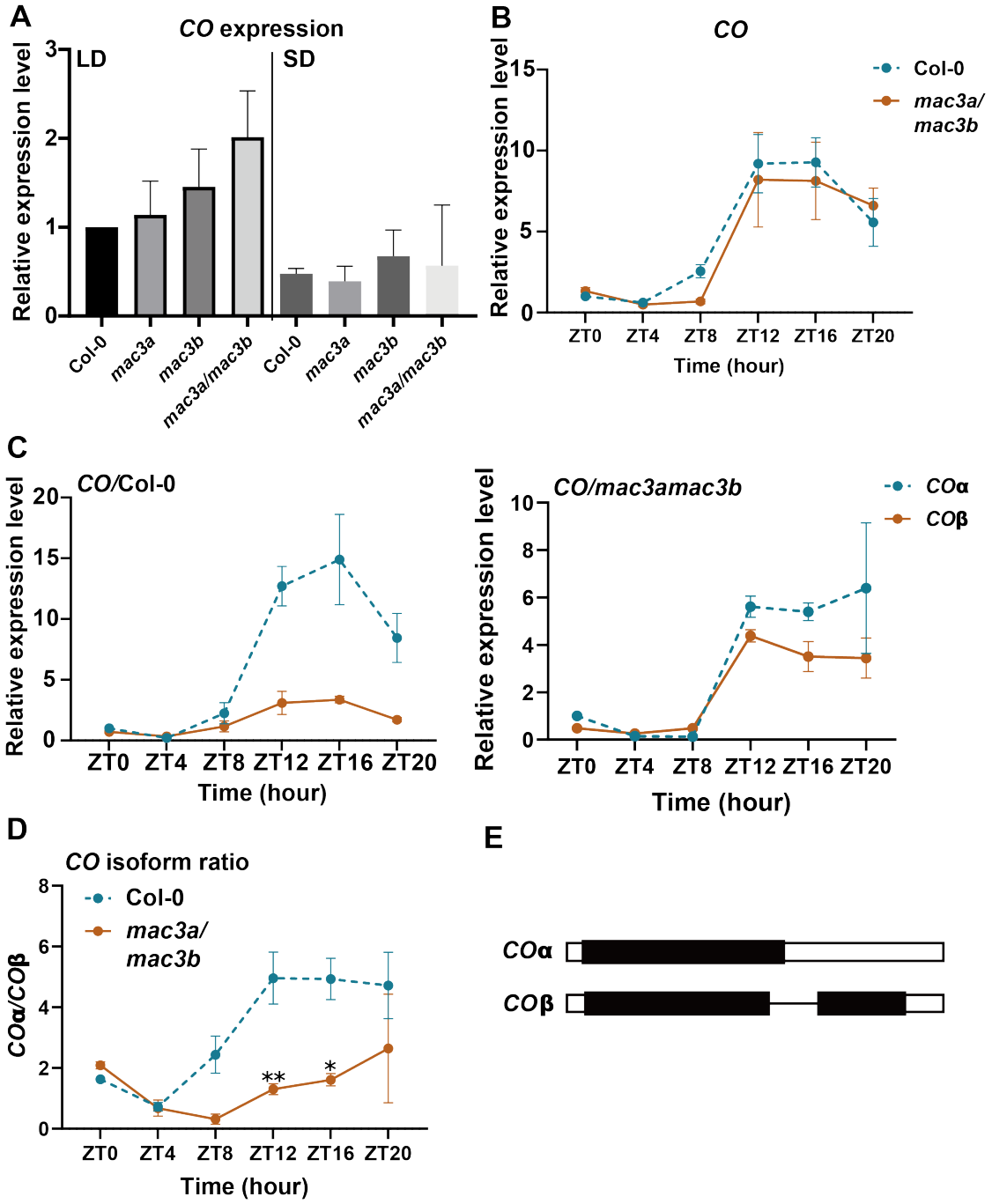

Figure 2. The expression of *CO* and its isoforms measured by RT-qPCR

(A) The relative transcript levels of *CO* in Col-0, *mac3a*, *mac3b*, and *mac3a/mac3b* mutants harvested at ZT16 under LD (16h light/8h dark) and ZT8 under SD (8h light/16h dark). The samples were harvested every 4 hours since dawn (ZT0). All time points were normalized with *UBQ10* expression and compared to the Col-0 sample at ZT0. **(B)** The diurnal expression profile of *CO* in Col-0 and *mac3a/mac3b* mutants under SD. **(C)** The relative expression of *COα* and *COβ* in Col-0 (left panel) and *mac3a/mac3b* (right panel) in SD. **(D)** The ratios of *COα* over *COβ* in Col-0 and *mac3a/mac3b* mutants in SD. **(E)** The diagram of transcript structure and the resulting protein isoforms of *COα* and *COβ*. The black rectangles are exons, and the lines connecting them are introns. The black bars are protein-coding regions. The error bars indicated standard deviations from three biological replicates. Data were analyzed using ANOVA and the Kruskal-Wallis test: **, $p < 0.01$; *, $p < 0.05$.

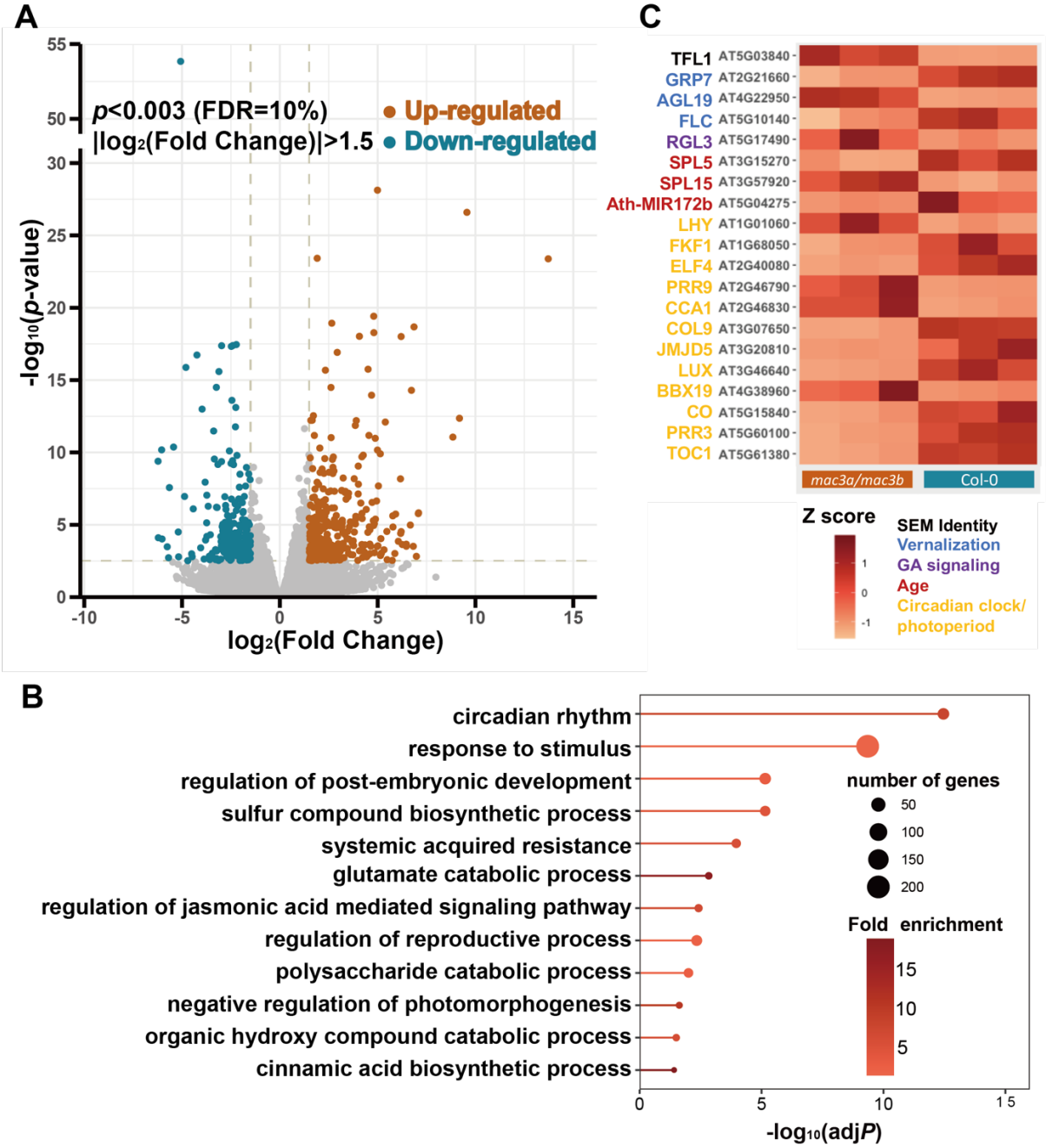

Figure 3. The differentially expressed genes (DEG) of SD-grown *mac3a/mac3b* mutant and their Gene ontology (GO) analysis

(A) The volcano plot of differentially expressed genes (DEG) in *mac3a/mac3b* mutants under SD compared to that in Col-0. The fold changes were calculated by comparing the means of normalized reads in three biological replicates of *mac3a/mac3b* and Col-0, and the p-values were calculated by T-Test of normalized reads. The up-regulated genes were marked in brown-orange, and the down-regulated genes were marked in blue with the criteria of $|\log_2(\text{fold change})| > 1.67$ and 10% FDR of accepted P values. **(B)** The top-ranked gene ontology (GO) of the biological processes category for the DEG. Selected GO terms were plotted on the lollipop plot, with gene numbers for each GO term in the DEG list represented by the dot size, and the darkness of the lollipops indicated the fold enrichment. **(C)** Heat map of DEG genes involved in flowering regulation. The color represents the Z-score, calculated by the normalized gene expression reads between samples. The genes belonging to specific flowering pathways were color-coded. FDR: false discovery rate.

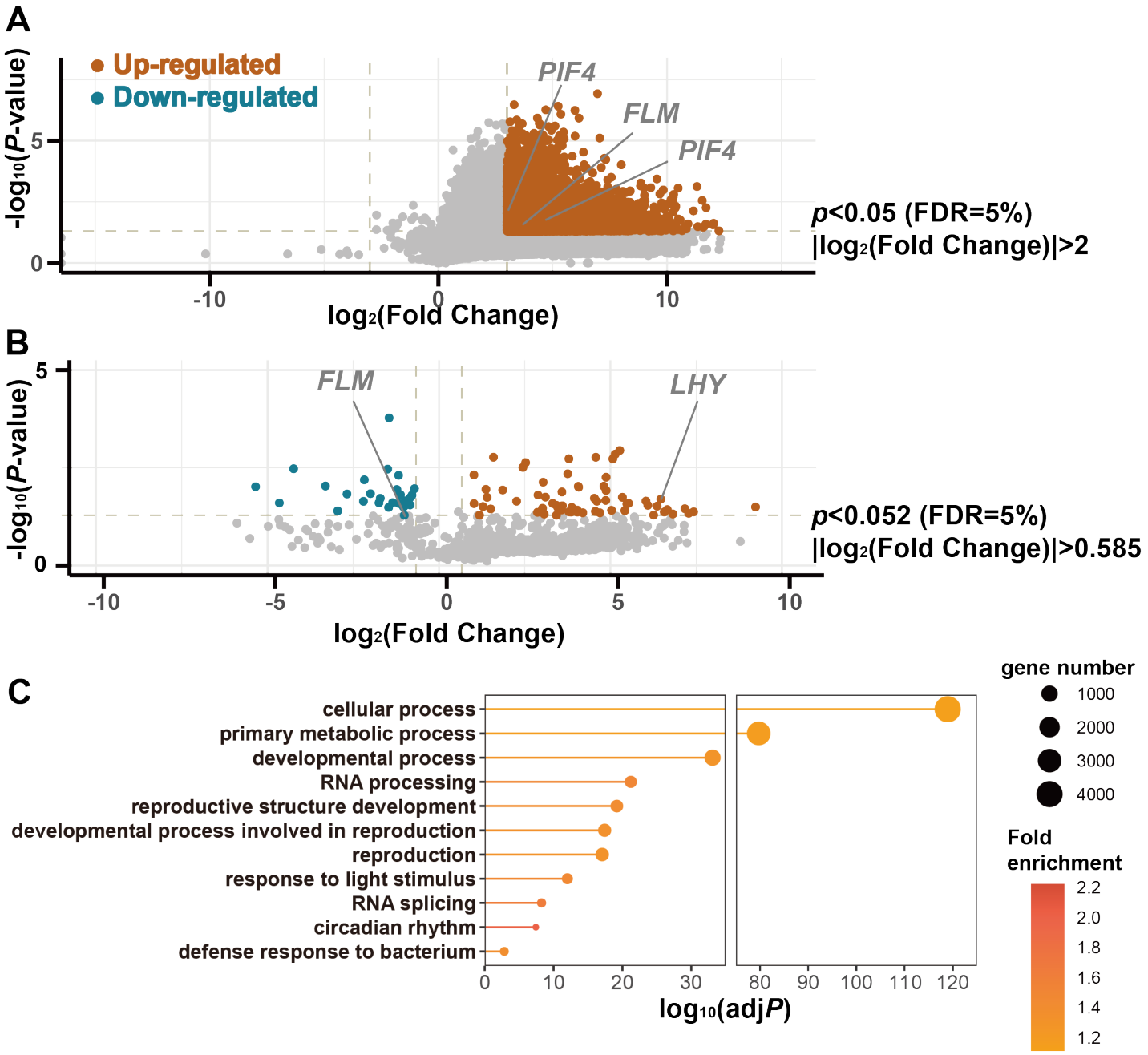

Figure 4. The differentially alternative spliced (DAS) events of SD-grown *mac3a/mac3b* mutant and their Gene ontology (GO) analysis

(A) The volcano plot of differentially intron retention (DIR) events between Col-0 and *mac3a/mac3b* identified by supporting reads ratio (|$\log_2$(fold change)|> 3, FDR< 0.05). **(B)** The volcano plot of differentially exon skipping (DES) events between Col-0 and *mac3a/mac3b* identified by supporting reads ratio (|$\log_2$(fold change)|> 0.585, FDR < 0.05). Genes related to flowering regulation, such as *PIF4*, *FLM*, and *LHY*, were labeled. **(C)** The top-ranked gene ontology (GO) of biological processes for all differential alternative spliced events. Selected GO terms were plotted on the lollipop plot, with gene numbers exhibiting in the dot size and the darkness of the lollipops for the fold enrichment. FDR: false discovery rate.

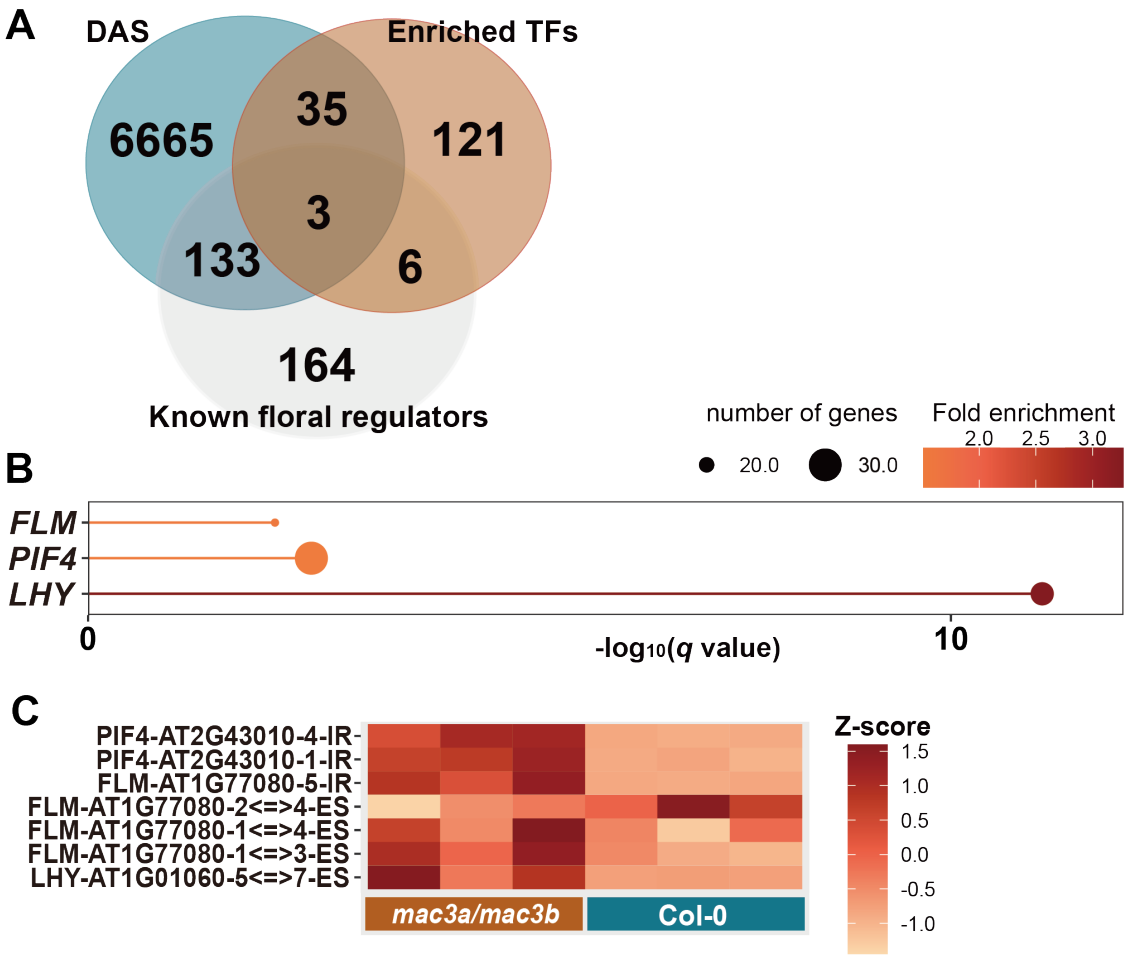

Figure 5. Identification of potential alternatively spliced targets of MAC3A and MAC3B for their flowering time regulation

(A) The Venn diagram represents the intersection of genes with differentially alternative spliced (DAS) events (Blue), the enriched transcription factors (TFs) upstream of the differentially expressed gene (DEG) (Orange), and known floral regulators (Grey). **(B)** *FLM*, *PIF4*, and *LHY* are the genes that overlap among these lists. The lollipop plot represents the numbers of DEG in the *mac3a/mac3b* potentially as downstream targets of FLM, PIF4, or LHY. The gene numbers were exhibited in the size of the dot, and the fold enrichment was shown in the darkness of the lollipops. **(C)** Heatmap of *FLM*, *PIF4*, and *LHY* DAS events found in the *mac3a/mac3b*. The color represented the Z-score among samples from respective normalized values of splicing events. The label of each row refers to the gene name, TAIR ID, and the location of the event.

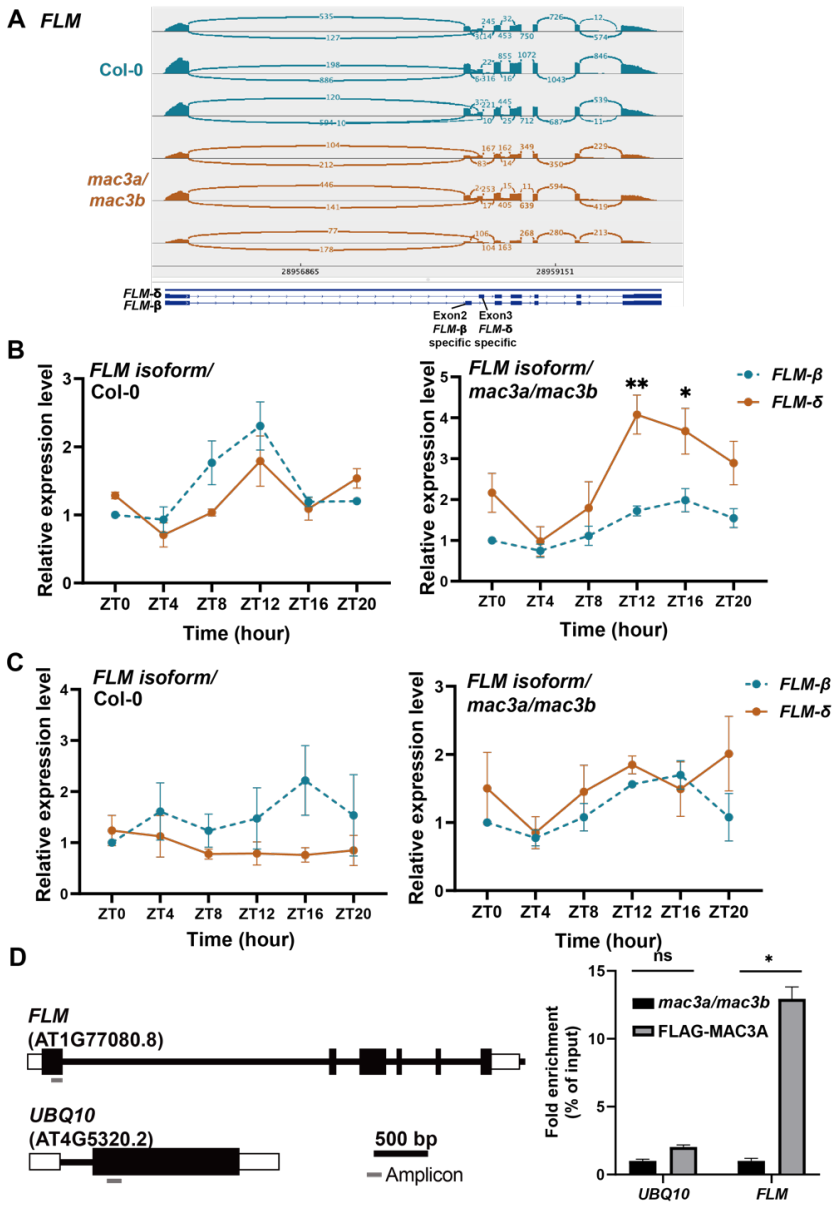

Figure 6. MAC3A and MAC3B regulate *FLM* splicing

(A) The sashimi plots on *FLM* locus in Col-0 (Blue) and *mac3a/mac3b* (Orange). The height of the base represented the relative read depth, and the read number across junctions was shown between specific splicing junctions. The *FLMβ*-specific 2nd exon and *FLMδ*-specific third exon were indicated. **(B and C)** The relative expression levels of *FLMβ* and *FLMδ* were measured with RT-qPCR in Col-0 (left panel) and *mac3a/mac3b* (right panel) seedlings under SD (B) and LD (C). All time points were normalized with *UBQ10* expression and compared to the *FLMβ* expression at ZT0. Error bars represented the standard deviations of three biological replicates. Data were analyzed using ANOVA and the Kruskal-Wallis test: *, $p< 0.05$; **, $p< 0.01$. **(D)** RNA-Immunoprecipitation followed by qPCR (RIP-qPCR) with anti-FLAG antibody in the FLAG-tagged MAC3A/*mac3amac3b* (FLAG-MAC3A) and *mac3amac3b* control. The locations of the amplicons were illustrated in the *FLM* and *UBQ10* gene structure (left panel), and the locations of the amplicons were labeled underneath the gene structure. The enrichment of immunoprecipitated RNA was calculated relative to the input RNA. The *mac3a/mac3b* mutant and the transcript of *UBQ10* were used as control and negative control, respectively. The values shown are means ± SD. Statistical analysis was performed using a two-tailed paired t-test (ns, non-significant, *$P< 0.05$). The other two biological replicates were included in the Supplemental Figure S4.

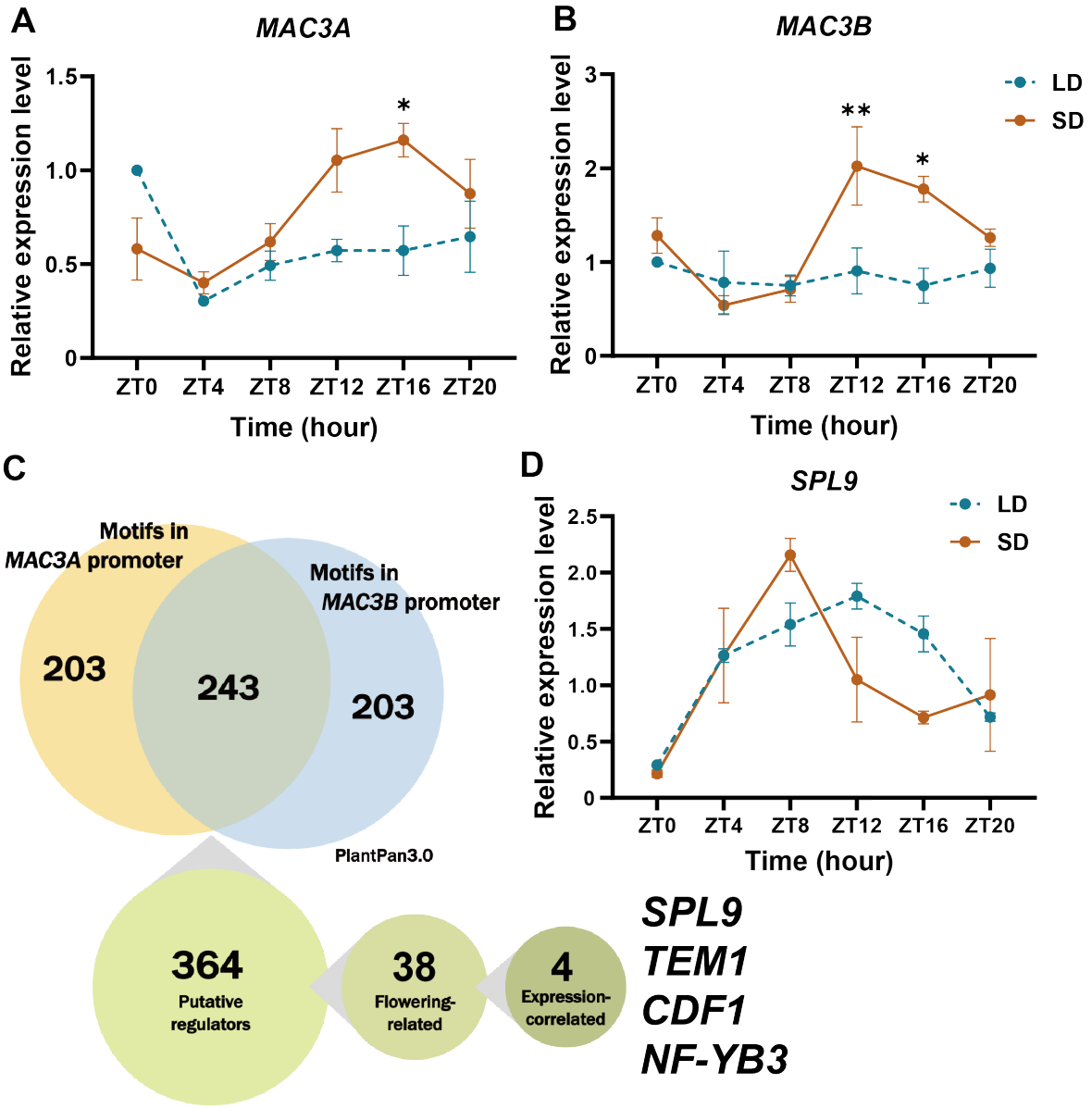

Figure 7. Identification of the upstream regulators mediating the photoperiodic expression of *MAC3A* and *MAC3B*

(A and B) The relative diurnal expression pattern of *MAC3A* (A) and *MAC3B* (B) in LD and SD were measured with RT-qPCR. The expression was normalized with *UBQ10* and compared to the expression at ZT0 in LD. Error bars showed the standard deviations of three biological replicates, and the data were statistically tested using the Kruskal-Wallis test: **, $p < 0.01$; *, $p < 0.05$. **(C)** The pipeline of identifying *MAC3A* and *MAC3B* upstream regulators. The TF binding motifs on the ~1.5 kb of *MAC3A* and *MAC3B* promoters were identified with the PlantPAN4 database (http://plantpan.itps.ncku.edu.tw/plantpan4, Chow et al., 2019), respectively. Then, 364 putative TFs binding to the motifs in both *MAC3A* and *MAC3B* promoters were selected. The TFs belonging to the flowering regulators in the list were further selected through analyses of their diurnal expression correlating with *MAC3A* and *MAC3B* shown in A and B. The diurnal expression data were extracted from the Photo-Graph database (https://gendron-lab.shinyapps.io/PhotoGraph/; Leung et al., 2023). **(D)** RT-qPCR measured the expression of *SPL9* under LD and SD. The expression was normalized with *UBQ10*. The error bars are the standard deviations of the mean from three biological replicates.

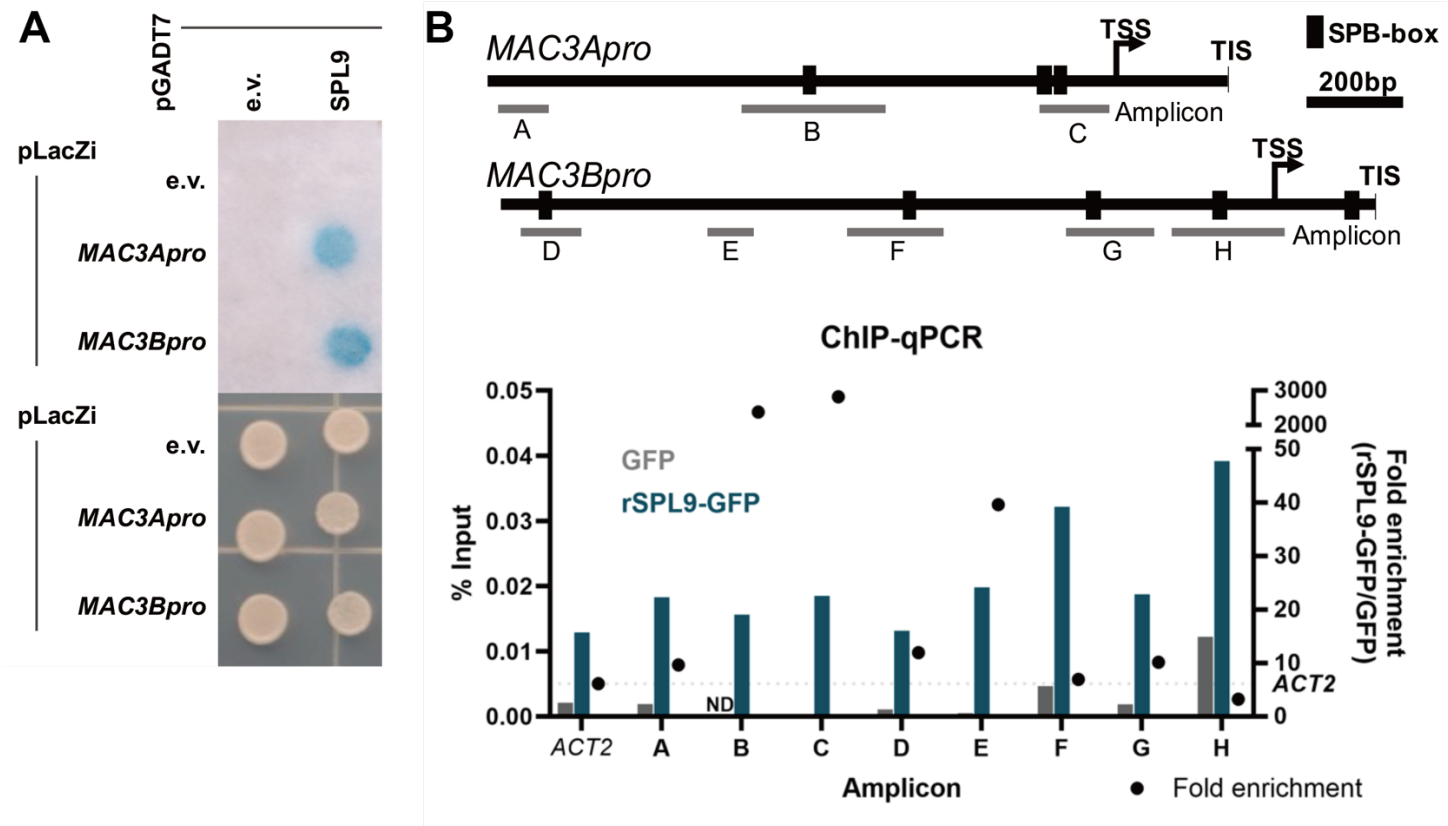

Figure 8. SPL9 interacts with the promoters of *MAC3A* and *MAC3B*

(A) SPL9 interacts with the *MAC3A* and *MAC3B* promoters in the yeast one-hybrid assays. The yeast bearing the *pLacZi* promoter-reporter vectors and *pGADT7* vectors expressing *SPL9* were grown on synthetic dropout medium (SD-Leu-Ura-Met). The colonies were blotted on the filter paper to test the β-Galactosidase (β-Gal) activity. The blue color indicates the interaction between 1.5 kb promoter fragments of *MAC3A* and *MAC3B* in the *pLacZi* vectors and the transcription factors in the *pGADT7* vectors. Empty vectors (e.v.) were used as negative control. **(B)** The chromatin immunoprecipitation (ChIP) assays in the Arabidopsis seeding expressing *rSPL9-GFP* or *GFP* only. The locations of SPL9 predicted binding sites (SPB-box, black boxes) were illustrated in the *MAC3A* and *MAC3B* promoters (upper panel). The amplicons were designed to surround SBP-Box (greys boxes labeled with A to H) or *ACTIN2* (*ACT2*) as controls. The chromatins in the Arabidopsis seedlings expressing *rSPL9-GFP* (dark blue bars) or *GFP* (grey bars) along with Col-0 were immunoprecipitated with anti-GFP antibody, and the relative enrichments of immunoprecipitated DNA relative to input were calculated as "%input." shown as a bar graph. The fold enrichment (black dots) was calculated by dividing "%input" in SPL9-GFP with "%input" in GFP. The grey horizontal dashed line represents the fold enrichment of negative control, *ACT2*. The "ND" stands for not detectable, and the transcription start site (TSS) and the translation initiation site (TIS) were labeled. Only one replicate is presented here.

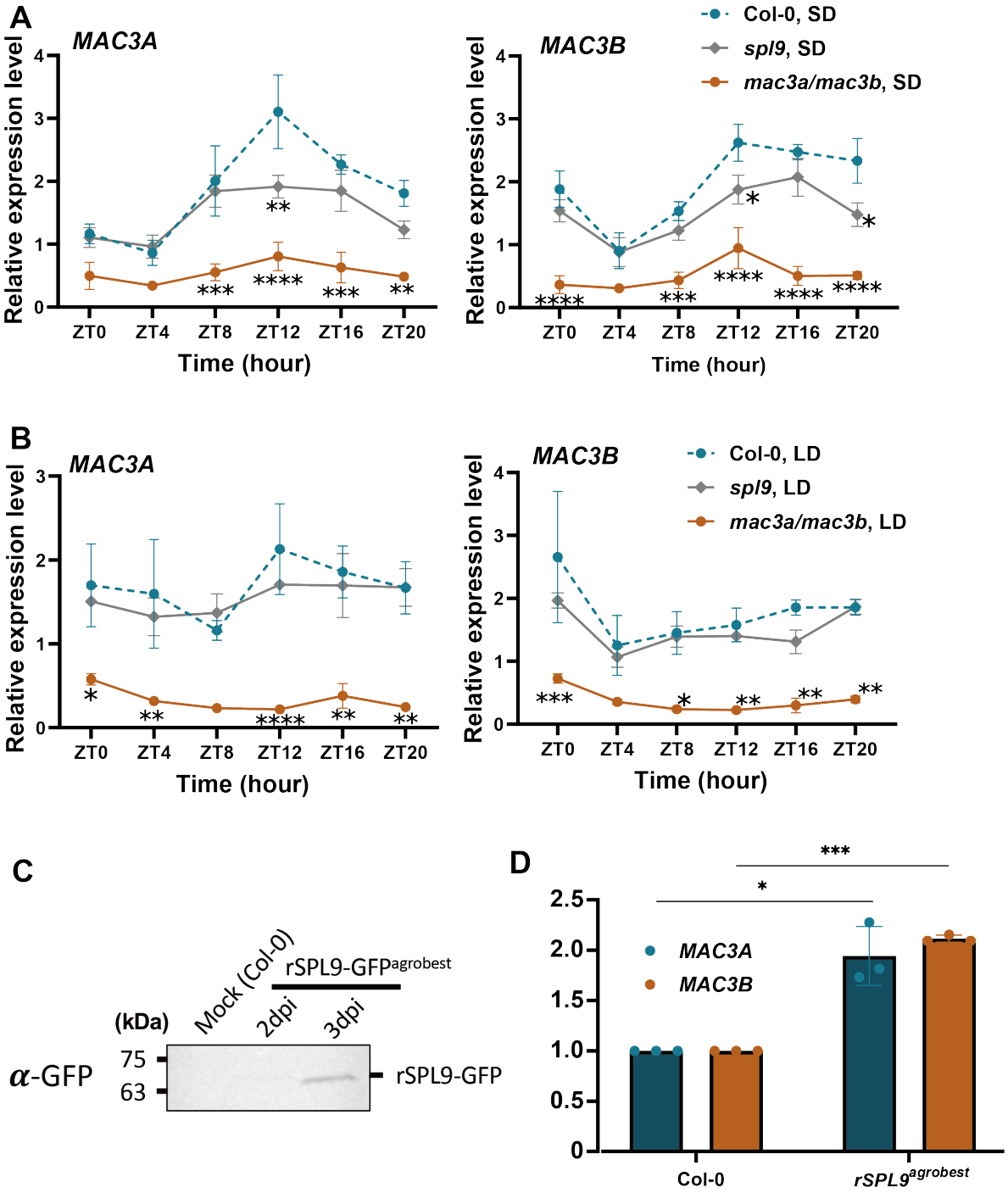

Figure 9. SPL9 activates *MAC3A* and *MAC3B* expression

(A and B) The diurnal expression of *MAC3A* (left panel) and *MAC3B* (right panel) in Col-0, *spl9*, and *mac3a/mac3b* mutant in SD (A) and LD (B) was measured with RT-qPCR. The samples were harvested every 4 hours after light on (ZT0). The significance of the differences between genotypes within time points was calculated from three biological replicates using two-way ANOVA with Dunnett's test. **(C)** Transient expression of *rSPL9-GFP* with the AGROBEST infection strategy. The rSPL9-GFP protein was detected by anti-GFP antibody in Western blotting to confirm their expression. **(D)** The expression of *MAC3A* and *MAC3B* in *rSPL9-GFP* over-expressed or Col-0 seedlings. The significance of the differences between the three biological repeats was tested using a T-Test. Significances were annotated by star marks (*:P< 0.05, **:P< 0.01, ***:P< 0.001, ****:P< 0.0001).

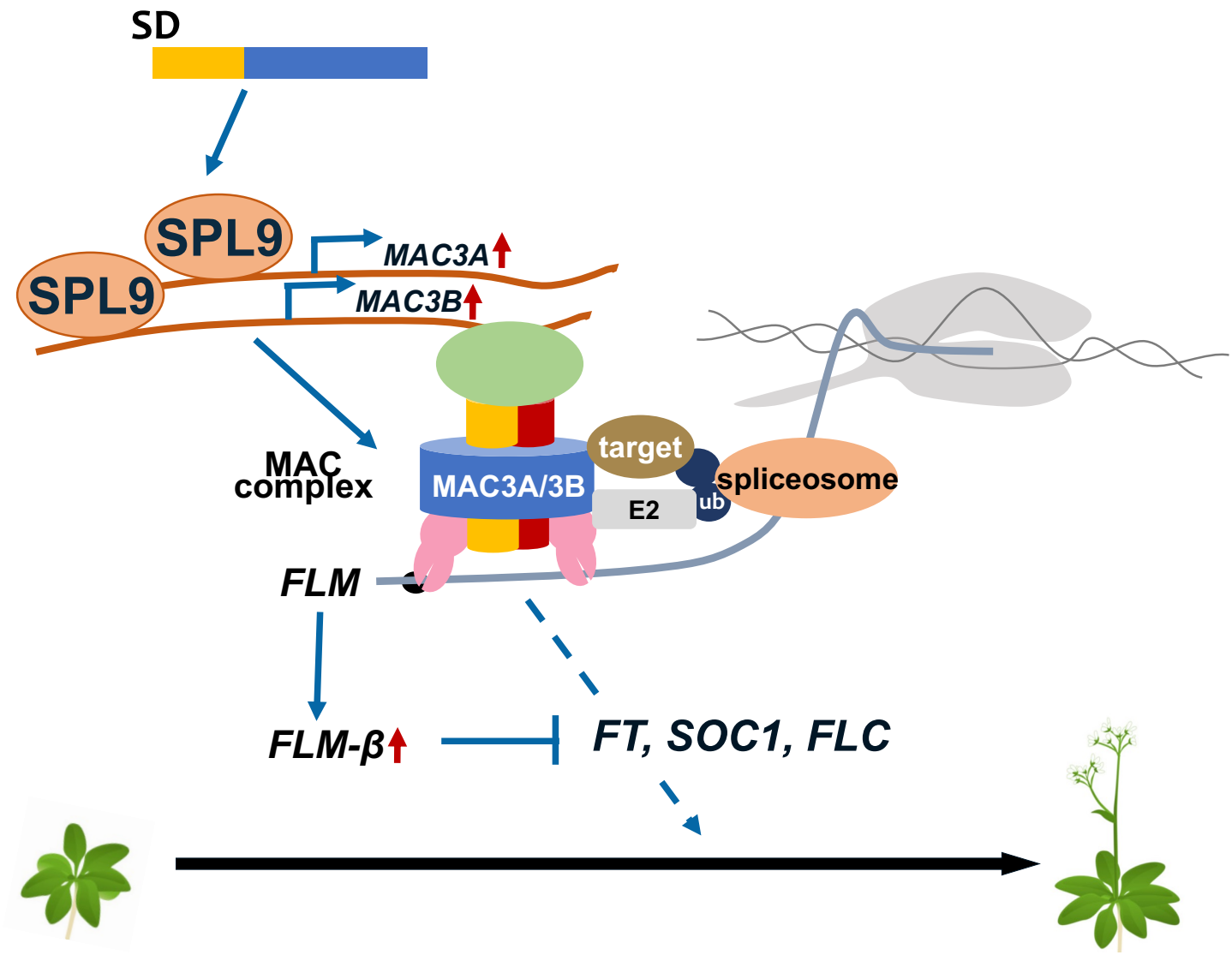

Figure 10. Proposed model of MAC3A and MAC3B mediated photoperiod signal to regulate flowering under SD

The working model of MAC3A and MAC3B repressing floral transition under SD. MAC3A and MAC3B proper the RNA splicing of *FLMβ* under SD, potentially acting with spliceosome, repressing floral transition. Under SD, SPL9 activates *MAC3A* and *MAC3B* transcription, which may enable MAC3A and MAC3B to modulate floral transition.

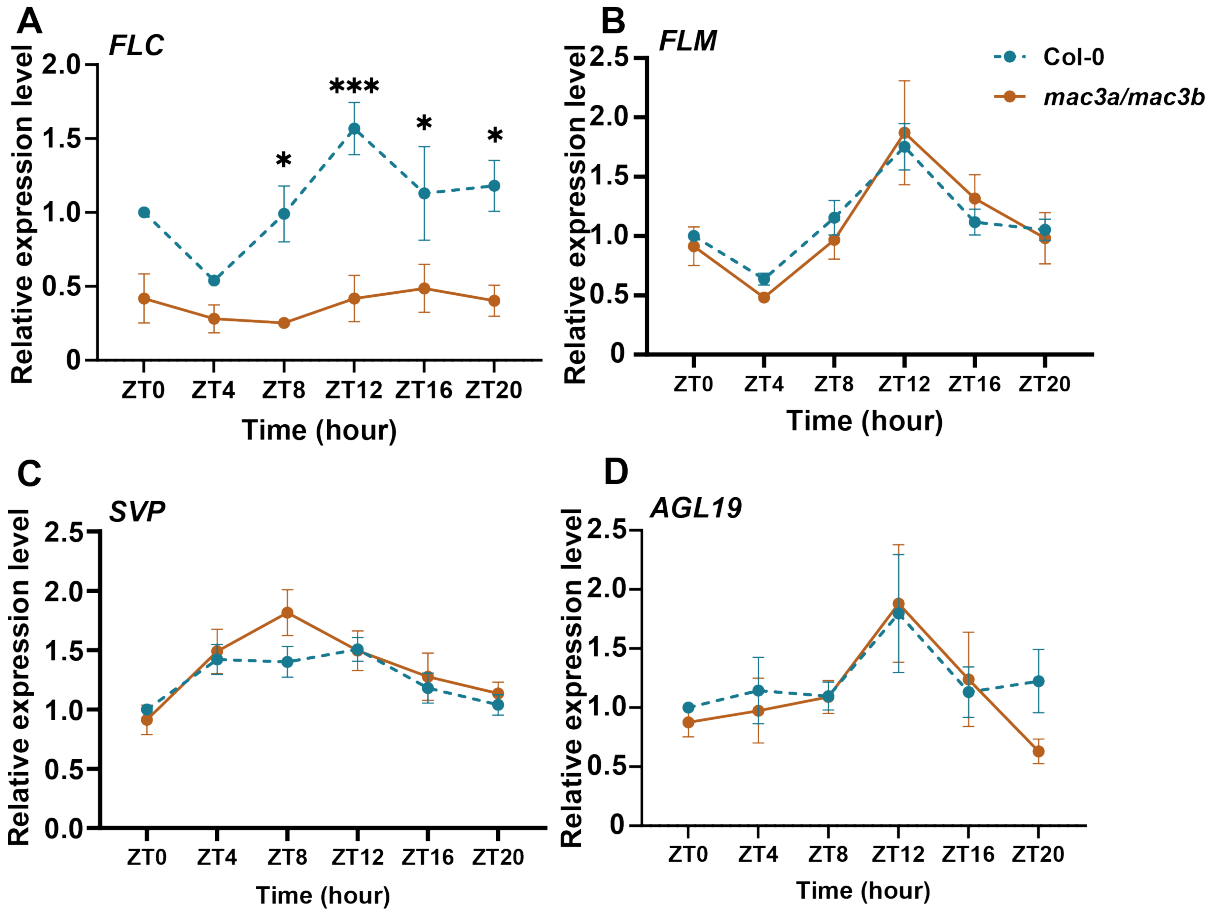

Supplemental Figure S1. The expression of *FLC*, *FLM*, *SVP*, and *AGL19* in SD measured by RT-qPCR

The diurnal expression levels of **(A)** *FLC*, **(B)** *FLM*, **(C)** *SVP*, and **(D)** *AGL19* in the Col-0 and *mac3a/mac3b* mutant seedlings under SD were measured by RT-qPCR. The relative expression levels were normalized with *UBQ10* and compared to Col-0 at ZT0. Error bars indicated standard deviations of three biological replicates. Data were analyzed using ANOVA and the Kruskal-Wallis test: ***, $p < 0.001$; *, $p < 0.05$.

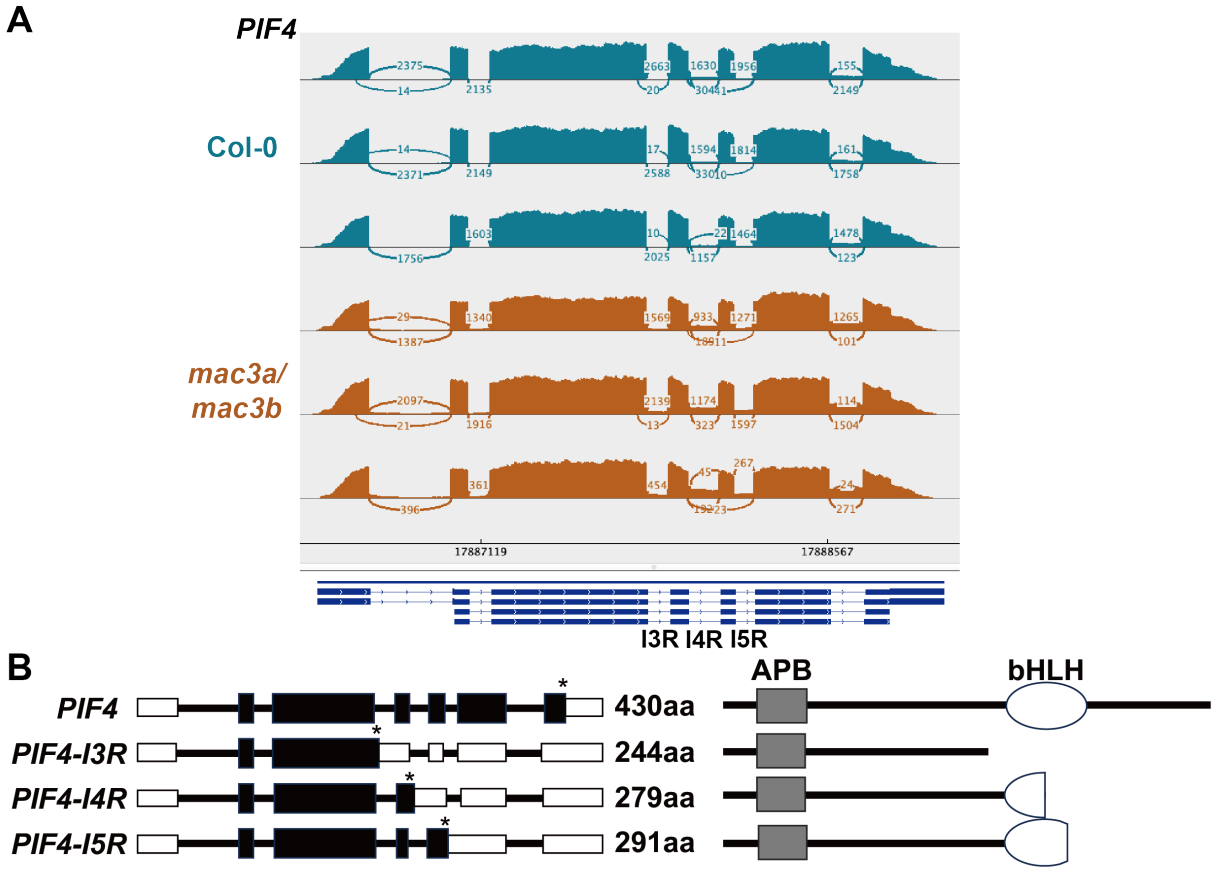

Supplemental Figure S2. Alternatively spliced events of *PIF4* were identified in the *mac3a/mac3b* mutant

(A) The sashimi plots demonstrate the splicing events found in Col-0 (Blue) and *mac3a/mac3b* (Orange) on the *PIF4* locus. The height of the base represents the relative read depth, and the read number across junctions was shown between specific splicing junctions. Intron 3, 4, and 5 (I3R, I4R, and I5R) annotated the IR events that may happen on the *PIF4* locus. In differentially alternative splicing events, only the I3R event out of these three events passes our statistical criteria, while its annotation is "PIF4-AT2G43010-4-IR" in Figure 5. The different annotations of intron numbers were due to the procedures of the RackJ algorithm. **(B)** The predicted *PIF4* isoforms with different retained introns. PIF4 and its intron-retained form of transcripts were drawn with untranslated regions (UTR) in white blocks, coding sequence (CDS) in black blocks, spliced introns in black lines, and translation stop codon in the star above (left). On the right panel, predicted peptides encoded from specific transcripts were annotated with active phyB-binding (APB, grey box) and complete/truncated bHLH (complete/sliced white oval) domains.

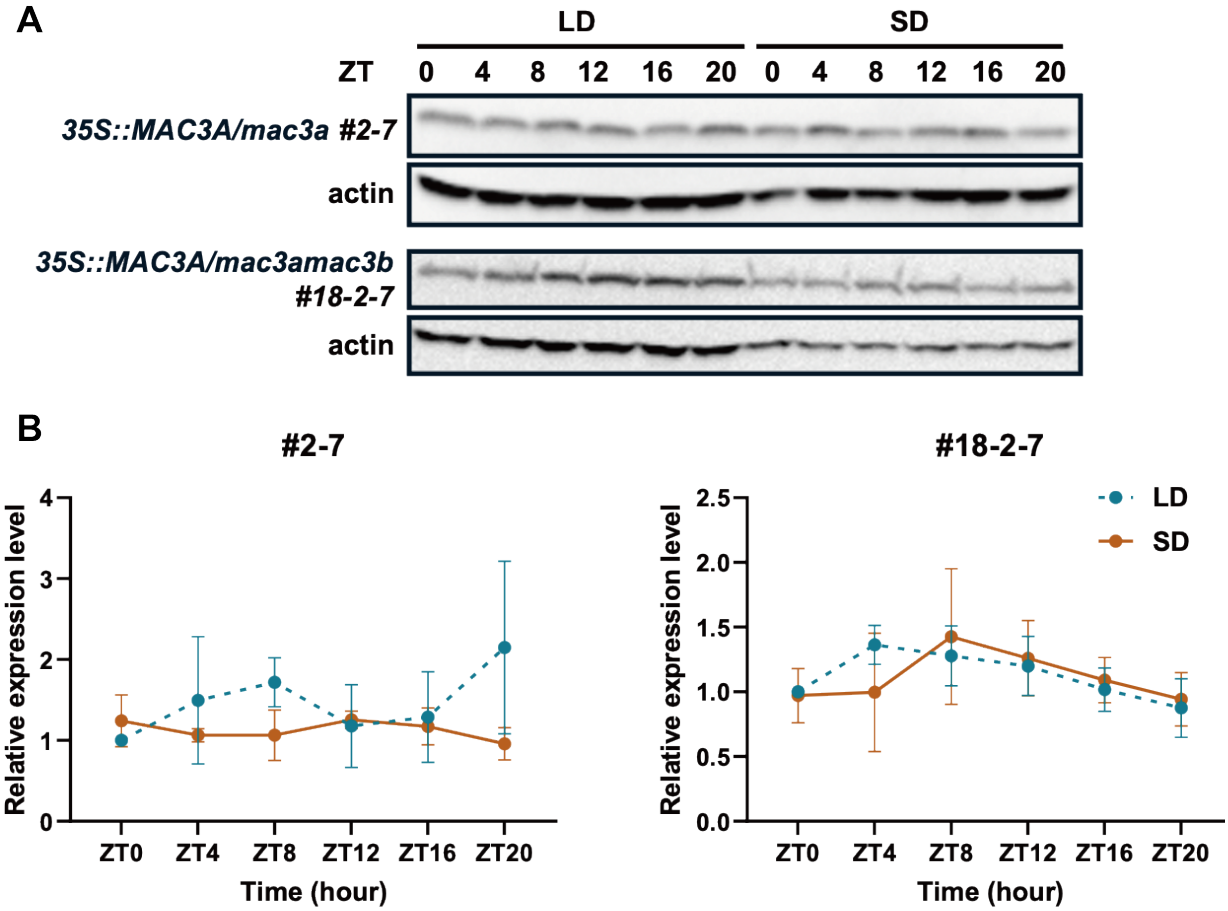

Supplemental Figure S3. Diurnal protein profiles of *35S::FLAG-MAC3A* in LD and SD

(A) The representative diurnal protein levels of *FLAG-MAC3A* fusions driven by the *CaMV 35S* promoter in the *mac3a* (*35S::MAC3A/mac3a*) or *mac3a/mac3b* (*35S::MAC3A/mac3amac3b*) Arabidopsis mutant in LD and SD. The 10-day-old seedlings in LD and 14-day-old seedlings in SD were harvested every 4 hours after light on (ZT0) for 24 hours. MAC3A proteins were immunologically detected using an anti-FLAG antibody, and actin levels were used as an internal control. **(B)** The quantification analysis of *35S::MAC3A* protein expression levels was plotted. Data were collected from three biological replicates and statistically analyzed using the Kruskal-Wallis test with no significant differences.

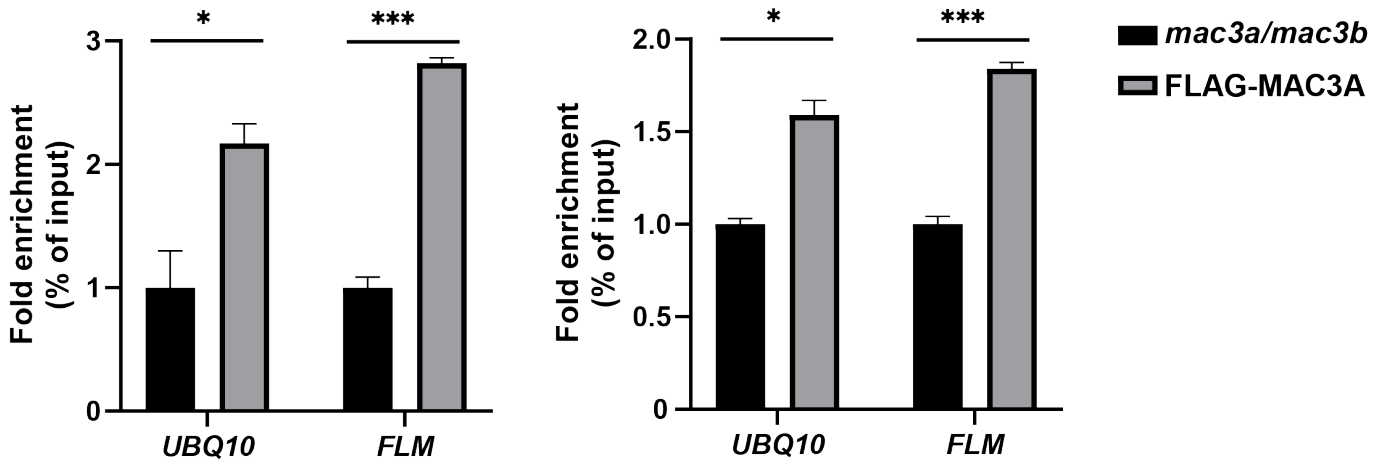

Supplemental Figure S4. The biological repeats of FLAG-MAC3A RIP-qPCR

RNA-Immunoprecipitation followed by qPCR (RIP-qPCR) with anti-FLAG antibody in the FLAG-tagged *MAC3A*/*mac3amac3b* (FLAG-MAC3A) and *mac3amac3b* control. The enrichment of immunoprecipitated RNA was calculated relative to the input RNA. The *mac3amac3b* mutant and the transcript of *UBQ10* were used as negative controls, respectively. The values shown are means ± SD. Statistical analysis was performed using a two-tailed paired t-test (ns, non-significant, *P< 0.05; ***P< 0.001). The representative replicates are shown in Figure 6D.

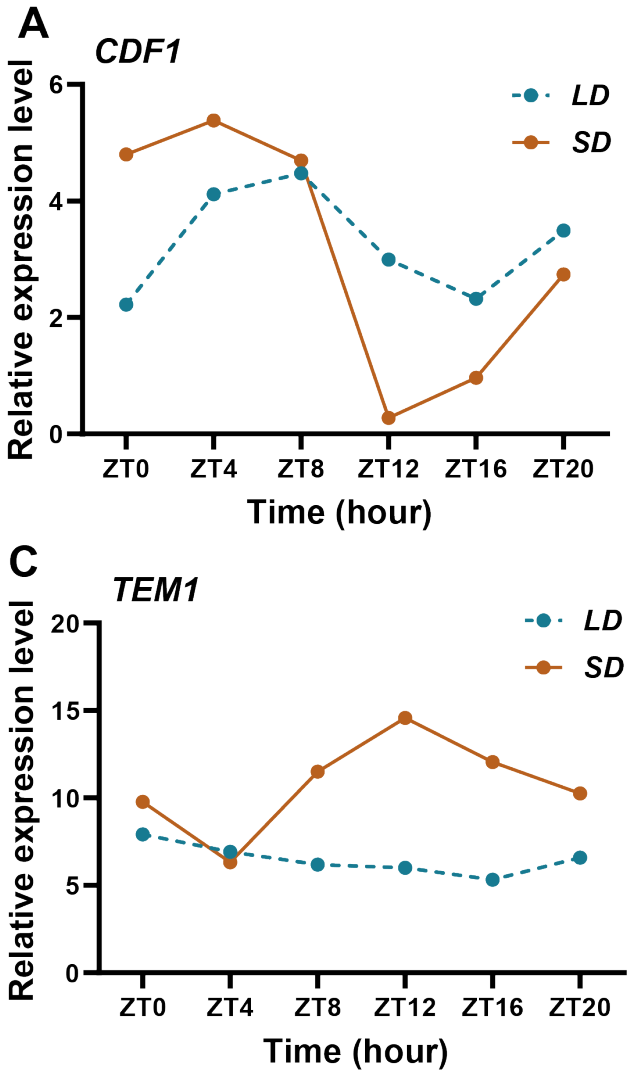

D

Correlation pair		Pearson's *r*	*P* value
SPL9	*MAC3A*	-0.593	0.0421
	MAC3B	-0.731	0.0069
CDF1	*MAC3A*	-0.830	0.0008
	MAC3B	-0.693	0.0125
TEM1	*MAC3A*	0.697	0.0118
	MAC3B	0.725	0.0076
NF-YB3	*MAC3A*	0.762	0.0040
	MAC3B	0.718	0.0086

Supplemental Figure S5. The expression profiles of *CDF1*, *NF-YB3*, and *TEM1* under LD and SD on the Photo-Graph database and their correlation to *MAC3A* and *MAC3B*

(A-C) The diurnal expression of (A) *CDF1*, (B) *NF-YB3*, and (C) *TEM1* under LD and SD were retrieved from the RPKM of RNA-seq data on the Photo-graph database (https://gendron-lab.shinyapps.io/PhotoGraph/; Leung et al., 2023). The dot noted the mean of normalized reads. The expression values under LD were represented by blue dots with lines and SD by orange dots with lines. The relative expression levels **(D)** The correlation between the expression pattern of *MAC3A* and *MAC3B* (Figure 7A and 7B) with *SPL9*, *CDF1*, *NF-YB3*, and *TEM1* across a day under LD and SD. The correlation was calculated in Pearson's r, by gene expression of correlation pair genes under LD and SD, and the significances of Pearson's r were shown on its right side.